Wrocław University of Technology
Centre of Advanced Materials and Nanotechnology

Materials Science

4th International Conference on Electronic Processes in Organic Materials ICEPOM-4

Lviv, Ukraine, 3-8 June, 2002

Guest Editor: Andrzej Miniewicz

Vol.20 • No. 4 • 2002

Oficyna Wydawnicza Politechniki Wrocławskiej

Materials Science is an interdisciplinary journal devoted to experimental and theoretical research into the synthesis, structure, properties and applications of materials.

Among the materials of interest are:

- glasses and ceramics
- sol-gel materials
- photoactive materials (including materials for nonlinear optics)
- laser materials
- photonic crystals
- semiconductor micro- and nanostructures
- piezo-, pyro- and ferroelectric materials
- high-T_c, superconductors
- magnetic materials
- molecular materials (including polymers) for use in electronics and photonics
- novel solid phases
- other novel and unconventional materials

The broad spectrum of the areas of interest reflects the interdisciplinary nature of materials research. Papers covering the modelling of materials, their synthesis and characterisation, physicochemical aspects of their fabrication, properties and applications are welcome. In addition to regular papers, the journal features issues containing conference papers, as well as special issues on key topics in materials science.

Materials Science is published under the auspices of the Centre of Advanced Materials and Nanotechnology of the Wrocław University of Technology, in collaboration with the Institute of Low Temperatures and Structural Research of the Polish Academy of Sciences and the Wroclaw University of Economics.

All accepted papers are placed on the Web page of the journal and are available at the address: http://MaterialsScience.pwr.wroc.pl

The Journal is supported by the State Committee for Scientific Research

Editorial Office

Anna Sofińska
Łukasz Maciejewski

Editorial layout

Hanna Basarowa

Cover design

Zofia i Dariusz Godlewscy

Printed in Poland

Drukarnia Oficyny Wydawniczej Politechniki Wrocławskiej
Zam. nr 930/2002.

Contents

Papers presented at the 4th International Conference on Electronic Processes in Organic Materials, ICEPOM-4, Lviv, Ukraine

Regular papers

Materials Science, Vol. 20, No. 4, 2002

Optical and photovoltaic properties of films and polymer composites based on near infra-red polymethine dyes*

A. ISHCHENKO[1**], N. DEREVYANKO[1], YU. P. PIRYATINSKII[2], A. VERBITSKY[2], D. FILONENKO[3], S. STUDZINSKY[3]

[1]Institute of Organic Chemistry of Ukrainian NAS, 02094, Murmanskaya Str. 5, Kyiv-94, Ukraine

[2]Institute of Physics of Ukrainian NAS, Prosp. Nauki 46, 03650, Kyiv-39, Ukraine

[3]Taras Shevchenko Kyiv National University, Volodymyrska Str. 64, 01033, Kyiv, Ukraine

Films and composites based on 1,3,3,1′,3′,3′-hexamethylindotricarbocyanine tetrafluoroborate (HITC) polymethine dye have been investigated. Optical, photovoltaic and luminescent properties were studied under different conditions. It is shown that the composites under investigation are photosensitive in the near IR region close to the region of maximal solar spectral photon flux.

Key words: *photovoltage, polymethine dye, polymer composite*

1. Introduction

The most effective inorganic solar elements from Si and $CuInSe_2$ can effectively transform solar illumination in the near IR region. On the other hand, most organic compounds have long-wavelength edge of absorption at <600 nm. This is one of the reasons of relatively small integral efficiency of photo-devices based on organic materials, such as photoconverters, photovoltaic elements, solar cells, etc. For example, the best of recently developed organic solar cells transform illumination at 400–600 nm spectral range only [1, 2].

Therefore our purpose was the development of flexible organic layers, photosensitive in near IR region close to the region with maximal solar photon flux (750 –850 nm), which can be used as components of organic photodevices, including solar cells.

---

*Paper presented at the 4th International Conference on *Electronic Processes in Organic Materials*, ICEPOM-4, 3–8 June 2002, Lviv, Ukraine.

**Corresponding author, e-mail: alexish@i.com.ua.

2. Experimental

To solve the problem mentioned above we selected polymethine dyes [3]. These dyes have maximum of the π-π absorpion in the 750–1050 nm spectral range. Their absorption and luminescence can be shifted over a wide spectral range by the modification of the structure of heterocyclic moieties and the length of polymethine chain. Besides, on modifying the structure of various fragments of dyes with synthesis, high solubility both in strong polar and in weak polar organic solvents has been achieved. Furthermore, $\pi \rightarrow \pi^*$ absorption bands generally are additionally red-shifted and broadened for films and polymer composites [4].

In this paper, we present the results of a study of films and polymer composites based on specially synthesized 1,3,3,1′,3′,3′- hexamethylindotricarbocyanine tetrafluoroborate (HITC) [5] (see Scheme 1). This dye was selected because of its stability, and good solubility in various media, as well as because of the position of the maximum of its absorbance close to the maximum of the solar photon flux (725–775 nm) [2].

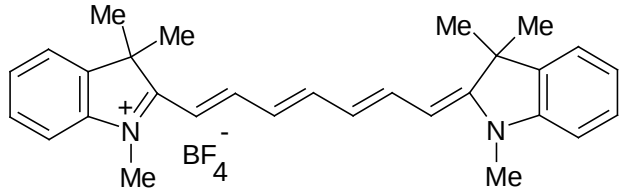

Scheme 1. Formula of HITC polymethine dye

To create polymer composites, poly-N-epoxypropylcarbazole (PEPC), synthesized in the Institute of Physical Organic and Coal Chemistry (Donetsk, Ukraine) [6] and polyvinylethylal (PVE) polymers [7], produced by "Azot" plant (Severodonetsk, Ukraine) (see Scheme 2) were used. It should be noted that PEPC is a photoconductive polymer whereas PVE does not exhibit any appreciable photoconductivity [4].

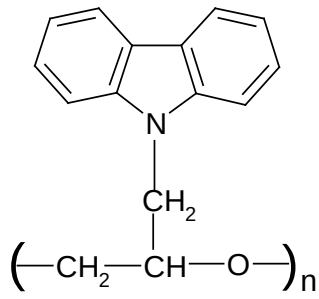

PEPC

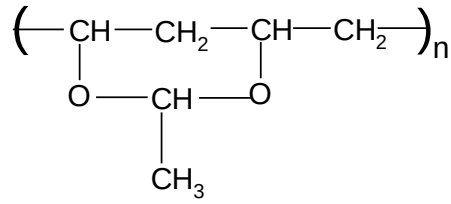

PVE

Scheme 2. Formulae of PEPC and PVE

Films of the dyes and of the dye-in-polymer composites were deposited from dichloroethane solution by the spin-coating technique. The films obtained were 1–2 μm thick, with different concentrations of HITC in PEPC ranging from 1 wt. % to 50 wt. %. The film of 50 wt. % HITC in PVE was obtained to compare the photosensitivity of composites based on different classes of polymers.

Absorption spectra were measured with a SPECORD M40 spectrophotometer. Photoluminescence (PL) was measured under the excitation with an UV nitrogen laser (λ = 337.1 nm) or with a red laser diode (λ = 651.2 nm) using the experimental set-up described in [8]. The technique and apparatus for photovoltage measurements were described elsewhere [9].

3. Results and discussion

Figure 1 shows absorption spectra of a HITC solution in dichloroethane, HITC solid film as well as dye-in-polymer composites in PEPC and PVE (30 wt. % of dye concentration). It can be seen that the absorption spectrum of HITC solution in 1,2-dichloroethane has the shape typical of polymethine dyes – the main band with a vibronic maximum at the short-wavelength edge. When applying a polymer matrix, a red shift of the dye absorption band has been observed both in photoconducting PEPC and in non-photoconducting PVE. The feature can be explained by the increase of dispersion interactions due to a higher refraction index of polymers as compared with 1,2-dichloroethane. The broadening of the absorption band, observed in the polymer matrices, is caused by a nucleophilic solvation of positively charged centres of HITC cations by polar groups of PEPC and PVE.

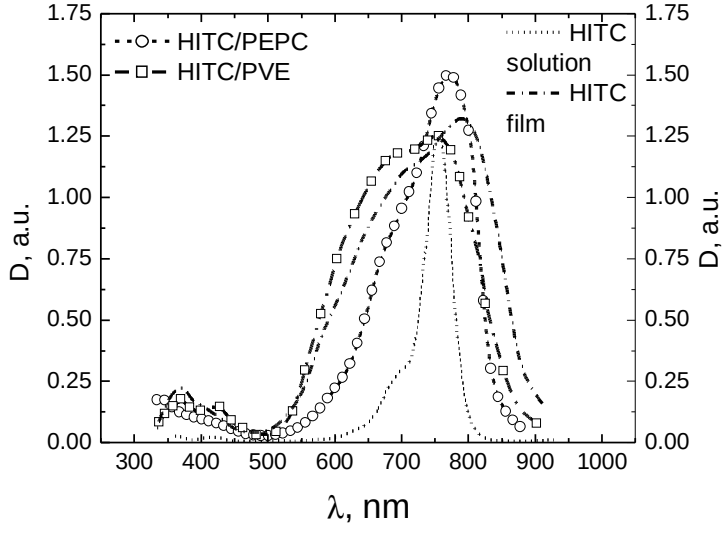

Fig. 1. Absorption spectra of HITC dye in different states

In Figure 2, the photovoltage spectra of HITC composite films in PEPC and PVE are shown. Their shapes generally correspond to the respective absorption spectra. Some slight changes in the intensity and bands position are observed.

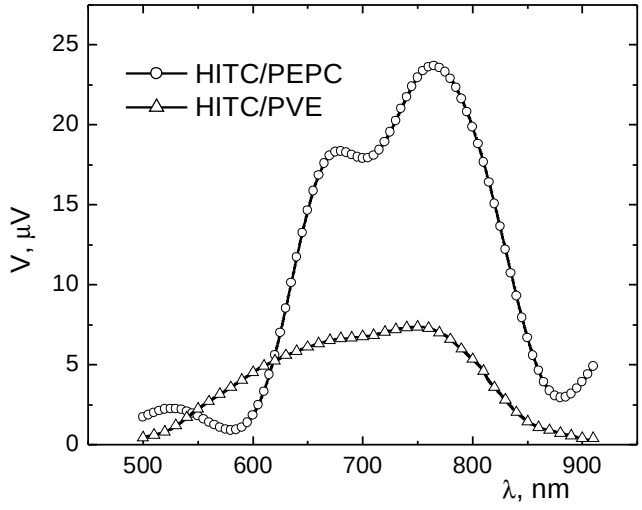

Fig. 2. Photovoltage spectra of HITC composite films

It is obvious that the photosensitivity of the samples contaning HITC in a photoconducting polymer (PEPC) is greater than that of the film of the dye in a non-photoconducting polymer matrix (PVE). This fact testifies that not only the dye concentration influences the efficiency of charge generation but also the type of polymer. Charge transfer between the dye and polymer molecules is much more effective in the PEPC composite than in the PVE-based film. This must result in the rise of the number of generated charge carriers.

In order to clarify processes in HITC/PEPC composite in which more effective photogeneration takes place, we studied the concentration dependence of the absorbance and photoluminescence (PL) under different conditions and using different sources of excitation.

The dependence of these quantities on the dye concentration in the 1–20 wt. % range is shown in Fig. 3. It is seen that the positions of maxima are weakly dependent on the dye concentration. An additional broadening of the absorption bands occurs on increasing the dye concentration due to the fact that macromolecular compounds have low dielectric permittivity. Salt-like dyes in these compounds are therefore completely dissociated. Because of this such dyes form different types of ionic pairs in polymer solutions [4]. When the concentration of the dye rises, the fraction of contact ionic pairs increases. A counter-ion, being localized in the region of one of the heterocycles, on

which a maximal positive charge is concentrated, destroys the electronic symmetry of the dye molecule [4]. This leads to the amplification of vibronic interaction and consequently to the band broadening.

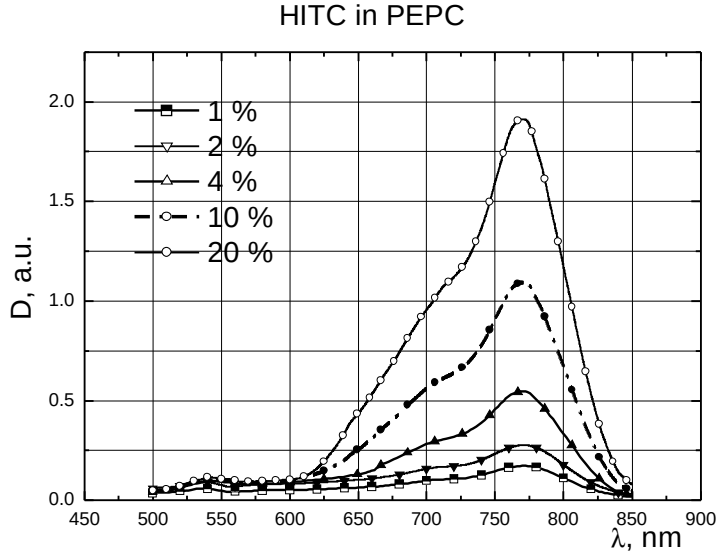

Fig. 3. Concentration dependence of absorption of HITC/PEPC composites

The above-mentioned effect is maximal in solid films of dye. Not only a significant broadening of the absorption band but also a strong deformation of its shape is observed (Fig. 1). Besides, an intermolecular interaction in the dye–dye system also influences the band shape in the film due to short distances between the dye molecules.

PL spectra for different concentrations of HITC dye are shown in Fig. 4. These spectra were measured under excitation with the nitrogen laser (λ_{ex} = 337 nm). The comparison of the PL spectra under excitation with the 337 nm N_2 laser band and with the 651 nm diode laser band (for the samples containing 2% of dye in PEPC) at 700 –900 nm range shows that the intensity of the PL band of the dye is greater for the diode laser excitation and its maximum is blue-shifted by 5 nm (Fig. 5). From Fig. 5 it is obvious that PL spectra of HITC both in the solution and in the polymer matrix are mirror-similar to the absorption spectra. The shape of PL bands remains the same for excitation in the region of the first (low-energy) electronic transition (λ_{ex} = 651 nm) as well as in the region of the second (high-energy) one (λ_{ex} = 337 nm). In the latter case, the PL intensity is weaker since the excitation energy is dissipated in the radiationless S_2–S_1 transition.

The results of low-temperature measurements of PL (at 4.2 K) are presented in Fig. 6. It can be seen that at low temperatures sharpening of PL band is observed together with a significant red shift (25 nm). It is explained by the decrease of the contribution to

the main vibronic transition of non-planar oscillations of dye molecules as well as of oscillations of polymer molecules in the field of dye charges. The mirror similarity of the absorption and PL spectra, and their shape independence on the wavelength of the excitation are the evidence that HITC dye in solutions and in polymer matrices are predominantly in the non-associated monocationic form.

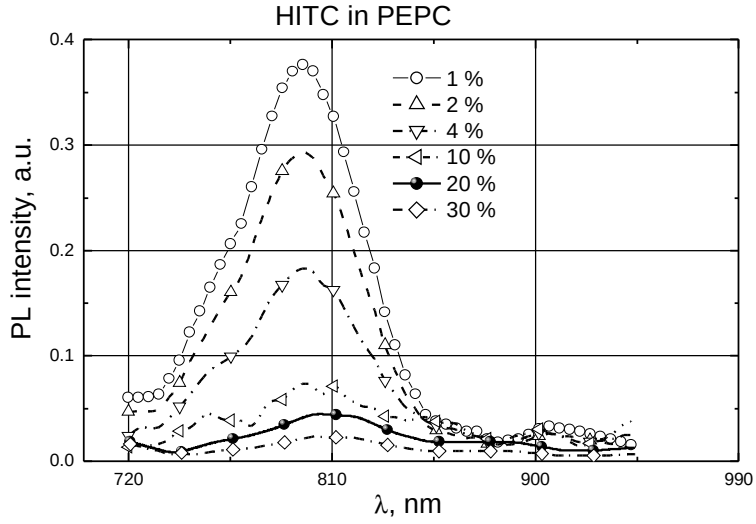

Fig. 4. Dependence of PL on concentration of dye

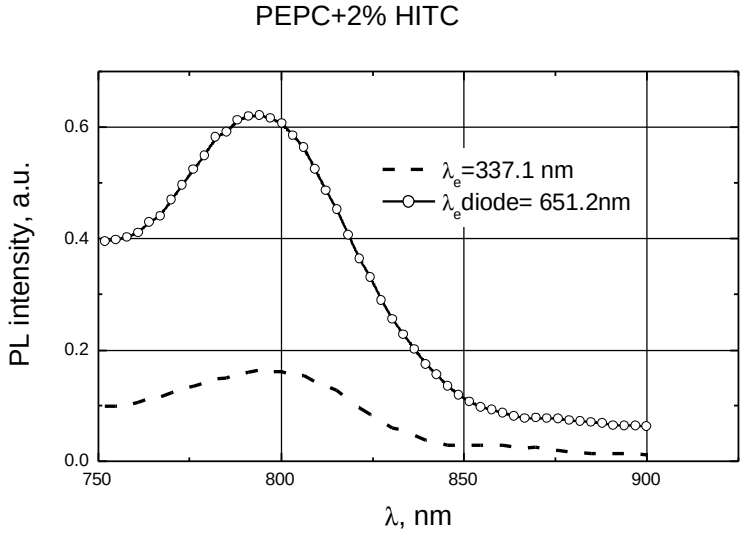

Fig. 5. PL spectra measured using different lasers

A strong luminescence quenching occurs with the concentration rise. In Fig. 7, the Stern–Volmer plot of luminescence intensity dependence on HITC concentration (open circles) is presented. A fitting analysis has shown that the dependence of the luminescence quenching on the concentration of the dye cannot be satisfactorily described by the linear Stern–Volmer equation (1), as is expected for the system with one luminophore and one quencher (it should be a linear dependence in Fig. 7).

$$\frac{I_0}{I_q} = 1 + K[\mathrm{Q}] \tag{1}$$

where I_0 is the PL intensity without a quencher, I_q is the PL intensity with a quencher Q, [Q] is the quencher concentration in mol/1000 g of polymer, K is the Stern–Volmer constant.

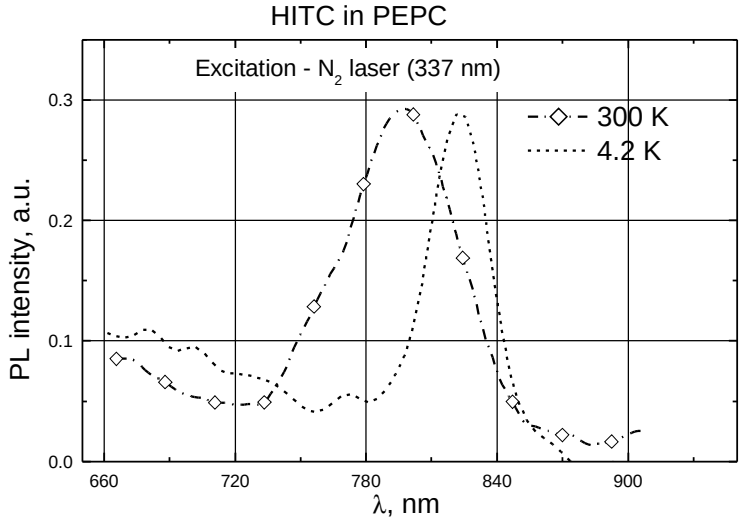

Fig. 6. Low-temperature measurement of PL

On the other hand, the dependence observed can be fitted by a quadratic Stern –Volmer equation (dashed line):

$$\frac{I_0}{I_q} = (1 + K[\mathrm{Q}])(1 + K'[\mathrm{Q}]) \tag{2}$$

where K and K' are the Stern–Volmer constants for different quenching processes.

The fitting analysis gives the following values for these constants (kg/mol): K = 2.25 and K' = 9.39. The presence of two kinetic processes of the luminescence quenching allows the conclusion that the process is not caused by the energy migration between dye molecules only but also by some other factor.

Probably, this second factor is the electron transfer from photoconducting PEPC to the cation of the dye. PEPC should form $(carbazole)^{+\bullet}$ cation-radical, and the cation of HITC can form a neutral radical $Ct^{\bullet}$. Since the dye molecules at high concentrations, as was mentioned above, occur mainly as contact ionic pairs, $Ct{\cdot}An^{-}$ anion-radical pairs are formed. The formed ions $(carbazole)^{+\bullet}$ and $Ct{\cdot}An^{-}$ are charge carriers in a PEPC photoconducting matrix doped with HITC dye. Their presence explains photovoltaic properties of HITC/PEPC composites. The fact that photosensitivity of the composite based on non-photoconducting PVE is much smaller than that of composites based on photoconducting PEPC (Fig. 2), is in agreement with this model.

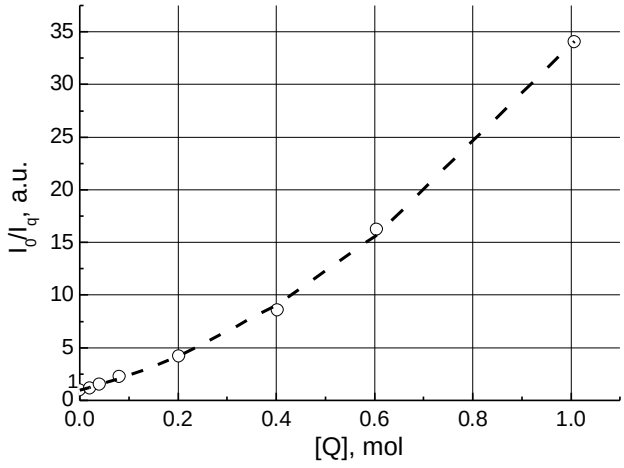

Fig. 7. Integral PL quenching in Stern–Volmer coordinates

Conclusions

Flexible composite films of HITC in conductive PEPC have noticeable photosensitivity in the region close to the maximum of solar photon flux. Therefore, such films may be used in perspective as components of organic photosensitive devices, including solar cells.

References

[1] ROSTALSKI J., MEISSNER D., Solar Energy Mater. and Solar Cells, 63 (2000), 37.
[2] BRABEC C. J., SARICIFTICI N. S.., HUMMELEN J.C., Adv. Funct. Mater, 11 (2001), 15.
[3] ISHCHENKO A.A., Theoretical and Experimental Chemistry, 34 (1998), 191.
[4] ISHCHENKO A.A., *Structure and spectral and luminescent properties of polymethine dyes* (in Russian), Naukova Dumka, Kiev, 1994.
[5] KOMAROV I.V., TUROV A.V., KORNILOV M.YU., DEREVYANKO N.A., ISHCHENKO A.A., Zh. Obshchei Khimii, 59 (1989), 2356.

[6] GETMANCHUK YU.P., DAVIDENKO N.A., DEREVYANKO N.A., ISHCHENKO A.A., KOSTENKO L.I., KUVSHINSKII N.G., STUDZINSKII S.L., SYROMYATNIKOV V.G., Polymer Science Ser. A., 44 (2002), 855.
[7] *Encyclopedia of Polymers* (in Russian), Soviet Encyclopedia, Vol. 1, Moscow, 1972, 227.
[8] PIRYATINSKII YU.P., YAROSHCHUK O.V., Optika i Spectroscopiya, 89 (2000), 937.
[9] VERBITSKY A.B., VERTSIMAKHA YA.I., KORBUTYAK D.V., Functional Materials, 4 (1997), 57.

Received 3 June 2002
Revised 28 October 2002

Materials Science, Vol. 20, No. 4, 2002

Effect of aggregation on optical and photovoltaic properties of an metallorganic compound*

N. DEREVYANKO, A. ISHCHENKO, A.VERBITSKY**

Institute of Organic Chemistry of Ukrainian NAS, 02094, Murmanskaya Str. 5, Kyiv-94, Ukraine

Institute of Physics of Ukrainian NAS, 03650, Prosp. Nauki 46, Kyiv-39, Ukraine

Optical and photovoltaic properties of an metallorganic compound – nickel(II)bis(dithiobenzil) (NBDB) in various states of aggregation (solution, vacuum-deposited film, polymer composite) have been studied. Its absorption spectra are explained by the formation of sandwich aggregates in deposited films, which are absent in the solution and polymer composites. The study of photovoltage spectra showed that both deposited and composite films are photosensitive at the range of 500–1000 nm, and the quantum efficiency of the photogeneration for the direct excitation of aggregates is greater than that for the excitation of monomer molecules.

Key words*: metallorganic compound, composite, aggregation, photovoltage*

1. Introduction

Most of organic compounds have a long-wavelength edge of absorption at 600–800 nm. This is one of the reasons of relatively limited use of organic compounds for different applications in IR region, such as dye lasers, organic light -emitting diodes, photoconverters, solar cells, etc.

Therefore, our purpose was to develop organic layers, which can be used in near IR region [1, 2]. The study of optical and photovoltaic properties of metallorganic films, photosensitive at near IR region is described.

2. Experimental

Films of nickel(II)bis(dithiobenzil) (NBDB) [3] were prepared by vacuum deposition onto glass substrates coated with SnO_2 layer at room temperature.

---

*Paper presented at the 4th International Conference on *Electronic Processes in Organic Materials*, ICEPOM-4, 3–8 June 2002, Lviv, Ukraine.

**Corresponding author, e-mail: avsky@iop.kiev.ua.

Films of NBDB-doped polymer composites were obtained from the solutions of both NBDB and polyvinylethylal (PVE) polymers ("Azot" plant, Severodonetsk, Ukraine) [4] in methylene chloride (CH_2Cl_2).

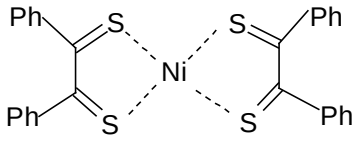

NBDB

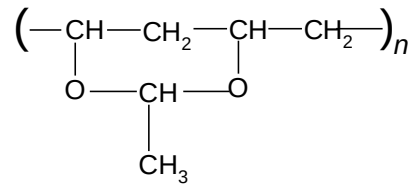

PVE

Absorption spectra were measured by the Specord M40 and Perkin-Elmer lambda 20 spectrophotometers. The experimental set-up and configuration of cells for the measurement of spectral characteristics of photovoltage (V) were described elsewhere [1, 2, 5]. All photovoltage dependences were measured using modulated illumination and they were corrected for the equal number of incident photons.

3. Results and discussion

Absorption spectrum of NBDB in solution can be described by two electronic transitions with maxima at 600 and 860 nm (Fig. 1). In Fig. 1 it can also be seen that absorption spectrum of NBDB-doped polymer composite film (~1 μm thickness) is similar to the spectrum of solution with a slight (~10 nm) red shift.

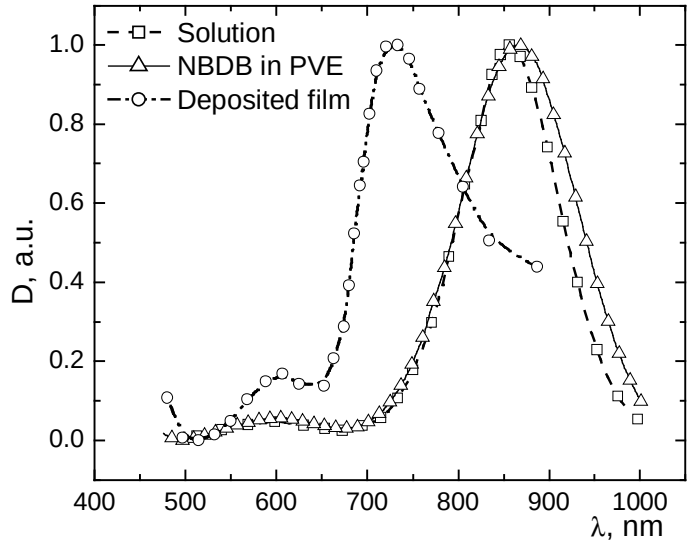

Fig. 1. Absorption spectra of NBDB

The morphology of these composite films is as follows: in a solid solution with randomly arranged crystallites most of them have a “cross-swords” shape. In Figure 2, the image of a polymer composite film made by means of a polarization microscope supplied by a digital photo-camera with high resolution (cross polarizers) is shown.

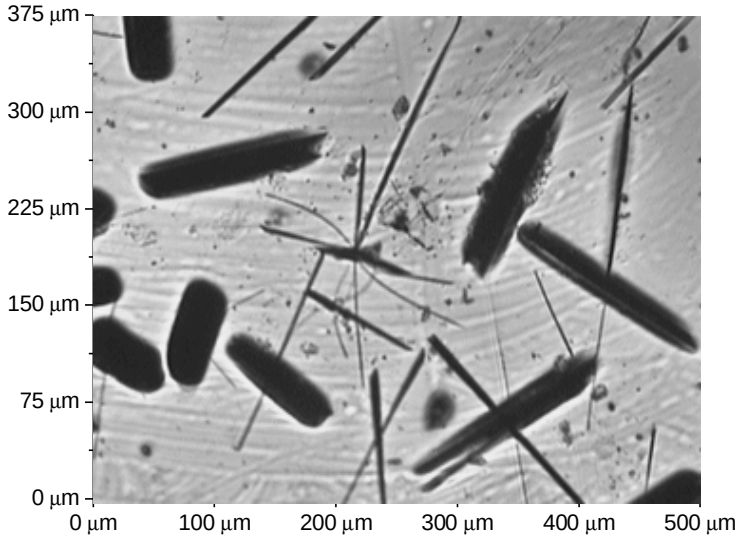

Fig. 2. Image of NBDB-PVE composite film

A strong deformation of the spectrum is observed when passing from the solution and composite to a solid deposited film. During the film formation both bands of a molecule are splitted (Fig. 3).

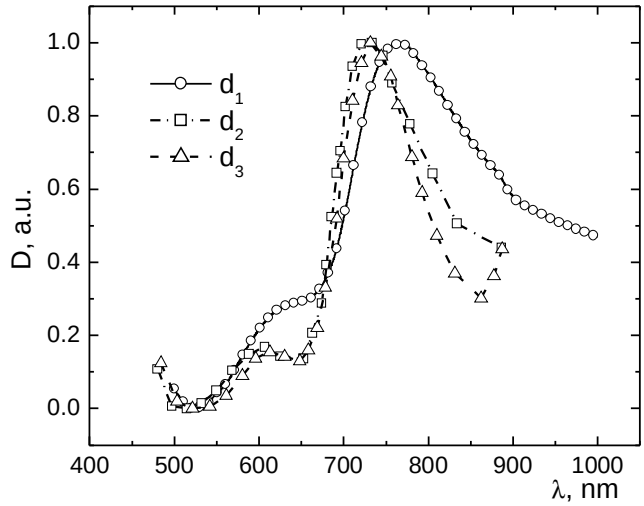

Fig. 3. Thickness dependence of the spectra of NBDB films

Figure 3 shows the absorption spectra of NBDB vacuum-deposited films of different thickness: 42 nm (d_1), 220 nm (d_2) and 410 nm (d_3). From the comparison of the spectra with those of solutions and polymer composites it is seen that due to the film formation both bands of the spectrum with the maxima at 600 nm and 860 nm are splitted. Since NBDB molecules have a planar structure, they most probably form aggregates in which planes of chromophore groups of dyes are parallel to each other – so-called sandwich-aggregates since dispersion and electrostatic interactions are maximal for such orientation of molecules [6]. Decrease of the long-wavelength absorption band intensity and appearance of new short-wavelength bands are in the agreement with the sandwich structure of aggregates [6].

According to the exciton theory, the interaction of chromophores in aggregates of dyes leads to the splitting of the first excited state S_1 into two states: S_1^h of higher energy and S_1^1 of lower energy [6]. The electronic transitions $S_0 - S_1^h$ and $S_0 - S_1^1$ correspond to short-wavelength- and long-wavelength bands in the absorption spectra of aggregates, respectively.

In sandwich aggregates, the long-wavelength transition is forbidden, and short-wavelength transition has doubled intensity [6]. Therefore, the formation of sandwiches is accompanied by the decrease in intensity of a long-wavelength band and increase of intensity of a short-wavelength band which is blue-shifted. Such a situation, as was mentioned above, is observed in our case. In thick films, the number of dye molecules participating in the process of aggregation increases. This causes, as follows from the exciton theory, additional splitting of the S_1 level, and consequently, amplification of the above-described effects in absorption spectra as the thickness of the film increases (Fig. 3).

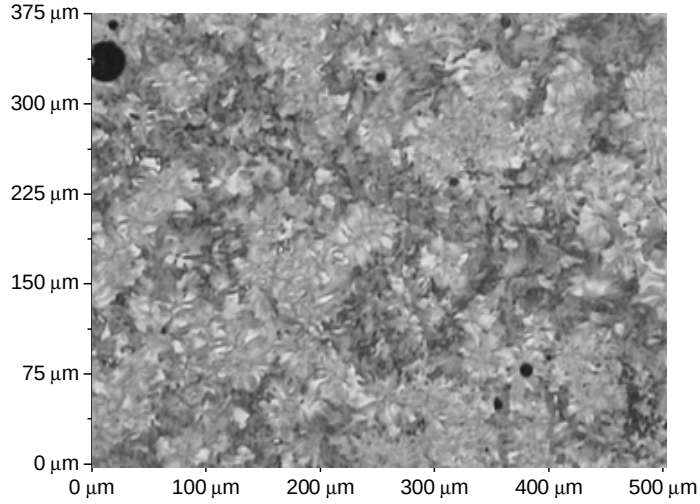

Fig. 4. Image of NBDB deposited film

Such a mosaic aggregate structure can be clearly seen in Fig. 4, where the photograph of vacuum-deposited film of 210 nm thickness (cross polarizers) is shown. The study of photovoltage spectra of deposited and composite films showed that both films are photosensitive at the range of 500–1000 nm (Fig. 5).

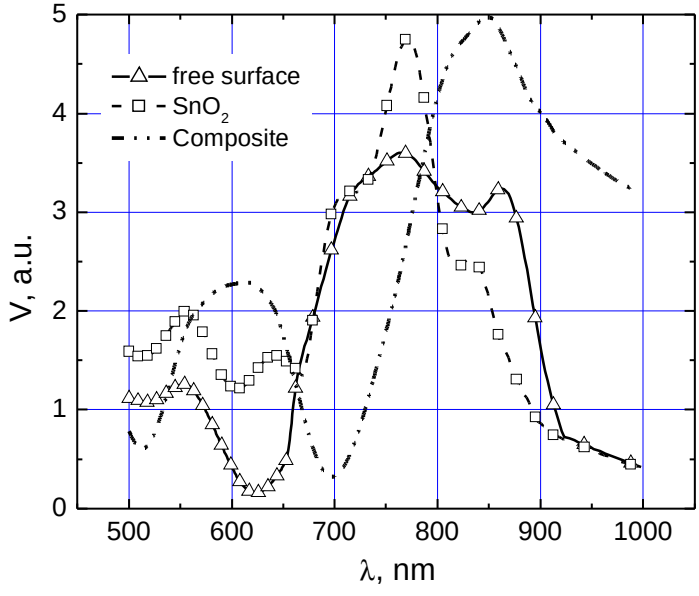

Fig. 5. Photovoltage spectra of NBDB deposited film and polymer composite

Figure 5 shows photovoltage spectra of vacuum-deposited films under the excitation from the side of the SnO_2 electrode as well as from the free-surface side, and the spectrum of photovoltage for polymer composite film which, in general, is similar to the absorption spectrum with a slight change in the ratio of bands intensity. Opposite picture is observed for deposited films.

During the film formation, the band with the maximum near 600 nm is splitted into the band at 640 nm and a weak band with the maximum at 550 nm. The more intensive band with the maximum near 860 nm in the spectra of films is splitted into bands with the maxima at about 770 and 860 nm. The shoulder at 700 nm is also observed. All these bands are clearly seen at the photovoltage spectra (Fig. 5).

Observation of photovoltage under illumination of deposited films from both sides confirms that during light absorption aggregates create carriers, which then are separated by internal electrical fields because of the formation of a potential barrier at the interface with SnO_2 electrode and at the free surface of NBDB film. Besides, it should be noted that the height of the potential barrier at the interface between NBDB and SnO_2 is higher than a bend of energetic bands at the free surface.

The higher relative intensity of additional bands in spectra of photovoltage than in absorption spectra of films testifies that the quantum efficiency of photogeneration for direct excitation of aggregates is greater than for the excitation of monomer NBDB molecules.

Conclusions

- We have shown that mosaic structure consisting of sandwich-aggregates is formed in vacuum-deposited films of NBDB contrary to NBDB-polymer films, which consist of crystallites randomly arranged in the composite.
- The study of photovoltage spectra, as well as of deposited and composite films are photosensitive at the range of 500–1000 nm. New bands due to sandwich-aggregates formation are observed for deposited films both in absorption and photovoltage spectra.
- It is found that relative quantum efficiency of photogeneration is maximal for the direct excitation of aggregates.

References

[1] VERTSIMAKHA YA., VERBITSKY A., ISHCHENKO A., DEREVYANKO N., *Photovoltaic Properties of Photosensitive in Wide Spectral Region Heterostructures*, [in:] A. Graja, B.R. Bulka, F. Kajzar (Eds.), *Molecular Low-Dimensional and Nanostructured Materials for Advanced Application*, NATO Science Series, II. Mathematics, Physics and Chemistry, Kluwer Academic Publishers, Dordrecht, 2002, p. 311.

[2] VERTSIMAKHA, YA., ISHCHENKO, A., MEISSNER, D., VERBITSKY, A., DEREVYANKO N., Proceedings of QUANTSOL-2001 International Workshop, Kirchberg, Austria, March 10–17, 2001, 71.
[3] MOURA J.C.V.P, OLIVEIRA-CAMPOS A.M.F., GRIFFITHS J., Dyes and Pigments, 33 (1997), 173.
[4] VERBITSKY A.B., VERTSIMAKHA YA.I., KORBUTYAK D.V., Functional Materials, 4 (1997), 57.
[5] *Encyclopedia of Polymers* (in Russian), Soviet Encyclopedia, Moscow, 1972, Vol. 1, p. 227.
[6] ISHCHENKO A.A., KRAMARENKO F.G., MAYDANNIC A.G., SEREDA S.V., VASILENKO N.P., J. Inf. Rec. Mater., 19 (1991), 207.

Received 3 June 2002
Revised 30 October 2002

Materials Science, Vol. 20, No. 4, 2002

Photoinitiation ability of some pentaaza-1,4-dienes*

OLENA O. NOVIKOVA[1], VOLODYMYR G. SYROMYATNIKOV[1**],
LARISA F. AVRAMENKO[1], NATALIYA P. KONDRATENKO[1],
TATYANA M. KOLISNICHENKO[1], MARC J. M. ABADIE[2]

[1]Kiev Taras Shevchenko University, Kiev 01033, Vladimirskaya Str., 64, Ukraine

[2]LEMP/MAO, University Montpellier 2, S.T.L., Place Bataillon,
34095 Montpellier Cedex 05, France

1,5-bis(4-methoxyphenyl)-3-methyl-pentaaza-1,4-diene, 1,5-bisphenyl-3-(2`-oxyethyl)-pentaaza-1,4-diene and 1,5-bisphenyl-3-methyl-pentaaza-1,4-diene were studied by differential scanning photocalorimetry (DPC) and dilatometry methods as photoinitiators of radical polymerization of vinyl monomers. Photoinitiation abilities of the compounds investigated were compared with those of industrial photoinitiator IRGACURE 1 700. Pentaazadienes exibit a high initiation capacity, the activation energy of polymerization process in the presence of pentaazadiene compounds being lower than that for IRGACURE 1700. An increase of the initiator concentration results in a decrease of the rate of the process. The phenomenon can be explained by autoinhibition.

Key words: *pentaazadiene-1,4; photoinitiator; polymerization*

1. Introduction

Due to their photosensitive properties and relative thermal stability azo compounds may be applied in non-silver photographic processes [1]. The usage of azo compounds as photosensitive materials in photolithography and laser ablation is well known [2]. Their photosensitivity and superior structuring properties are mainly due to the liability of substituents binding to the N=N groups. During the ablation process, these bonds are cleaved, and nitrogen atoms as well as other small organic fragments of a molecule are released without leaving any residuals on the surface.

Pentaazadiene compounds under our investigation contain five nitrogen atoms in a row forming two conjugated azo groups. In view of the lability of this arrangement,

---

*Paper presented at the 4th International Conference on *Electronic Processes in Organic Materials*, ICEPOM-4, 3–8 June 2002, Lviv, Ukraine.

**Corresponding author, e-mail: svg@macro.chem.univ.kiev.ua,

they appear to be predestined for utilization in photochemical experiments [3, 4]. The first representative of these aromatic pentaaza-1,4-dienes was synthesized in 1866 by Griess [5] in the reaction of diazotized aniline with ammonia. Since then, a wide variety of aromatic pentaazadiene model compounds and polymers have been synthesized to investigate the influence of the substituents on the photolability [6]. A comprehensive discussion of the electronic structure of the pentaazadienes was made. With respect to the electronic structure and therefore to the photochemical properties, the class of pentaazadienes is similar to aromatic triazenes and aromatic diazonium salts [7].

The studies of a photochemical reaction under UV-Vis exposition and thermolysis behaviour have been carried out. It was found that electron-donating aromatic substituents increase photosensitivity and decrease their thermostability [6]. The quantum yield of photolysis is quite high compared with relative triazenes, which is attributed to the sterical hindrance of the competitive reaction channel, i.e. isomerization [8]. The thermolysis in the solution was followed with NMR spectroscopy [6]. Electronic paramagnetic resonance (EPR) experiments of pentaazadiene compounds were performed to establish whether an ionic or radical reaction take place during the UV -photolysis. Using a spin trap, aryl and alkyl radicals have been detected for all model compounds. For photolysis (mercury lamp), the photocleavage mechanisms were postulated. Depending on the solvent polarity, the compound is cleaved either into ionic or radical transient products after an initial isomerization. In acetonitrile and benzene as solvents, radical intermediates were verified by EPR spectroscopy [9].

For the study of initiation ability of the titled compounds and thus their application possibility as photoinitiators of radical polymerization processes, a convenient method of differential scanning photocalorimetry (DPC) was chosen [10, 11]. The DPC method is based on differential scanning calorimetry DSC, making possible a delicate thermal analysis (measurement of heat flow as a function of time). The exothermal character of the polymerization of vinyl monomers allows one to study it by thermal analysis.

Differential scanning photocalorimeter Du Pont 930 with differential calorimeter 912 was used. The apparatus allows heating two samples simultaneously with Indium as a standard. Program selection, monitoring and calculations were fulfilled with computer IBM PC-2 connected with the calorimeter. The apparatus was supplied by UV light source (Hg high-pressure lamp, 200 W), fitted for irradiation the samples which were heated to assigned temperature.

2. Experimental

Compounds of the following general structure were synthesized for investigations of initiation ability of pentaazadienes. They were obtained by the reaction of aromatic diazonium salts and primary amines [6].

For polymerization studies 1,6-hexandioldiacrylate (HDODA) CH_2=CH–COO –$(CH_2)_6$–OOC–CH=CH_2 was used as a monomer, which does not polymerize in such con-

ditions without an initiator. Initiators were dissolved in monomer in the amount of 1 wt. %. Samples of (1.5±0.5) mg weight were set up in standard Du Pont aluminium pans. For equal distribution of the solution layer, the samples were covered with a thin polyethyleneterephthalate film. Pans were fitted in a thermostated head of the calorimeter and the samples were irradiated with integral UV light of 3 mW/cm^2 intensity.

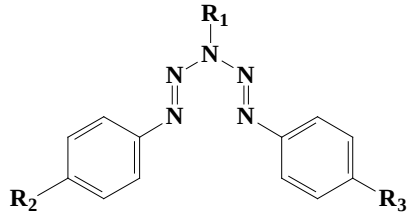

I. R_1 = –CH_3, R_2 = R_3 = –H
II. R_1 = –CH_3, R_2 = R_3 = –OCH_3
III. R_1 = –CH_3, R_2 = R_3 = –NO_2
IV. R_1 = –CH_3, R_2 = R_3 = –COOBu
V. R_1 = –CH_2–CH_2–OH, R_2 = R_3 = –H

According to a selected program, samples were heated to pre-set temperatures, kept at the final temperatures for 1 min isothermally and then were subjected to 15 min irradiation in isothermal conditions. The reaction of polymerization can manifest itself as an exothermal dependence of the heat flow versus time [8].

Dilatometry investigations were carried out in a quartz dilatometer, thermostated at 30 °C. The measurements of volume contraction were conducted with a katetometer. Samples were irradiated with the integral light of a high pressure Hg lamp. The methyl methacrylate (MMA) was chosen as a monomer and its 15% DMF solution was examined. Kinetics curves of polymerization in the presence of 1% (of monomer weight) pentaazadienes of different structures were obtained.

3. Calculations

From the dependences heat flow versus time, the enthalpy of polymerisation (ΔH_{exp}, J/g); induction time (time of 1% monomer conversion); time of achievement of maximum on DPC curve (peak maximum, s) and monomer conversion in this maximum (reacted at THE peak) were obtained. The monomer conversions were calculated according to equations

$$C = \frac{\Delta H_{\text{exp}}}{\Delta H_t}$$

where ΔH_{exp} – experimental enthalpy at the time t (J/g), ΔH_{theor} – theoretical enthalpy (J/g),

$$\Delta H_{\text{theor}} = \frac{f\left(\Delta H_f\right)}{M}$$

where f – the number of double bonds in the molecule (only for similar double bond), ΔH_f – enthalpy of double bond opening (J/mol), M – molecular weight of the monomer. For HDODA $f = 2$, $M = 226$ g/mol, $\Delta H_f = 80.3$ kJ/mol [10], $\Delta H_t = 710$ J/g.

For kinetic calculations we assumed that the reaction rate can be described by differential equation [11]:

$$\frac{d\alpha(t,T)}{dt} = k_{(T)} f(\alpha)$$

where α – fraction of the monomer converted, $k_{(T)}$ is given (according to Sestak and Berggren [11]) by the following differential equation:

$$R_{(T)} = \frac{dC_{(t,T)}}{dt} = k_{(T)} C^m (1-C)^n [-\ln(1-C)]^p$$

where C – conversion of monomer; m, n, p – partial reaction orders for the initiation, propagation and termination stages, respectively. As at the beginning of reaction $p = 0$, the above expression reduces to:

$$R_{(T)} = \frac{dC_{(t,T)}}{dt} = k_{(T)} C^m (1-C)^n$$

The values of $k_{(T)}$ were calculated at the primary step of reaction, in an interval between opening of diaphragm and achievement the maximum on DPC curve. The parameter n was fixed and equal 1.5, and the parameter m was calculated.

The measurements for each of the compounds studied were carried out at several temperatures and then the values of the activation energy of the polymerization process were calculated using the Arrhenius equation.

3. Results and discussion

The results of DPC investigations are shown in Figs. 1–6 and in Tables 1 and 2. From the kinetic curves (Fig. 1) and calculated parameters (Table 1) one can see that in the presence of pentaazadiene compounds (I, II, V) the maxima on DPC curves can be achieved a little later than in the presence of IRG, but the maxima of conversion are higher in the presence of compounds I, II, V. Moreover, as is clear from Fig. 1, the polymerization proceeds further attaining a higher conversion. The initiation ability is higher for the compound II with electron donating OCH_3 substituent in the phenyl ring.

These results are in a good accordance with the degree of photosensitivity and values of the photolysis quantum yields of the data compounds [8].

Table 1. DPC data of HDODA polymerization
in the presence of the compounds investigated at various temperatures

Compound	Temperature /°C	Enthalpy /(J/g)	Peak maximum/s	Induction time/s	Reacted at peak/%
I	24.8	560.6	9.6	5.1	16.0
	38.9	450.8	8.8	3.7	14.8
	49.0	634.1	6.8	2.6	21.1
	59.1	614.0	7.1	2.6	23.8
	69.3	479.9	5.0	2.2	13.9
	79.3	754.2	4.9	2.0	20.5
II	27.2	570.7	6.9	3.4	20.3
	33.8	660.7	5.5	2.2	23.0
	43.9	648.3	5.2	2.0	20.5
	54.0	591.7	4.8	1.9	17.6
	64.1	664.4	4.5	1.8	21.7
	74.2	593.6	4.4	1.7	20.4
V	25.4	470.0	9.6	4.9	16.1
	33.8	482.3	7.9	3.4	15.0
	43.9	616.6	7.5	3.0	18.1
	54.0	564.1	6.9	2.8	19.0
	64.1	529.4	4.9	2.3	10.9
	74.3	606.6	5.3	2.1	19.3
	84.5	660.8	4.9	2.1	15.5
IRGACURE 1700	23.9	420.0	4.6	2.8	15.7
	33.8	489.2	3.4	1.7	15.2
	43.8	522.4	3.4	1.7	17.0
	53.9	584.3	3.7	1.6	21.9
	64.1	570.0	3.6	1.7	15.7

Upon increasing the temperature in the range of 25–75 °C, the polymerization rates increase (Figs. 2, 3). The activation energies determined from these experiments are given in Table 2. As results from the measurements, the activation energies in the experiments with pentaazadienes are lower than those in the experiments with IRG. The dependences of $\ln k_{(T)}$ versus $10^3/RT$ for pentaazadienes (I, II, V) are shown in Figs. 4–6, respectively.

The kinetics of MMA polymerization (Fig. 7) shows that the polymerization rate in the presence of pentaazadienes is only weakly dependent on the electronic structure of substituents in the aromatic rings of the molecules. It was found that with the increasing of pentaazadiene concentration from 0.5% to 4%, the rate of MMA polymerization

decreases to some extent (Fig. 8) and when the concentration of the initiator was 5%, the process did not occur at all.

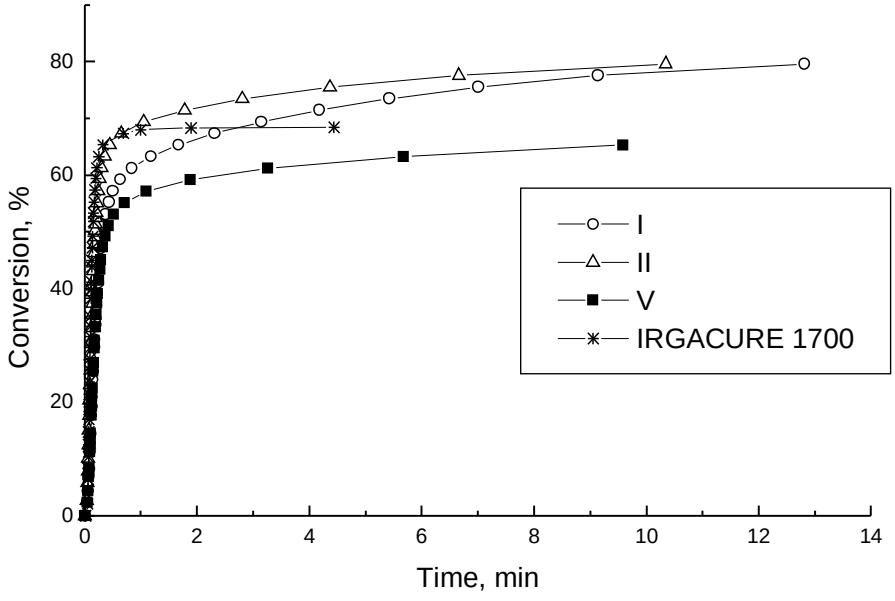

Fig. 1. Kinetic curves of HDODA polymerization in the presence of 1% (of monomer weight) of pentaazadienes and IRGACURE 1700 at room temperature

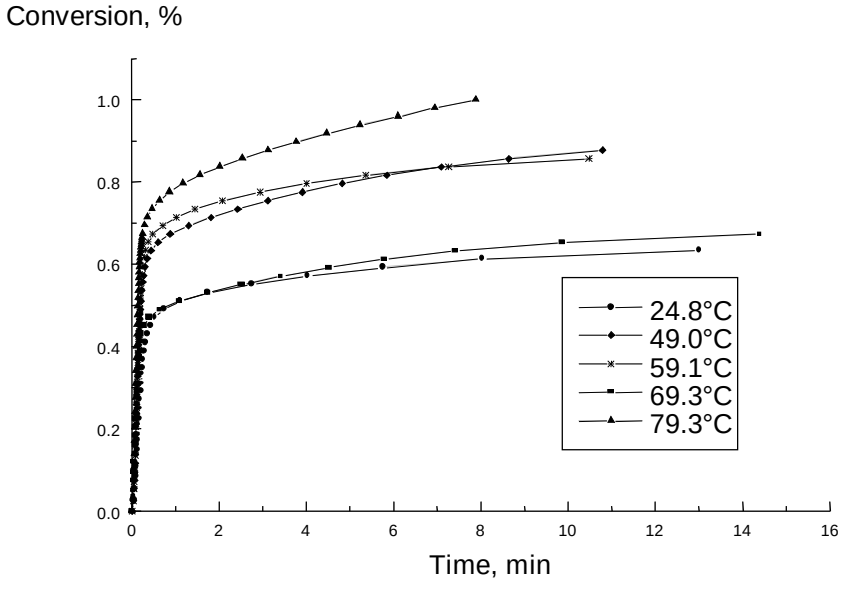

Fig. 2. Kinetic curves of HDODA polymerization in the presence of 1% (of monomer weight) of 1,5-bisphenyl-3-methyl-pentaaza-1,4-diene (I) at several temperatures

Table 2. Activation energy E_a of HDODA polymerization in the presence of pentaaza-1,4-dienes and Irgacure 1700, obtained graphically from dependence of $\ln k_{(T)}$ versus 1/T and calculated from the Arrhenius equation

Compound	E_a, /(kJ/mol)	Coefficient of correlation
I	9.6	0.952
II	5.6	0.999
V	8.5	0.978
IRGACURE 1700	10.1	0.982

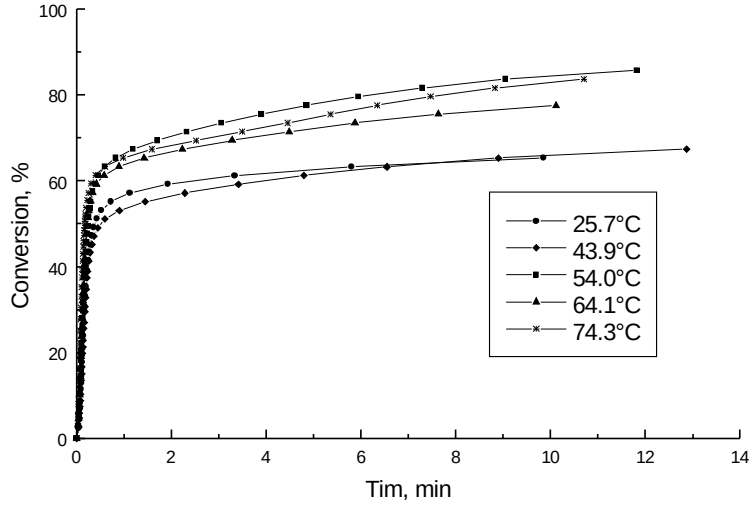

Fig. 3. Kinetic curves of HDODA polymerization in the presence of 1% (of monomer weight) of 1,5-bis(4-methoxyphenyl)-3-methyl-pentaaza-1,4-diene (II) at several temperatures

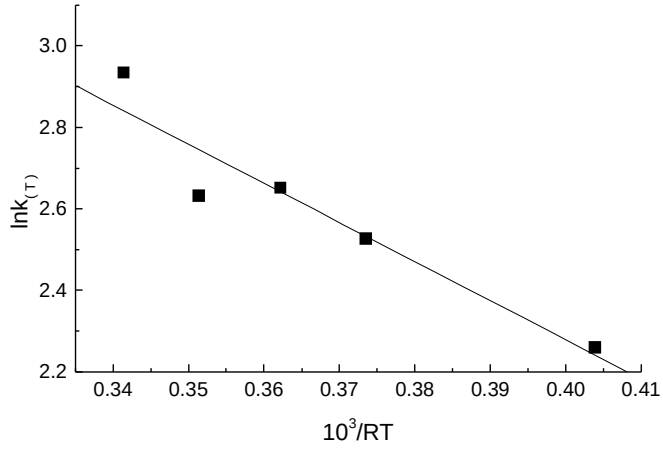

Fig. 4. Dependence of $\ln k_{(T)}$ versus 1/T for HDODA polymerization in the presence of 1% (of monomer weight) of 1,5-bisphenyl-3-methyl-pentaaza-1,4-diene (I)

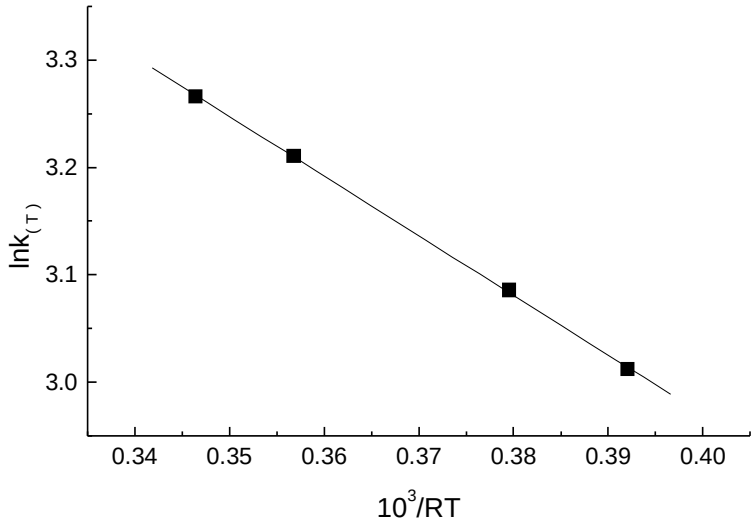

Fig. 5. Dependence of ln$k_{(T)}$ versus 1/T for HDODA polymerization in the presence of 1% (of monomer weight) of 1,5-bis(4-methoxyphenyl) -3-methyl-pentaaza-1,4-diene (II)

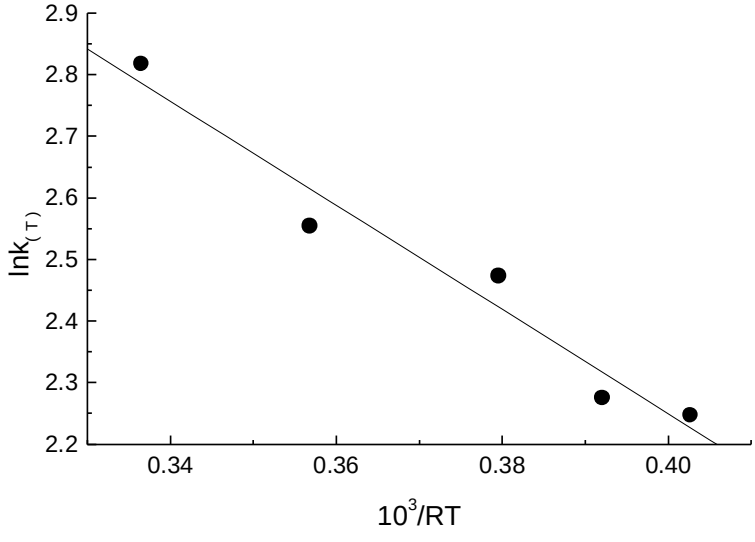

Fig. 6. Dependence of ln$k_{(T)}$ versus 1/T for HDODA polymerization in the presence of 1% (of monomer weight) of 1,5-bisphenyl -3-(2′-oxyethyl)-pentaaza-1,4-diene (V)

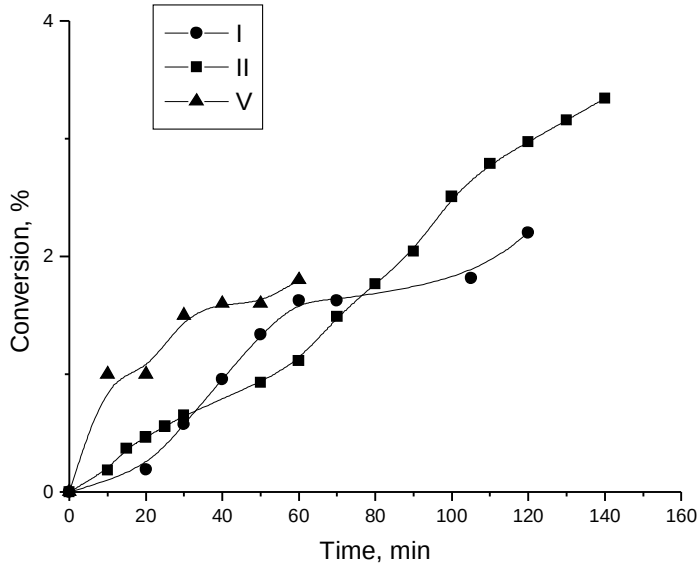

Fig. 7. Kinetic curves of polymerization of 15% MMA solution in DMF in the presence of pentaazadienes

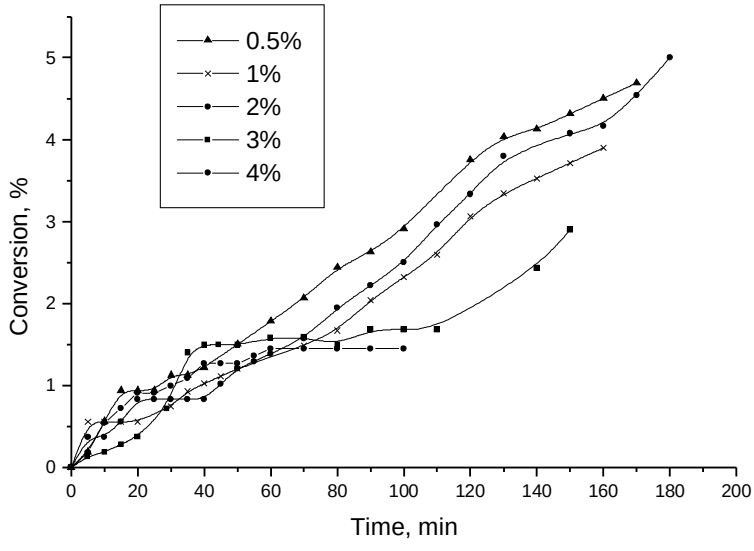

Fig. 8. Kinetic curves of polymerization of 15% MMA solution in DMF in the presence of 1,5-bis(4-methoxyphenyl)-3-methyl-pentaaza-1,4-diene (II). Concentrations of the initiator are given in % of the weight of monomer

As a result of this work, a conclusion can be made that the investigated pentaaza-1,4-diene compounds appear as effective photoinitiators of radical polymerization of vinyl monomers, which can be used in a suitable UV-Vis region (300–450 nm).

References

[1] NUYKEN O., WEIDNER R., Adv. Polym. Sci., 73/74 (1986), 145.
[2] LIPPERT T., STEBANI J., IHLEMANN J., NUYKEN O., WOKAUN A., J. Phys. Chem., 97 (1993), 12296.
[3] CSSR Pat., 169589 (1974), 31.10.1974.
[4] USSR Auth. Cert., 1356800 (1986),.
[5] GRIESS P., Liebigs Ann. Chem., 81 (1894), 137.
[6] BAINDL A., LANG A., NUYKEN O., Macromol. Chem. Phys., 197 (1996), 4155.
[7] BUGAEVA L.N., KONDRATENKO P.A., J. Appl. Spectry, 53 (1990), 873.
[8] BUGAEVA L.N., KONDRATENKO P.A., Fundam. Osnovy. Optich. Pamyati i Sredy, Kiev, 20 (1989), 86.
[9] STASKO A., ERENTOVA K., RAPTA P., NUYKEN O., VOIT B., Magn. Reson. Chem., 36 (1998), 13.
[10] *Radiation curing*, P. Pappas (Ed.), Plenum Press, New York, 1992, 448.
[11] ABADIE M.J.M., Eur. Coatings J., 11 (1991), 788.

Received 7 June 2002
Revised 30 October 2002

Materials Science, Vol. 20, No. 4, 2002

Non-linear optical properties of epoxy-based polymers with covalently attached chromophores and metallic complexes*

A. BORSHCH[1], M. BRODYN[1], V. LYAKHOVETSKY[1], V. VOLKOV[1**], A. KUTSENKO[2], S. MALOLETOV[2]

[1]Institute of Physics NASU, 46, Pr. Nauki, 03028, Kiev, Ukraine

[2]Institute of Physical Chemistry NASU, 31, Pr. Nauki, 03039, Kiev, Ukraine

Non-linearl refraction and absorption in polymer structures based upon diglicidylether of bisphenol A has been studied. The polymers contain organo-metallic complex of nickel(II) $NiL(ClO_4)$ 2- or 4-amino-azobenzene as non-linear optically active side groups covalently attached at each monomer unit. The studies have been carried out by polarization technique together with a real time pump and probe technique, dynamic holography and *Z*-scan. The materials were shown to exhibit fast non-linear response (relaxation time is about 20 ns) together with slow one (relaxation time of the order of tens of hours). This makes it possible to record fast- and long-lived (quasi-stationary) phase holograms. The analysis of possible mechanisms for the polymer refractive index non-linear response in the time range from 10^{-8} to 10^5 is presented. In particular, the role of electron polarizability, thermal excitation of the polymer, orientation of the chromophore molecules, and *trans-cis* isomerization processes are discussed.

Key words: *non-linear refraction; non-linear optical susceptibility; dynamic holography; azobenzene; isomerization*

1. Introduction

Molecular design is a new field in the materials science. This direction of scientific activity based upon practically unlimited opportunities in organic material synthesis has opened wide perspectives for development of new materials for the non-linear optics (NLO) [1]. By the end of XX century, sufficient progress has been made in the field of quadratic optical non-linear materials based on organic polymers [2]. In these materials, NLO active chromophores with large dipole moments have been as a rule covalently

---

*Paper presented at the 4th International Conference on *Electronic Processes in Organic Materi*als, ICEPOM-4, 3–8 June 2002, Lviv, Ukraine.

**Corresponding author, e-mail: volkov@iop.kiev.ua.

attached to polymer chains as side groups. Polymer matrices used for those purposes have to be thermally stable. This property made it possible to freeze the orientation of π-conjugated side groups so that the medium in question could be non-centrosymmetric. Thermally stable polyamide materials turned out to be the most suitable for those purposes. Regarding third order optical non-linear materials, the progress in their syntheses is not essential. Though it is clear that the perspectives of their practical application are very high.

To obtain effective cubic non-linear optical (NLO) polymer systems, it is necessary to use molecules with large effective length of π–π^* conjugation, which guarantee prompt electron excitation transfer over polymer chain and effective electron movement along the macrochains. The highest values of the third order optical non-linearity have been obtained in polymers (polyacetylene, polydiacetylene) with large effective π–π^*-conjugation length [3, 4], especially in the case of molecules with large dipole moments. However, the achieved values of optical non-linearity were too small to be used for the purposes of optical communication, information technology, transient holography and so on. Besides, it is well known that the increase of the π–π^*-conjugation length leads to an increase of absorption which, in turn, may cause overheating and thermal damage of the material under laser excitation. Also one has to take into account that the conjugated polymers are as a rule non-soluble. This limits their performance as well.

To obtain effective organic third order NLO materials we used non-conjugated polymer chain based upon epoxide (diglycidyl ether of bisphenol A) instead of a material with the strong π-conjugation along the polymer chain. To make the material optically and thermally stable and NLO sensitive, the following optically stable chromophores have been covalently attached to the polymer chain as side groups during polymerization:

- weakly conjugated organo-metallic complex of nickel(II) $NiL(ClO_4)_2$;
- photochromes capable of photoinduced isomerisation (*trans-cis* transition).

Polymers based on the monomers are transparent in the visible and IR spectral range as well as optically stable.

2. Third-order NLO response of epoxy polymer with nickel(II) complex, $NiL(ClO_4)_2$

One of the most promising approaches to increase thermal and radiation resistance is the modification of organic systems by organo-metallic or metal-complex compounds [1, 5]. In such a case we can expect that the role of the metal ion will be manifested in several ways: 1) manifestation of intrinsic hyperpolarizability through electronic transitions between molecular orbitals of the metal-containing compound (charge transfer from a metal to a ligand or from a ligand to a metal) and related possibilities of additive

or synergistic effects in the metal-modified organic matrix; 2) strengthening of NLO characteristics of the organic matrix itself as a result of the polarizing donor-acceptor and/or electrostatic influence of the metal ion; 3) heat and light stabilization of polymers by the metal ion through deactivation of the triplet states of the macromolecules themselves and also singlet oxygen present in the polymers.

For the studies we have synthesized a new material consisting of a linear polymer based on an organic α-oxide with a covalently attached amine complex of nickel(II), $NiL(ClO_4)_2$. This particular compound was selected for the following reasons: 1) it contains a primary amino group that is sterically accessible and reactive in relation to the monomer, and this amino group can be incorporated into the polymer chain; 2) the macrocyclic complexes have high thermodynamic stability so that dissociation of the metal ion in the process of thermal polymerization and or under intense laser radiation can be avoided.

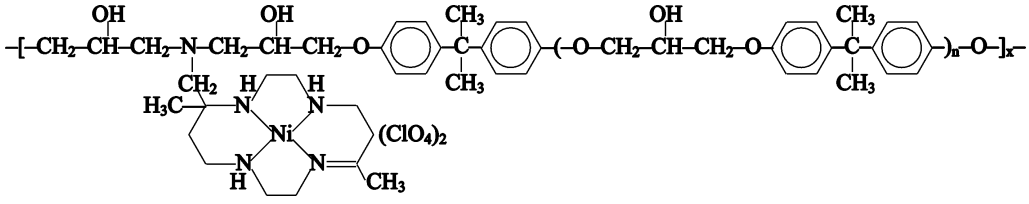

Fig. 1. Molecular structure of a linear polymer with metallocomplex of Ni(II) covalently attached at each unit of diglycidyl ether of bisphenol A, n = 0; 1; 2

The nickel(II) complex (Fig. 1) was synthesized and purified by procedures described in [6]. The complex was characterized by elemental analysis and by IR and electronic spectroscopy. As the epoxide monomer we used the diglycidyl ether of bisphenol A, which contained approximately 21% of epoxy groups. The metallopolymer was obtained by thermally initiated polymerization of a mixture of the epoxide monomer and the nickel complex in a ratio 3:1, with the reaction time of 7 h at 120 °C.

A comparison of IR spectra of the original α-oxide and the final polymer demonstrates that the polymerization is accompanied by spectral changes that are typical of epoxide systems, i.e., a decrease of intensity of the 917 cm^{-1} band corresponding to asymmetric stretching vibrations of the epoxide ring [7, 8]. Grafting of the nickel(II) complex, with the formation of a covalent bond, is evidenced by the fact that the spectrum of the polymer does not contain any bands of stretching vibrations of primary amino groups (ν = 3174 cm^{-1}). Moreover, in the IR spectrum of the polymeric material, in comparison with that of the monomer, we observe a redistribution of intensities for the series of absorption bands in the 1000–1200 cm^{-1} region, possibly related to the appearance of intense bands of stretching vibrations of perchlorate ions in this region.

In Figure 2, we show electronic absorption spectra of acetone solutions of the original nickel complex (curve 2) and the synthesized polymer material (curve 1). The

vertical line corresponds to the light wavelength λ = 532 nm used to investigate NLO properties of the material.

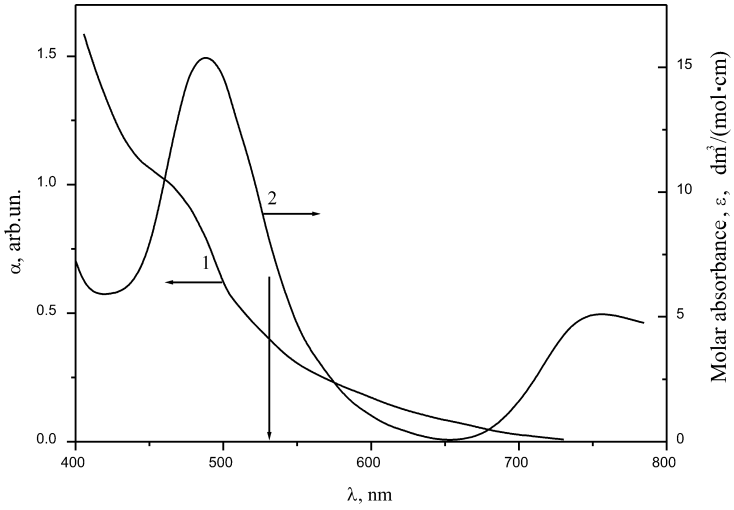

Fig. 2. Electronic absorption spectra: 1) acetone solution of the synthesized NLO polymeric material; 2) acetone solution of nickel(II) complex $NiL(ClO_4)_2$. The vertical arrow indicates the position of the Nd^{3+}:YAG second harmonic wavelength 532 nm

The spectrum of the $NiL(ClO_4)_2$ complex solution has a form that is typical of a six-coordinated nickel(II) ion [9] indicating that the primary amino group interacts with the metal ion. At the same time, in the spectrum of the polymer, against a background of organic matrix intense absorption (apparently produced by superposition of several bands of different types), we observe a shoulder at approximately 460 nm. Since this is the exact region in which we should observe a relatively intense band of the d–d transition of a square-planar complex of nickel(II) [9], such a feature of the spectrum can be regarded as indirect evidence of covalent insertion of the complex into the polymer matrix. As a consequence of the polymer formation, which proceeds through alkylation of the primary amino group, decoordination of the amino group should take place with a transition of nickel(II) from a six- to four-coordinated state.

For our study of the NLO properties of the synthesized polymer material, we prepared samples in the form of a polymer layer with a thickness of 100 μm between two glass plates. As the characteristic feature to be studied, we selected the non-linearity of refraction, which is the most promising NLO phenomenon from the standpoint of practical application in devices for controlling the parameters of laser radiation, and which is described by the tensor of third-order optical non-linear susceptibility $\chi^{(3)}_{\omega}(\omega, \omega, -\omega, \omega)$ [1].

The non-linear refraction of the medium in question have been studied by dynamic gratings recording using a scheme of the degenerate two-wave mixing. As a source of

radiation we used a pulsed single mode frequency doubled YAG:Nd^{3+} laser (τ = 10 ns, λ = 532 nm, TEM_{00}).

In the course of the investigation, we measured an exposure characteristic of the samples, i.e., the dependence of the first-order diffraction pulse energy on the recording pulse energy. The experimental dependence shown in Fig. 3 is well described by the cubic equation $E_1 = aE_0^3$. This indicates that the phase dynamic gratings were recorded on the third-order optical non-linearity. The relaxation time of the non-linearity was estimated to be < 2 s. The positive sign of the non-linear refractive index was determined by the *Z*-scan method.

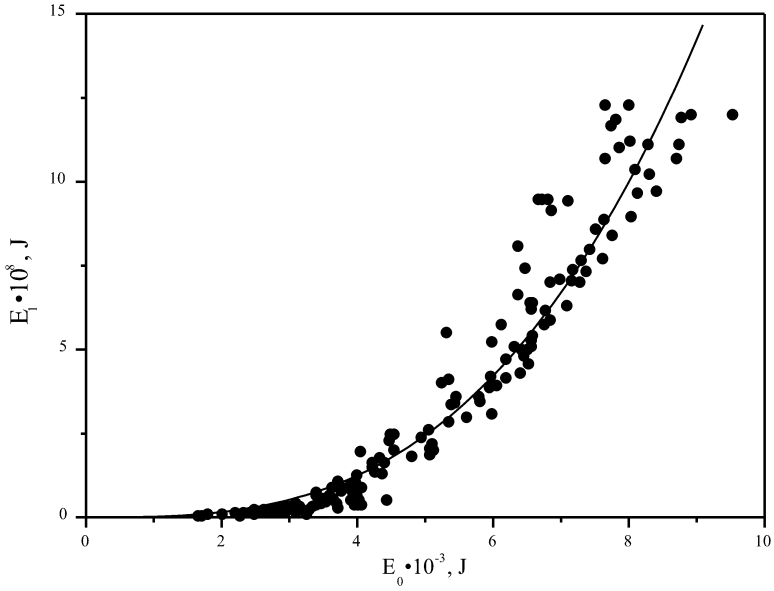

Fig. 3. First-order diffraction energy E_1 as a function of recording energy E_0

The value of $\chi_{\omega}^{(3)}$ was estimated using data obtained from the measurements of the diffraction efficiency by means of the following relationship [10]:

$$\left|\chi_{\omega}^{(3)}\right| = 3\left(\frac{n_0}{4\pi}\right)^2 \lambda \frac{\sqrt{\eta}}{\pi l I_0} \tag{1}$$

where n_0 = 1.67 is the refractive index of the sample; l = 100 μm is the thickness of the polymer layer; η = $1.25 \cdot 10^{-4}$ is the diffraction efficiency; λ = 532 nm and I_0 = 5 MW/cm^2 are the wavelength and the intensity of the recording radiation. The value of $\chi_{\omega}^{(3)}$ was found to be $(2.6 \pm 1.3) \cdot 10^{-10}$ esu.

It is known that with an increase of the intensity of irradiation (I > 1 GW/cm^2) of organic systems with conjugated bonds, the diffraction efficiency is gradually decreased

as a result of damage of the conjugation system. Many tests on our material have shown that there is no such a decrease. However, with an irradiation power greater than 7 GW/cm^2, we observed a sharp disappearance of self-diffraction of the recording beams as a result of the polymer damage. Because of such a behavior the potential practical applications of the polymer material in question are restricted to a range of laser radiation power up to 7 GW/cm^2.

3. Third-order NLO response of epoxy polymer with chromophores*

For the synthesis of non-linear polymer with chromophores we used the epoxy monomer (diglycidylether of bisphenol A), which contained about 21% of epoxy groups. For the thermal polymerization of the monomer we used chromophore-4 -aminoazobenzene (AA). The amino group of every AA molecule combined two epoxy groups so that aminoazobenzene was covalently attached to the polymer chain. The information about the polymerization process and the structure of the resulting polymer can be obtained from the analysis of the changes in IR spectra [7, 12]. Actually, the polymerization leads to a rise of new OH groups in macromolecules and to an increase of the hydrogen bond amount. The presence of a large number of OH groups in macromolecules may lead to additional transverse bonds between polymer chains resulting in formation of a three-dimensional structure involving hydrogen bonds [7, 12]. The polymer obtained by us remained linear because it was soluble in polar solvents. When the polymer is heated over T_g, the hydrogen bonds break and the polymer turns into liquid state.

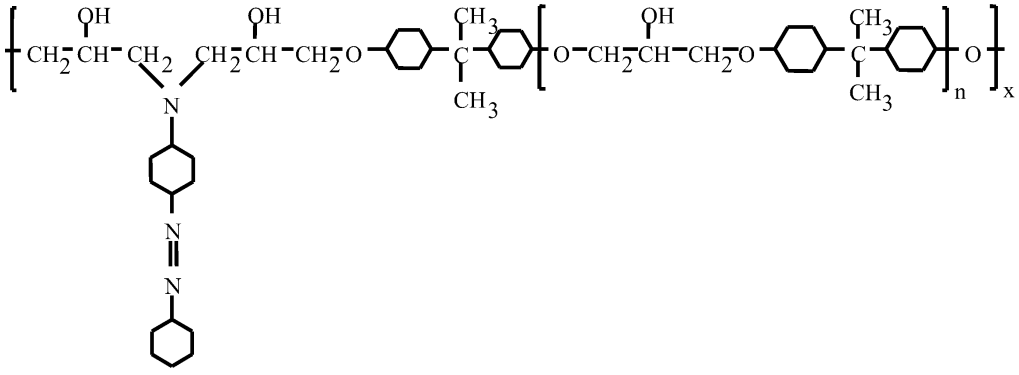

Fig. 4. Molecular structure of a linear polymer with 4-aminoazobenzene chromophore (AA), n = 0; 1; 2

The molecular structure of the synthesized linear polymer is shown in Fig. 4. The AA molecule can be viewed as a side group with respect to the polymer chain. In such a

* Data presented in the chapter are mainly based on previously published results [11].

configuration, the azobenzene is capable of *trans-cis* isomerization upon light excitation. The absorption spectrum of the polymer in the visible spectrum range is shown in Fig. 5. The strong long-wave absorption band of the *trans* isomer of azobenzene (430–460 nm) is associated with the $n \rightarrow \pi^*$ transitions [13, 14], while a weak $\pi \rightarrow \pi^*$ absorption band is shifted towards short-wave spectral range and for the *trans* isomer of AA it is positioned at about 300 nm [15]. In Figure 5, the band $\pi \rightarrow \pi^*$ is not seen since it coincides with the absorption band of the sample glass substrate.

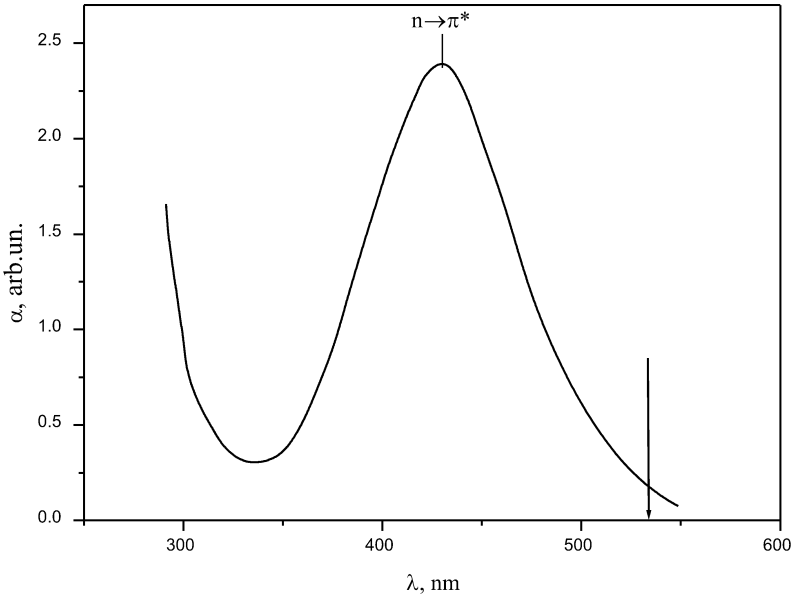

Fig. 5. Absorption spectrum of the structure shown in Fig. 4 in the visible spectrum range for AA (4-aminoazobenzene). The vertical line indicates the position of the Nd^{3+}:YAG second harmonic wavelength 532 nm

It is known that the *trans-cis* isomerization takes place for the excitation of both $n \rightarrow \pi^*$ and $\pi \rightarrow \pi^*$ transitions. However, the excitation of $n \rightarrow \pi^*$ transition is more preferable because the quantum yield of the isomerization in this case is two times higher [16]. The vertical line in Fig. 5 indicates the position of the wavelength 532 nm used for the sample excitation. It is seen that it coincides with the long-wavelength side of the absorption band so that the excitation of the $n \rightarrow \pi^*$ transition of AA is not resonant.

The samples studied were in the form of a thin polymer layers with the thickness of 140 μm placed between two glass plates. Two AA samples with the glass transition temperature T_g = 100 °C and T_g = 35 °C were prepared by thermal initialization.

The non-linear refraction was studied in the samples in question by means of recording transient phase gratings in the scheme of the degenerate two-wave mixing. The experimental set-up is shown in Fig. 6. A frequency doubled single-mode Nd^{3+}:YAG laser (λ = 532 nm) was used as a source of radiation. The laser delivered light pulses

with the energy of 3 mJ and the pulse length of 10 ns. The laser pulse energy was changed by means of a polarizer attenuator A (a $\lambda/2$-plate together with a polarizer) and measured by a photodiode.

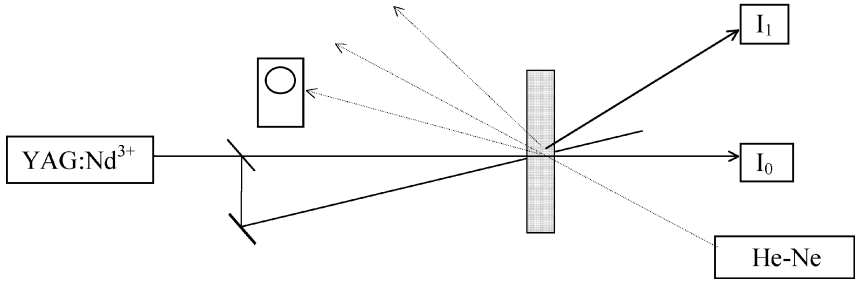

Fig. 6. Experimental set-up. Dynamic grating recording. YAG:Nd^{3+} – frequency-doubled single-mode pulsed laser (τ = 10 ns, λ = 532 nm, TEM_{00}). He-Ne – cw laser for reading out the recorded dynamic gratings

The laser beam was split into two beams of equal intensity. The beams intersect each other at an angle of $2\theta = 3°$. Our sample was placed where the beams were totally overlapped. The sample was excited by the interference pattern of the two beams so that a refractive index transient grating causing self-diffraction of the writing beams was induced in the sample. The first diffraction order pulse energy was measured by a photodiode. For our samples with AA molecules covalently attached to the polymer chain the self-diffraction pattern contains up to eight diffraction orders at recording energy of 0.4 mJ. In this case, the diffraction efficiency, $\eta = I_1/I_0$, (where I_0 is the recording beam intensity, I_1 is the first diffraction order beam intensity) of 20% can be achieved.

The exposition characteristic of the transient grating recorded in the sample with the glass transition temperature T_g = 100 °C is presented in Fig. 7. Actually it is the dependence of the first diffraction order intensity upon the recording one. The dependence is described by the cubic equation of a type $I_1 \sim a I_0^3$ fairly well. One can conclude that the transient gratings are recorded incorporating the non-linearity of the third order in the electric field, which is described by the non-linear susceptibility $\chi_\omega^{(3)}(\omega, \omega, -\omega, \omega)$. The value of $\chi_\omega^{(3)}$ can be estimated using the measured value of the diffraction efficiency and Eq. (1). For the following experimental data: η = 10%, E_0 = 0.3 mJ, l = 140 μm, n_0 (0.53) = 1.8, [17] the laser beam diameter d = 2 mm and the laser pulse duration τ = 10 ns the value of $\chi_\omega^{(3)}$ was shown to be of $(4.7–2.4)\cdot10^{-8}$ esu.

By means of *Z*-scan method we have found that the non-linear changes of the refractive index in our samples are negative that is the refractive index decreased in the field of the laser light.

To understand the mechanism of the medium non-linear response, it is important to determine the response time of the system that is the time of the refractive index

changes. The kinetics of the refractive index non-linear variation was measured by means of pulsed recording (λ = 532 nm) and cw reading out the dynamic grating. A cw He-Ne laser (λ = 633 nm) was used for the grating reading out.

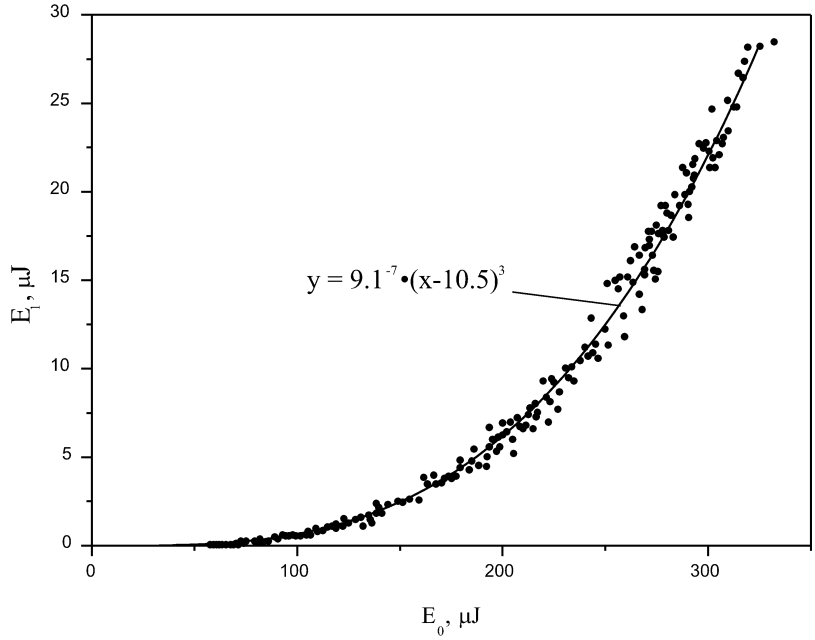

Fig. 7. The first order diffraction pulse energy versus writing pulse energy. Polymerized state. Experimental data (dots) and the solid line which presents an approximation by the equation shown in the figure

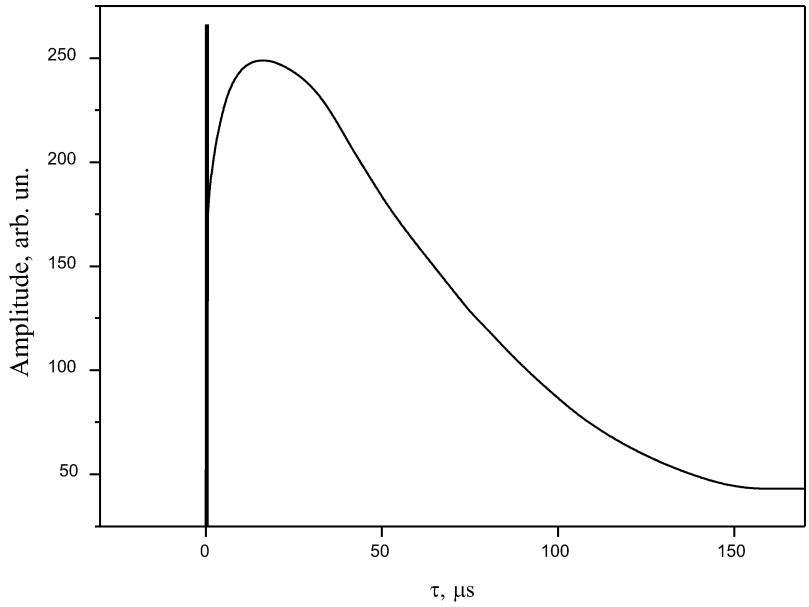

Fig. 8. Fast relaxation of the dynamic grating. Oscilloscope trace of a light pulse diffracted into the first order at reading out the grating by cw laser beam (He-Ne laser, λ = 0.63 μm)

The oscilloscope trace of the signal is shown in Fig. 8. Both grating writing and erasing occur with two different times: one in ns-, the other – in μs time scale. The μs component maximum is reached when the recording pulse is already absent. So that the measured $\chi_{\omega}^{(3)}$ value corresponds to ns component. Therefore it can be concluded that two different mechanisms participate in a fast non-linear process. It should also be mentioned that the samples with T_g = 100 °C and T_g = 35 °C have the same value of the diffraction efficiency in the μs time region.

Except the fast non-linear mechanism which is observed over a wide range of the writing intensities, a slow non-linearity with the characteristic relaxation time about 24 h appears starting from the recording intensity I = 300 kW/cm^2 (see Fig. 9). The slow grating mechanism has the maximum diffraction efficiency of about 15%. The self-diffraction pattern contains up to ten diffraction orders in this case. Thus the non-linear refractive index relaxation time range for the polymer with AA is from 10^{-8} to 10^5 s.

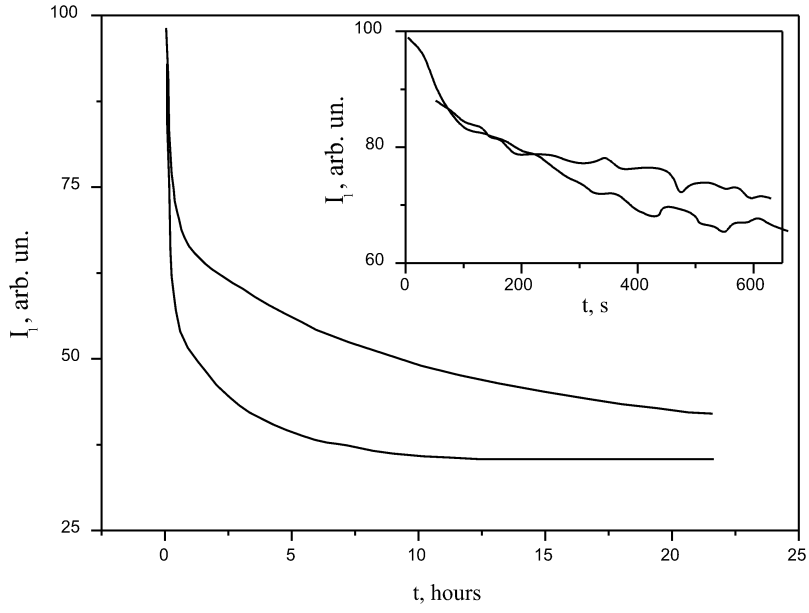

Fig. 9. Slow relaxation of the dynamic grating recorded by a single pulse taken as in Fig. 8. The insert shows in more detail the beginning of the dependence

The same experimental scheme was used for the studying the kinetics of the grating relaxation in this case. The grating was written by a single laser pulse with the intensity I = 0.8 MW/cm^2 and λ = 0.53 μm. Then it was read by cw He-Ne laser. The data on the diffraction efficiency were being taken every 10 s. The results are shown in Fig. 9. The insert shows the beginning of the dependence in more detail. Curve 1 has been obtained for the sample with T_g = 100 °C, curve 2 – for the sample with T_g = 35 °C. From the figure one can see that both curves are coincided in the time region from 0 to 200 s. Then the curves show sufficiently different character of relaxation. It is clear from the curves that the decreasing the T_g value of the polymer material leads to the faster decreasing of the diffraction efficiency of the long lived grating.

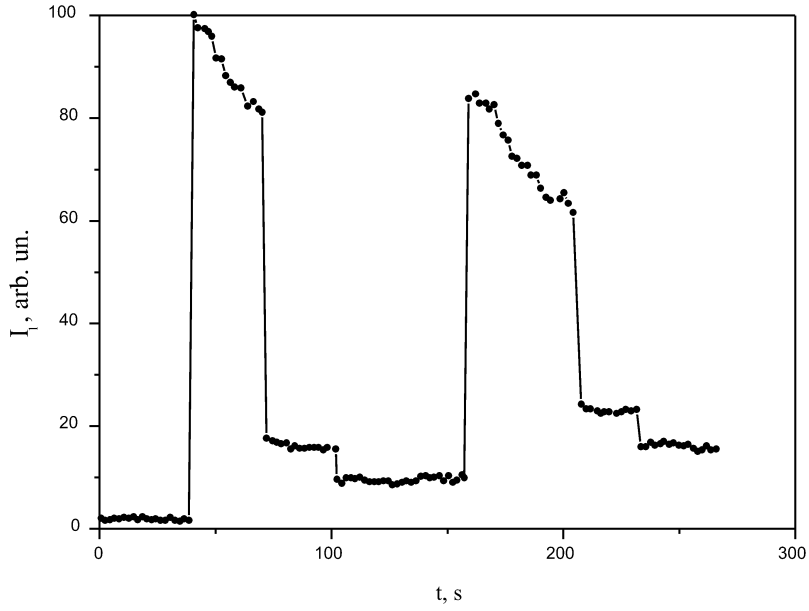

Fig. 10. Reversible writing and erasing a quasi-stationary grating

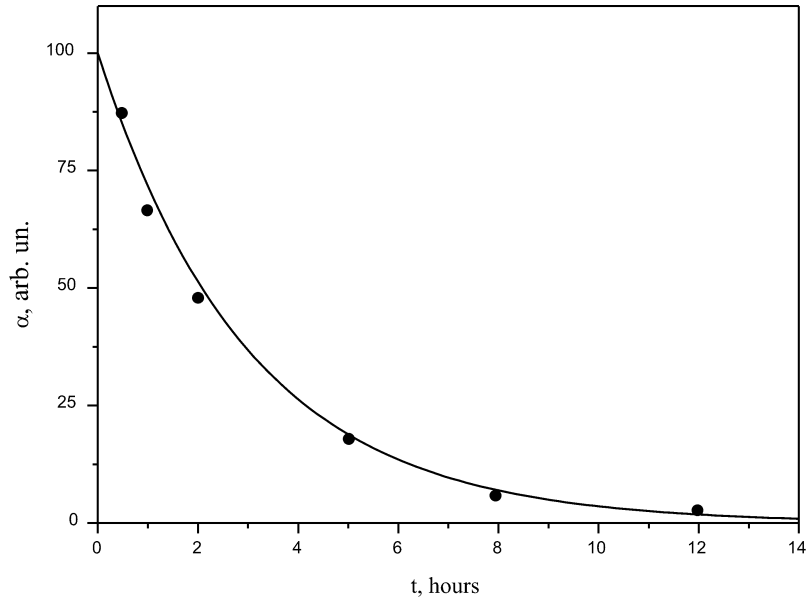

Fig. 11. *Cis* → *trans* relaxation curve for the T_g = 100 °C obtained by means of UV spectrometry

Writing the dynamic gratings with the relaxation time higher than 10 h makes it possible to use the polymer in question as a memory medium for information storage. We have carried out studies on the possibility of reversible writing of the phase gratings

in a polymer with 4-aminoazobenzene (T_g = 100 °C). We have chosen the sample because its damage threshold intensity is much higher than that of the sample with T_g = 35 °C. The dynamic grating has been written by a single laser pulse (λ = 0.53 μm) with the intensity I = 0.8 MW/cm^2. Then the grating was erased by one of the writing beams with the intensity I = 2 MW/cm^2. The writing and erasing cycles were then repeated several times. The reading out the recorded grating was carried out by the cw radiation of a He-Ne laser. Results of the studies are shown in Fig. 11. The results vividly manifest that the polymer with AA can be used as a recording medium for holographic reversible writing and storage of information.

4. Analysis of non-linearity mechanisms of epoxy polymers with chromophores

The phase dynamic diffraction gratings are usually the result of periodic modulation of the refractive index caused by contribution of population of electronic or vibration states (phonons) or medium density modulation caused by heat or electrostriction. However in the case of polymer optical non-linear materials isomerization and reorientation of azo dye molecules make sufficient contribution into the writing and erasing the dynamic gratings. Therefore in this chapter we dwell upon these non-linear mechanisms.

4.1. Isomerization

The long-wave shift of the absorption band accompanied by the absorption increase was observed during the dynamic grating recording in our samples. The complete restoration of the initial spectrum took about 11 h. The kinetics of the absorption spectrum restoration is shown in Fig. 11. These variations of the absorption spectrum are caused by the *trans-cis* isomerization of the aromatic azo compounds (AA) induced by rotation of one part of the AA molecule around the double bond N=N [15, 18–20].

Trans and *cis* forms of the azobenzene molecules are shown in Fig. 12a. Among possible mechanisms of the isomerization associated with the N=N and C=N bonds, it is necessary to distinguish a rotational mechanism that is rotation around X=Y bond and an inversion mechanism as the movement of a part of a molecule in plane without rotation as for instance in azo compounds with AA [15, 20].

The scheme of the inversion mechanism is shown in Fig. 12b [15]. The linear configuration along X=Y–a bond corresponds to a transition state. The inversion isomerization is possible only in the case when one of the atoms forming double bond possesses not only a substituent but also not shared electron pair or unpaired electron. For the azo compounds with AA such as unsubstituted azobenzene, the inversion mechanism takes place for both the *trans-cis* photoisomerization and the thermal *cis*

-trans isomerization [15, 20]. Figure 12c shows simplified energy diagram where the route of the thermal *cis-trans* isomerization is shown separately (γ).

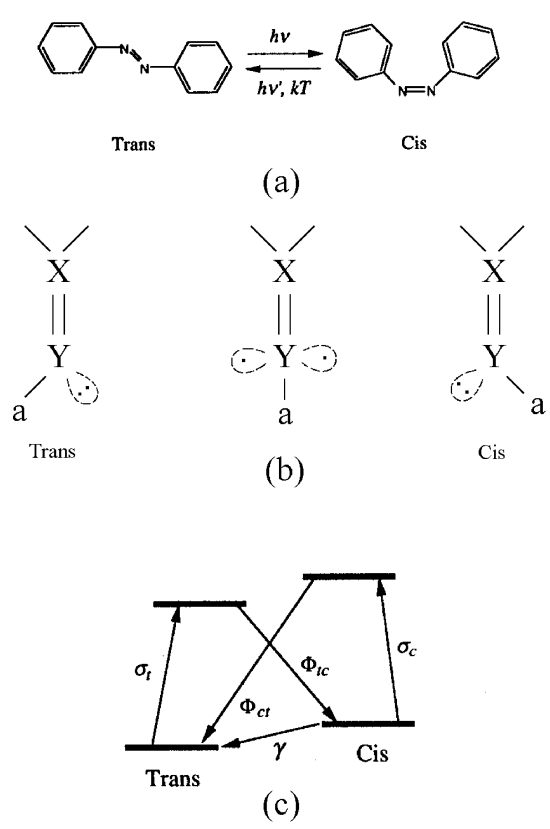

Fig. 12. Isomerization of AA (4-aminoazobenene): (a) azobenzene molecule change under the *trans-cis* isomerization, (b) the inversion isomerization mechanism scheme, (c) a simplified model of the molecular states. σ_t and σ_s are the cross sections for absorption of the one photon by a molecule in the *trans* and *cis* forms, respectively; γ is the thermal relaxation rate; and Φ_{ct} and Φ_{tc} are the quantum yields of photoisomerization

Such an isomerization can be viewed as a possible way of non-radiative relaxation of the molecular excitation [15, 18, 20]. That is why the fluorescence is not observed in many *trans* and *cis* isomers of azo compounds. The luminescence is not observed in our samples under laser excitation. The response time of the *trans-cis* photoisomerization of the azo compounds in solvents with different viscosity is from 10 to 100 ps [21]. Any triplet or other short-lived states in *trans-cis* transitions of the azobenzene have not been found by means of picosecond photolysis although the triplet nature of the isomerization is assumed [15, 20]. By means of the measurements of time-resolved absorption spectra it was shown [22] that in azo compounds dissolved in liquid crystals, the *trans-cis* tran-

sition time is about 10 ns under pulsed excitation (τ_p = 10 ns) at the wavelength of 355 nm. So the *trans-cis* isomerization is a fast process the response time of which could be comparable with the laser pulse duration (20 ns in our experiments).

It is known that the *cis-trans* thermoisomerization time is dependent upon the medium used as a solvent for chromophore molecules and may be of the order of minutes or even hours for the azobenzene without luminescence [15, 19]. The kinetics of the absorption spectrum restoration (reflects the *cis-trans* transition) measured in our samples after the pulsed laser excitation is fairly well approximated by the exponential relation of the form $y = y_0 e^{(-t/\tau)}$ (where time constant τ = 3 h) in the time range from several minutes to 12 h when the spectrum is restored completely (see Fig. 11). Such a long transition time could be connected with the thermally activated rotational mobility of side or end polymer chain branches (β-relaxation at a temperature lower than T_g) [15, 23, 24].

4.2. Orientation

It is known [25–27] that the light polarized linearly orients azobenzene molecules in the plane perpendicular to the plane of oscillation of the electric field light wave. The orientation of the azobenzene molecules can be established during a very short time period. Thus, it was shown [28] that the azobenzene molecules in the polymer are oriented during 1 ps under excitation by the linearly polarized light pulse with the duration of 100 fs.

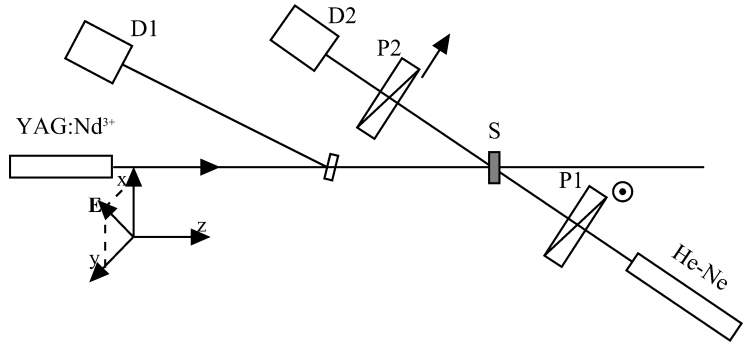

Fig. 13. Experimental set-up. Studies of the effect of induced birefringence due to azo dye molecules orientation in the field of linearly polarized YAG:Nd^{3+} laser light. P1, P2 – crossed polarizes, S – sample, D1, D2 – photodiodes

The contribution of the molecular reorientation into non-linear refraction of the polymers with 4-aminoazobenzene has been studied by means of the measuring the induced anisotropy. The experimental set-up is shown in Fig. 13. A frequency doubled

single-mode pulsed Nd^{3+}:YAG laser (λ = 532 nm, τ_p = 10 ns, E_p = 0.3 μJ, TEM_{00}) was used as a source of radiation. The linearly polarized laser beam with the Gauss intensity profile was directed at the sample. The plane of the electric field oscillation is oriented at 45° to the vertical plane. The pulse energy was measured by a photodiode D_1. cw radiation of a He-Ne laser with a vertical polarization was directed at the sample at a small angle towards the pump beam. The He-Ne beam passed through two crossed polarizers and the pumped area of the sample placed between the polarizers. Initially our samples were isotropic so that the system "crossed polarizers–sample" was not transparent for the He-Ne radiation. However, in the case when the polarized pulsed radiation induced birefringence in the sample as a result of chromophore molecule orientation, the radiation of the Ne-He laser appeared at the output of the crossed polarizers. The radiation passed through the system "crossed polarizers–sample" is monitored by a photodetector D_2. The system makes it possible to study the dynamics of anisotropy induced in the sample in the time range from microseconds to hours.

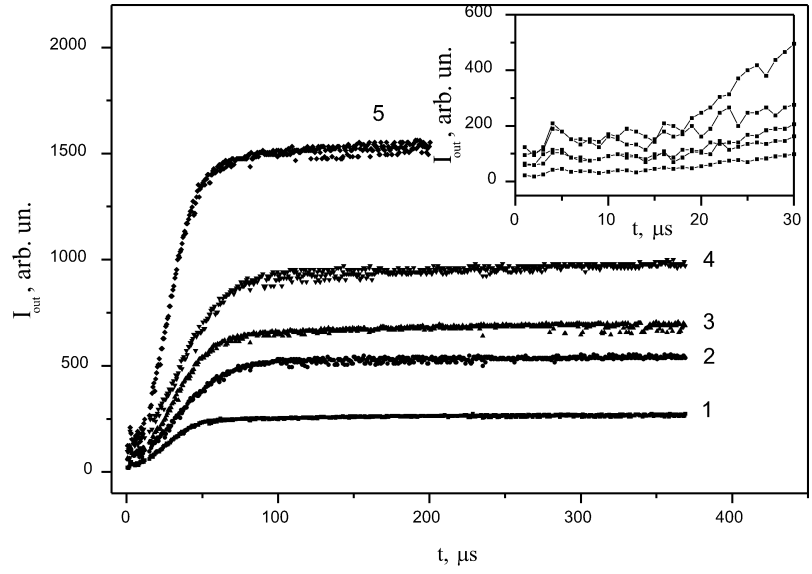

Fig. 14. Time dependence of induced anisotropy onset (He-Ne laser radiation amplitude at the output of the system "crossed polarizers-sample") for different pump pulse energy: 1 – 340 μJ; 2 – 560 μJ; 3 – 680 μJ; 4 – 1080 μJ; 5 – 1500 μJ

Figure 14 shows dependencies of the amplitude of the He-Ne laser radiation passed through the system versus time in the range from 0 to 400 μs for different values of the energy of the pump pulse. Each curve is a response of the sample at the single pulse action. The insert shows the beginning of the dependencies in detail. It is seen from the figure that the anisotropy appeares in spurts (see insert) under pulsed excitation and then after the pump pulse end the anisotropy continues to grow on during 50–70 μs until saturation. The level of the saturation linearly depends upon pump pulse energy.

The relaxation of the induced anisotropy is shown in Fig. 15. It was found that induced anisotropy relaxation has two time components: a fast one, τ_1 ~5–10 s and a slow one, τ_2 of the order of hours. It should be noted that the anisotropy does not decay completely. Some part of it remains for a long time. It could be removed by heating the sample above the glass transition temperature T_g.

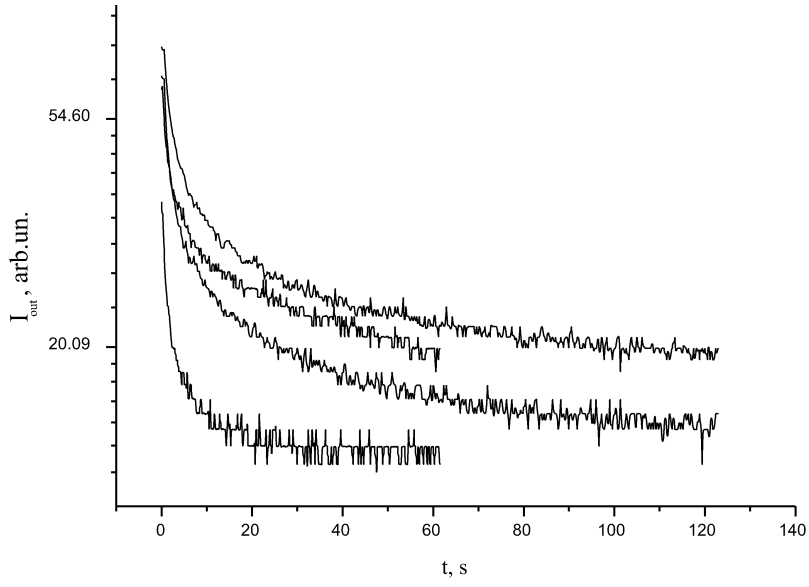

Fig. 15. Time dependence of the induced anisotropy decay (He-Ne laser radiation amplitude at the output of the system "crossed polarizers-sample") for different pump pulse energy: 1 – 340 μJ; 2 – 560 μJ; 3 – 680 μJ; 4 – 1080 μJ

Photochromic, anisotropic molecules of azo dyes are characterized by double bond –N=N– between two phenyl rings and have a rod-like shape. Delocalization of π-electrons along the principal axis of the molecule leads to a strong anisotropy of polarisability and absorption dichroism ($\alpha_{II} >> \alpha_{\perp}$). The dipole transition moment is oriented along the long axis of the molecule. Initially, all chomophore molecules are oriented randomly in the polymer so that the sample is isotropic. Linearly polarized light excites molecules selectively with the probability dependent on $\cos^2\theta$ where θ is the angle between the molecule axis and the electric field vector **E**. As the result of such a selective excitation some number of *trans* molecules transform into long-lived *cis* form. It leads to an anisotropic decrease of a number of *trans* molecules in some angle close to the light polarization plane. This effect is called "angular hole burning" [27]. It also could be viewed as a latent reorientation. *Trans-cis* isomerization of azo molecules takes place through excitation levels with very short lifetimes so that it takes 10 to 100 ps [21].

Earlier we have observed *trans-cis* isomerization in the samples in question under pulsed excitation (τ_p = 10 ps). Therefore the observed fast onset of the anisotropy (see insert in Fig. 14) could be attributed to angular hole burning in the angular distribution of the *trans* azo molecules.

Not all molecules are transformed into *cis* form due to steric hindrance [29] that is some molecules have not enough free volume for the transition into *cis* form. In this case the excitation energy transforms into heat. However, if the excitation energy is increased, the number of isomerized *trans* molecules may be increased due to additional molecules, which could overcome steric potential barriers. This effect is observed in the experiment. The level of the fast anisotropy onset is increased with the pulse energy (see insert in Fig. 14).

As we have already mentioned, in the field of the linearly polarized light azo molecules trend to reorient in a position perpendicular to the polarization plane of the light wave as a result of multiple acts of absorption-deactivation. This effect is called angular redistribution of azo molecules and contrary to latent orientation is direct reorientation that also gives its contribution to the induced anisotropy. As it was pointed out above, some molecules cannot transform into *cis* form due to conformational limiting. In that case absorbed energy is transformed into heat. Thermal oscillations of the surrounding of the azo molecule increase the rotational mobility of the azo molecules in the steric potential of the surrounding [29]. This effect causes direct reorientation of the molecule during laser pulse (10 ns) and dark reorientation of the molecules after laser pulse end. It is seen from the Fig. 14 that the process of the dark reorientation takes about 50–70 μs. The nature of such a strong reorientation is not clear at the moment. It needs to be studied additionally. It could be however supposed that azo dye molecules covalently attached to the polymer chains which occupy new position as a result of reorientation pull the polymer chain and cause reorientation of some its fragments [30]. Such a movement of the medium mass is an inertial process and it could not occur during short laser pulse because the conformational mobility of the matrix is much smaller than that of azo dye molecules.

Relaxation curves of the induced anisotropy decay are presented in Fig. 15. One can see that the relaxation has two characteristic times. Some part of induced anisotropy decays during 5–10 s and could be connected with the thermal diffusion of some oriented molecules. More slow decay (relaxation time about hours) is supposed to be connected with *cis-trans* isomerization that is the decay of the latent orientation. Such a relaxation time is in agreement with the *cis-trans* relaxation [11] (see Fig. 11).

Now we can distinguish different contributions into the non-linear refraction in the samples under study incorporated in dynamic grating recording [11]. Figure 16 shows the diffraction pulse of He-Ne laser radiation (curve 1) at dynamic grating recorded in the samples by two beams of a frequency doubled neodymium laser. Curve 2 obtained at the same pump pulse energy shows a contribution due to induced anisotropy. Curve 3 is a result of subtracting of curve 2 from curve 1. The curve manifests the contribution

relaxing during 30 μs. This contribution could be attributed to the thermal effect. Actually this time is a time of erasing the thermal dynamic grating due to thermal diffusion. Taking into account that the period of the recorded grating Λ is equal to 6.5 μm, it is possible to calculate the coefficient of the thermal diffusion in the material under study:

$$D_T = \frac{\Lambda^2}{4\pi^2\tau} = 3 \cdot 10^{-7} \text{ m}^2/\text{s} \qquad (2)$$

Here τ = 30 μs is the thermal grating relaxation time deduced from curve 3 in Fig. 16.

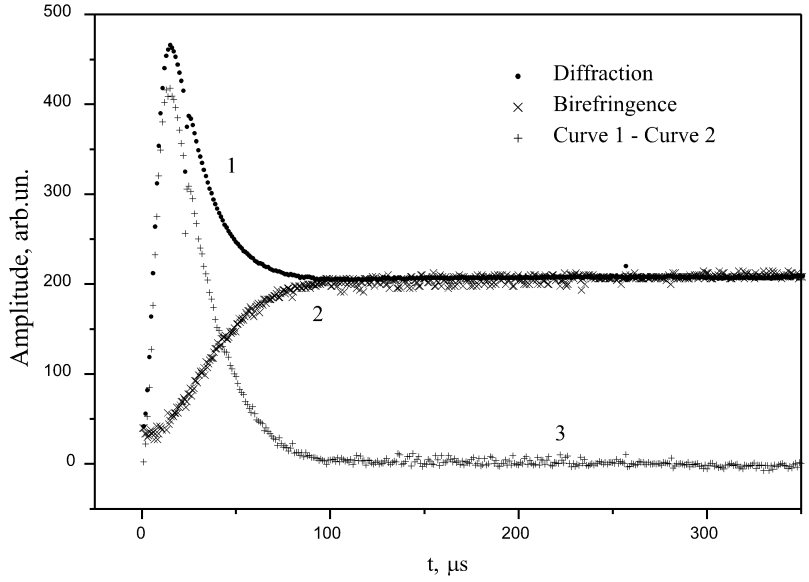

Fig. 16. He-Ne laser radiation diffraction at dynamic grating recorded in the sample by the frequency doubled neodymium laser pulse (1); anisotropy contribution (2); thermal grating contribution (as a result of subtracting curve 2 from curve 1) (3)

Conclusions

We have shown the possibility of creating new, effective, third-order non-linear polymer materials without strong π-conjugation along polymer chains but having π-conjugation in the side groups.

The results on non-linear refraction in epoxy-based polymer materials with covalently attached metal complex of nickel and NLO chromophores are presented. Third order optical non-linear susceptibility $\chi_{\omega}^{(3)}(\omega, \omega, -\omega, \omega)$ has been measured in the materials by means of degenerate two-wave mixing using frequency doubled pulsed YAG:Nd^{3+} laser. The kinetics of the dynamic grating recording and erasing in the materials in question have been studied in the time range of 10^{-8}–10^{5} s. The role of such

mechanisms of non-linear refraction as electron, thermal isomerization and orientation has been discussed.

It should be finally pointed out that unlike second order polymer materials in which matrixes with high T_g are usually used to freeze molecular orientation in third order optical non-linear materials, it is recommended to use matrixes with not high T_g to guarantee free molecular reorientation and insomerization. Besides, using matrixes with different T_g makes it possible to control the relaxation time of the third order optical non-linear polymer materials.

References

[1] CHEMLA D.S., ZYSS J., *Non-linear Optical Properties of Organic Molecules and Crystals*, Academic Press, Orlando, 1987.
[2] SEHWERZEL R.E., EPA Newsletter, 6 (1994), 3.
[3] SEHWERZEL R.E., The Spectrum, 6 (1993), 1.
[4] ZHAO M.T., SAMOC M., SINGH B.P., PRASAD P.N., J. Phys. Chem., 93 (1989), 7916
[5] KORENEVA L.G., ZOLIN V.F., *Non-linear Optics of Molecular Crystals* (in Russian), Nauka, Moscow, 1985.
[6] KOLINSKI R.A., KORYBUT-DASZKIEWICZ B., Inorg. Chim. Acta, 14 (1975), 237.
[7] KUTSENKO A.S., MALOLETOV S.M., Teor. Eksp. Khim., 31 (1995), 308.
[8] MELESHEVICH A.P., *Radiation Chemistry of Epoxide Compounds* (in Russian), Naukova Dumka, Kiev, 1982.
[9] YATSIMIRSKII K.B., LAMEKA YA.D., *Physical Chemistry of Metal Complexes with Macrocyclic Ligands* (in Russian), Naukova Dumka, Kiev, 1985.
[10] GIBBS H.M., *Optical bistability*, Academic Press, Orlando, 1985.
[11] KUTSENKO A.S., MALOLETOV S.M., BURIN O.M., VOLKOV V.I., BORSHCH A.A., BRODYN M.S., J. Non-lin. Opt. Phys. Mat., 10 (2001), 311.
[12] PAQUIN A.P., *Epoxydverbindugen und Epoxydharze*, Springer-Verlag, Berlin, 1958.
[13] BISLE H., ROMER M., RAU H., Ber. Bunsenges, Phys. Chem., 80 (1976), 301.
[14] KRONER J., BOCK H., Chem. Ber., 101 (1968), 1922.
[15] ELTSOV A.V., (Ed.), *Organic Photochroms* (in Russian), Khimiya, Leningrad, 1982 .
[16] FANGHANEL E., HANSEL R., HOHLFIELD J., J. Pract. Chem., 319 (1977), 485.
[17] JUNGBAUER D., TERAOKA I., YOON D.Y., RECK B., SWALEN J.D., TWEIG R., WILSON C.G., J. Appl. Phys., 69 (1991), 8011.
[18] BROWN G.H. (Ed.), *Photochromism*, Vol. 4, Wiley, New York, 1971.
[19] GUILLET J., *Polymer Photophysics and Photochemistry*, Cambridge University Press, Cambridge, 1985.
[20] RAU H., Photochem. Photophys., 2 (1990), 119.
[21] KOBAYASHI T., DEGENKOLB E.O., RENTZEPIS P.M., J. Phys. Chem., 83 (1979), 2431.
[22] TSUTSUMI O., SHIONO T., IKEDA T., GALLI G., J. Phys. Chem., B101 (1997), 1332.
[23] EISENBACH C.D., Makromol. Chem., 179 (1978), 2489.
[24] EISENBACH C.D., Makromol. Chem., 180 (1979), 565.
[25] RAMANUJAM P.S., HOLME N.C.R., NIKOLOVA L., BERG R.H., HVILSTED S., KRISTENSEN E.T., KULINNA C., NIELSEN A.B., PEDERSEN M., SPIE, 3011 (1997), 319.
[26] BARRETT C.J., NATANSOHN A.L., ROCHON P.L., J. Phys. Chem., 100 (1996), 8836.
[27] DUMONT M., Mol. Cryst. Liq. Cryst., 282 (1996), 437.

[28] HOLME N.C.R., NIKOLOVA L., NORRIS T.V., HVILSTED S., PEDERSEN M., BERG R.H., RASMUSSEN P.H., RAMANUJAM P.S., Macromol. Symp., 137 (1999), 83.
[29] PALTO S.P., KHAVRICHEV V.A., YUDIN S.G., BLINOV S.G., UDAL'YEV A.A., Mol. Mater., 3 (1992), 63.
[30] PUCHKOVS'KA G.A., RESHETNYAK V.YU., TERESHCHENKO A.G., YAROSHCHUK O.V., LINDAU J., Mol. Cryst., Liq. Cryst., 321 (1998), 31.

Received 11 July 2002
Revised 30 October 2002

Materials Science, Vol. 20, No. 4, 2002

Electrochromic transitions in polyaminoarene films electrochemically obtained on transparent electrodes*

OKSANA I. KONOPELNIK[1], OLENA I. AKSIMENTYEVA[2**], MYROSLAV YA. GRYTSIV [1]

[1]Physical Department of Ivan Franko Lviv National University

[2]Chemical Department of Ivan Franko Lviv National University,
6 Kyryla-Mefodia, 79005, Lviv, Ukraine,

The processes of electrosynthesis, electrochemical behaviour and electrochromic properties of polyaminoarenes of different nature and position of substitutents in benzene ring – poly-*o*-(*m*)-aminophenols, poly-*o*-toluidine, poly-*o*-methoxyaniline and polyaniline have been studied in aqueous acid electrolytes. It has been shown that particularities of electrochemical and electrochromic transitions in polyaminoarene films obtained on SnO_2 electrodes are defined by the charge transport parameters depending on the molecular structure of the polymers, type of electrolyte anion and associated with an ion-diffusion phenomena on the polymer–solution interface.

Key words: *polyaminoarene; electrochromic transitions; structure; charge transport*

1. Introduction

Conducting polymers, especially polyaminoarenes such as polyaniline and its derivatives have a potential application as modified electrodes in chemical power sources. During the last years the electrochromic properties of these polymers aroused a great interest [1–3]. It is known that electrochromic displays on the base of organic dyes harmonize with the background and are soft for human eyes, but their erasing-rewriting rate is slow [1]. This rate may be increased by using conducting polyaminoarenes with electroactive chromophore groups [2, 3]. Numerous investigations have been realized for polyaniline films in organic and aqueous electrolytes [1, 3–5] but molecular structure and electrochromic properties of its derivatives, except the poly-*o*-methoxyaniline

---

*Paper presented at the 4th International Conference on *Electronic Processes in Organic Materials*, ICEPOM-4, 3–8 June 2002, Lviv, Ukraine.

**Corresponding author, e-mail: aksimen@org.lviv.net.

[2, 6], have not been studied in detail. This is particularly true in the case of polyaminophenols, poly-*o*-toluidine and others. In the present paper, we report on the effect of structure and electrolyte on electrochemical behaviour and electrochromic properties of polyaminoarenes of different nature and position of substitutents in benzene ring – poly-*o*-aminophenol (POAP), poly-*m*-aminophenol (PMAP), poly-*o*-toluidine (POTI), poly-*o*-methoxyaniline (POMA) and polyaniline (PANI).

2. Experimental

Preparation of polyaminoarene films was carried out in a three-compartment electrochemical cell by electrolysis of 0.1 M solutions of purified monomers (*o*-toluidine, *o*-methoxyaniline, aniline, *o*- and *m*-aminophenols) in 0.5 M H_2SO_4. The glass, spin-coated with SnO_2 working electrode, Pt-wire counter electrode and Ag/AgCl (in saturated KCl) as a reference were employed. The potentiostat PI-50M was used as a power source. Cyclic voltammetry experiments were carried out on CVA-1 voltamperometric system at potential sweep rate ν of 5–200 mV/s. The EPR spectra were recorded *in situ* during the chemical oxidation of 0.1 M aminoarenes by 0.1 M $(NH_4)_2S_2O_8$ in 0.5 M sulfuric acid in quartz cells. The X-band radiospectrometer RE-1306 operating in the high frequency (100 kHz) modulation mode of magnetic field at T = 293 K was used. The value of g-factor and unpaired spin concentration were estimated using DPPH as a reference. The UV-Vis absorption spectra were obtained in a quartz electrochemical cell with SnO_2 working electrode using spectrophotometer SF-26 in the 320–1000 nm spectral range. The molecular structure of polymers was studied by IR-spectroscopy by means of the spectrophotometer Specord M-80 (400–4000 cm^{-1} spectral range) for samples pressed in KBr wafers. The content of doping ions was estimated by X-ray microprobe analysis with a Camebax analyzer. Film thickness was measured by micro-interferometer MII-4 or calculated from electrochemical data.

3. Results and disscussion

The formation of electrochromic films of a required thickness on the transparent surfaces may be provided by Langmuir–Blodgett technology [6], or by electrochemical synthesis [3–5]. In the latter case, the regularity of the film thickness may be achieved by the control of the charge passed during electrolysis, and by cyclic voltammetry method [4, 5]. The thickness of the film is determined by sweep cycle number (N) in a certain interval of potentials. In the case of polyaminoarenes, the cycle number and quantity of charge (Q), are connected by the empiric equation proposed by Zotti et al. [5], which for PANI can be written as

$$Q \approx c^2 \left(\frac{N}{\nu}\right)^2 \exp\left[\left(\frac{2\alpha nF}{RT}\right) E_\lambda\right] \quad (1)$$

where Q is the total deposition charge obtained for the fully reduced polymer after N cycles, c – monomer concentration, ν – sweep rate, α – transfer coefficient, n – number of electrons participating in the redox process, F – Faraday's constant, E_λ is the switching potential.

The electrolysis of aminoarene solutions in acid electrolyte at potential of monomer oxidation is accompanied by the formation of conducting polymer film on the metal or oxide electrodes [1–5]. The oxidation proceeds over the aminogen with the formation of cation-radical particles. Previously it has been found that electrochemical oxidation of *o*- and *m*-aminophenols on Pt and graphite electrodes is an irreversible process and proceeds by both (amino- and hydroxyl-) functional groups [7]. It has been established that on transparent tin oxide electrodes the process of oxidation of isomeric aminophenols, unsubstituted phenol and aniline proceeds in similar conditions. Depending on the mutual position of substitutents in benzene ring of the monomer, the oxidative potential (E_{ox}) and the rate of charge transport (k_s) calculated as in [7] are significantly different. As can be seen from Table 1, the presence of hydroxyl groups in aniline molecule and amino groups in phenol molecule causes the decreasing of oxidation potential in comparison with phenol and aniline, and arising of the heterogeneous constant of charge transport for oxidation of OH groups. The rate of aminophenol oxidation over the NH_2 groups is decreased comparably to aniline monomer. This observation is in a good agreement with the data of EPR spectra, presented in the Table 1. In the process of aminoarene chemical oxidation at T = 293 K, an EPR signal appears, increasing in time. The shape of line with g-factor 2.003 ±0.001 without hyperfine structure is typical of conducting polyaminoarene polymers [8]. The intensity of the signal, recorded after 60 min from the initiation of the polymerization, is significantly higher for aniline oxidation in comparison with aminophenols. A lower intensity of signal, associated with smaller unpaired spin concentration (N_s), broadening of the peak-to-peak distance (ΔHpp) indicates a slower polymerization rate of aminophenols as compared with aniline.

Table 1. Electrochemical parameters of electrooxidation of aminoarenes (C = 0.1 M) in 0.5 M H_2SO_4 and characteristics of EPR spectra (T = 295 K) of chemical oxidation of aminoarenes

Monomer	Functional group				Parameters of EPR spectra		
	–OH		–NH_2				
	E_{ox}/V	$k_s \cdot 10^5$ /(cm/s)	E_{ox}/V	$k_s \cdot 10^5$ /(cm/s)	g-factor	ΔHpp/Oe	N_s/(1/g)
Phenol $(C_6H_5)OH$	1.02	4.8	–	–	–	–	–
m-Aminophenol $(C_6H_5)(mNH_2)OH$	0.90	5.4	0.42	4.3	2.0037	8.5	$9.4 \cdot 10^{17}$

o-Aminophenol (C_6H_5)(*o*NH_2)OH	0.62	8.3	0.37	6.7	2.0045	12.8	$6.1 \cdot 10^{18}$
Aniline $C_6H_5NH_2$	–	–	0.80	27.0	2.0036	3.2	$4.7 \cdot 10^{19}$

For electrochemical preparation of polyaminophenol films on SnO_2 electrodes the potential cycling between E = –0.2 and 0.8 V with ν = 40 mV/s was used. Coloured polymer films were obtained only after 50 (PMAP) or 60 (POAP) cycles of potential sweeping. The IR-spectroscopy of film material (pressed in KBr pellets) confirmed that in this potential region only the amino group of *m*-aminophenol undergoes anode oxidation while the hydroxyl group remains unchanged. The absorption bands of *para*-substituted aromatic ring (3080, 1520, 760 cm^{-1}), amino group (3350, 1574 cm^{-1}) and OH group at 3600, 1410, 1200 cm^{-1} were found. In the case of *o*-aminophenol the close values of oxidative potentials causes subsequent oxidation by two functional groups, which leads to heterocycle formation [7, 9]. This is confirmed by absorption bands at 1270–1200 cm^{-1} (ether oxygen) and 3400–3200 cm^{-1} (bound hydroxyl). The molecular structure of polyaminophenols in comparison with polyaniline is presented in Fig. 1.

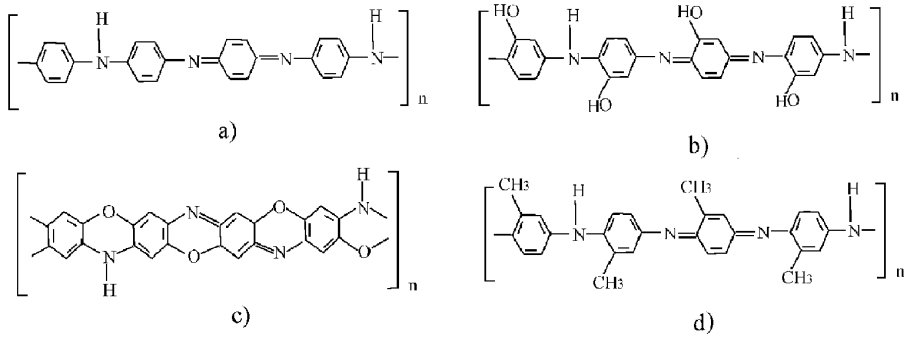

Fig. 1. Molecular structure of polyaminoarenes: a) polyaniline, b) poly-*m*-aminophenol, c) poly-*o*-aminophenol and d) poly-*o*-toluidine

The study of POMA, POTI and PANI films formation on the SnO_2 surface showed that polymerization takes place at significant lower anode potentials (E = 0.52–0.70 V) in comparison to monomer oxidation (E = 0.82–0.96 V), thus the primary formed layer is the catalyst of the process (Fig. 2a, b).

The polymer formation proceeds by the autocatalytic mechanism according to the known scheme for the reaction of electrochemical coupling of aromatic amines and includes the steps of monomer oxidation over amino group with cation-radical formation and coupling of cation-radicals accompanied by deprotonation [3, 5]. The compact, uniform films of POMA and POTI on the SnO_2 electrodes were obtained after 15–30 cycles of potential sweeping between E = 0 and E = 1.0 V. The molecular structure of POMA and POTI (Fig. 1d) films obtained in such conditions is similar to PANI and PMAP [3, 6].

In the process of potential cycling in acid aqueous electrolytes between E = –0.3 V and E = 1.2 V, the reversible multicolour transitions in polyaminoarene films are observed. In the case of POAP the rose-red-brown colouration is observed in the interval of potentials E of –0.1–0.4 V. In the case of PMAP the switching potential E (yellow -green-brown) lies in a more negative range – from –0.25 V to 0.05 V. For the POTI and POMA films on SnO_2 the colourless-yellow-green-blue-violet transition is observed in the potential interval of –0.3–1.2 V, whereas for PANI film similar colour variations are observed in the range of –0.2–0.8 V [3]. The switching potential of observed electrochromic transitions corresponds to potentials of redox maximums on CVA curves (Fig. 2c, d) which confirm the running of oxidation-reducing reactions in a conjugated polymer chain.

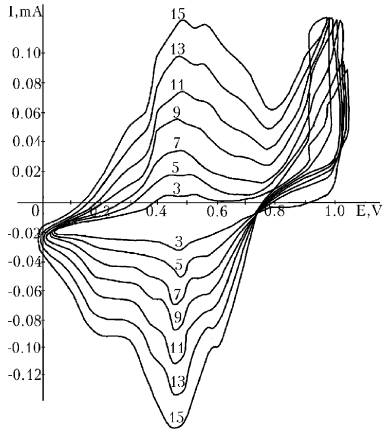

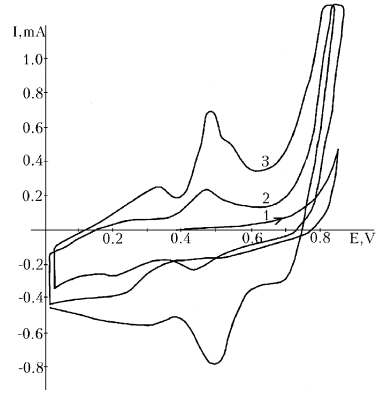

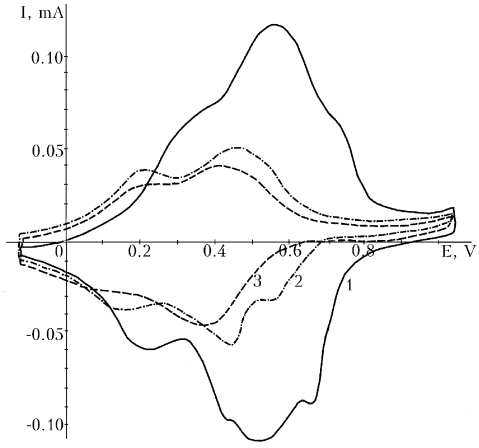

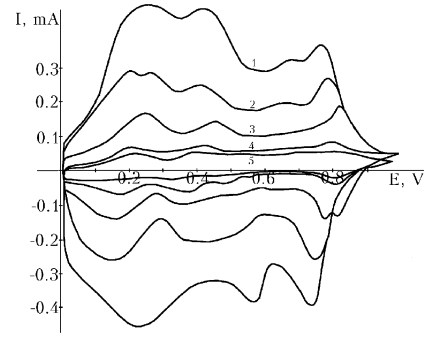

Fig. 2. Cyclic voltammograms obtained in the process of electrodeposition on the SnO_2 electrode: a) poly-*o*-toluidine from 0.1 M *o*-toluidine solution in 0.5 M H_2SO_4; b) poly-*o*-methoxyaniline from 0.1 M *o*-methoxyaniline solution in 0.5 M H_2SO_4, sweep rate 20 mV/s, the numbers refer to the sequence of cycles; c) cyclic voltammograms for poly-*o*-toluidine film in aqueous electrolytes: 0.5 M H_2SO_4 (1); 1 M HCl (2) and 1 M TSA (3), sweep rate 20 mV/s; d) cyclic voltammograms for poly-*o*-methoxyaniline film in 1 M TSA solution at sweep rate 80 (1), 40 (2), 20 (3), 10 (4) and 5 (5) mV/s. The polymer films obtained after 15 cycles of potential sweeping

The influence of anions on polymer redox properties one can see from the CVA curves recorded in acid electrolytes (Fig. 2c, d). In all electrolytes studied (HCl, H_2SO_4, HNO_3, toluenesulfonic acid (TSA)) on the CVA of POTI and POMA films two or three reversible redox peaks are observed. The first peak (E = 0.18–0.25 V) corresponds to the oxidation of fully reduced leucoemeraldine form of polyaminoarene to emeraldine (semiquinone cation-radical) form. The second peak (E = 0.45–0.60 V) is caused by fast oxidation (ΔE < 30 mV) of emeraldine to fully oxidized pernigraniline (dication), where all nitrogen atoms are in the quinone-diimine form [3]. The appearance of small intermediate maxima on the CVA curves may be related to reactions of oligomers or film degradation with formation of a soluble product [10]. Similar to polyaniline, the highest electrochemical activity of POMA and POTI films (estimated as peak current on CVA) has been observed in the sulfuric acid solution. At the same time, a shift of redox potentials to positive values has been observed. It was suggested [10] that anions (especially SO_4^{2-}) strongly interact with radical-cations of polyaminoarenes, promote the localization of charge and facilitate the polymer degradation, since the localized charge is more prone to the nucleophilic attack of water molecules. The highest peak currents are achieved in conditions, in which the process of polymer degradation is difficult. However, those peak currents observed in different electrolytes are also associated with the diffusion of ions on polymer–solution interface [2, 4]. The high peak currents of polyaminoarene films in sulfuric acid may be explained by higher ion mobility of SO_4^{2-} anions in comparison with Cl^- and large TSA anions [11] and strong hydrophilic properties of SO_4^{2-}, determining the kinetics of the electron transfer reaction [4].

The rate of colour transitions is controlled by the electron transport rate in polymer layer immobilized at the electrode surface. This rate may be characterized by the heterogeneous constant of charge transport (k_s) or by the effective coefficient of diffusion (D_{ef}) for charge transport across the film [12]. The study of electrochemical behaviour of polyaminoarene films in acid electrolytes demonstrated that in the case of polyaminophenols, the charge transport is diffusion-limited and a linear dependence of peak current on the square root of the sweep rate ($i_p \sim v^{1/2}$) is observed. This feature permits to calculate the effective diffusion coefficient D_{ef} using model of semi-infinite diffusion [13]. The following equations follow from the model:

$$i_p = 2.69 \cdot 10^5 n^{3/2} S D_{ef}^{1/2} v^{1/2} C^* \qquad (2)$$

$$C^* = \frac{Q}{nFSd} \tag{3}$$

where n is the number of electrons participating in the redox process, S – the area of the film (cm^2), C^* – concentration of active centres in the film (mol/cm^3), Q – total charge, calculated by the integration of anode or cathode cyclic voltammetric currents at slow sweep rate, d is a film thickness, F – Faraday's constant.

The calculated values of the effective diffusion coefficients (D_{ef}) for polyaminophenols films in acid electrolytes (Table 2) show that the parameters of charge transport correlate with the absolute mobility of doping anions [11]. The strong difference in the values of the diffusion coefficient found for polyaminophenols and PANI films suggests, however, that the main factor determining the rate of charge transport across the film is the molecular structure and segment mobility of polymer chains. The presence of the electron-donor substitutents in the benzene rings causes, as a rule, some loss of conductivity and electron-transport rate [3]. For the rigid ladder polymer structure of POAP the values of D_{ef} are lower by 2–4 orders compared to PANI, indicating a low rate of charge transport in poly-*o*-aminophenol film.

Table 2. Absolute mobilities of anions (u_c) and effective diffusion coefficients (D_{ef}) of polyaminoarene films in acid solutions

Polyaminoarene film, area and thickness	Electrolyte	u_c, m^2/Vs	$D_{ef} \cdot 10^{10}$, cm^2/s
Poly-*o*-aminophenol, S = 3.4 cm^2, d = 0.25 μm	CH_3COOH (1 M)	3.7	0.0 8± 0.02
	HCl (1 M)	6.8	0.15 ± 0.02
	H_2SO_4 (0.5 M)	7.1	0.23 ± 0.04
Poly-*m*-aminophenol, S = 4.0 cm^2, d = 0.28 μm	HCl (1 M)	6.8	1.17 ±0.07
	H_2SO_4 (0.5 M)	7.1	1.56 ±0.07
Polyaniline, S = 4.0 cm^2, d = 0.28 μm	CH_3COOH (1 M)	3.7	40.2 ± 0.5
	$HClO_4$ (1 M)	6.7	73.7 ± 0.5
	H_2SO_4 (0.5 M)	7.1	90.2 ± 0.5

The best charge transport characteristics were obtained for POMA and POTI thin films. From CVA study in aqueous electrolytes it has been found that electrodeposited polymer layers at $N \leq 15$ demonstrate the electrochemical behaviour attributed to oxidation-reduction of electroactive species strongly adsorbed or immobilized on the electrode surfaces.

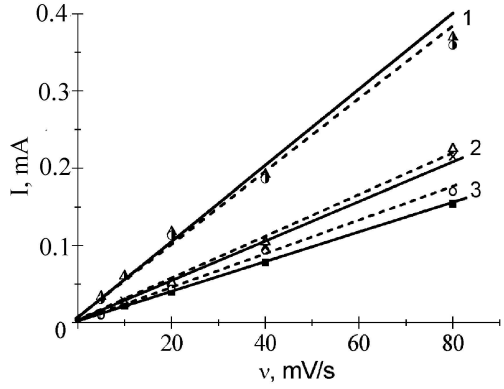

Fig. 3. Peak current dependence on potential sweep rate of poly-*o*-toluidine film in aqueous electrolytes: 0.5 M H_2SO_4 (1), 1 M TSA (2) and 1 M HCl (3); solid line indicates the anode peak and dashed line indicates the cathode peak

The evidences for this behaviour are the high reversibility of redox processes in the films (ΔE is in the range of 30 mV, $I_a/I_к \approx 1$, peak potentials slightly depended on sweep rate) and the linear dependence of anode and cathode peak current (I_a, $I_к$) from potential sweep rate v as shown in Fig. 3.

The doping current i of this polymer layer may be described by the equation [14]

$$i = \frac{n^2 F^2 A v \Gamma_i \exp\theta}{RT(E + \exp\theta)^2}, \qquad \theta = \frac{nF(E - E_0)}{RT} \tag{4}$$

where n is the number of electrons, A – area of the electrode surface, Γ_i – surface concentration of electroactive substances, the sum of concentration of oxidized and reduced form (Γ_{ox} + R_{ed}), E, E_o – electrode potential and standard electrode potential, F– Faraday's constant. The surface concentration of electroactive substances for POTI film, estimated from Eq. (4) based on i and E parameters of the second CVA maximum in the sulfuric acid solution at v = 20 mV/cm is nearly 10^{-9} mol/cm^2.

It has been found that in electron spectra of polyaminoarene films changes in positions of absorption maxima and optical densities occur under the potential applied. These changes are accompanied by reversible colour transitions in the films. As is shown in Fig. 4, the shapes of electron spectra of polyaminoarene in sulfuric acid solution depend on the electrode potential and usually are related to the polyaminoarene structure and the nature of functional groups.

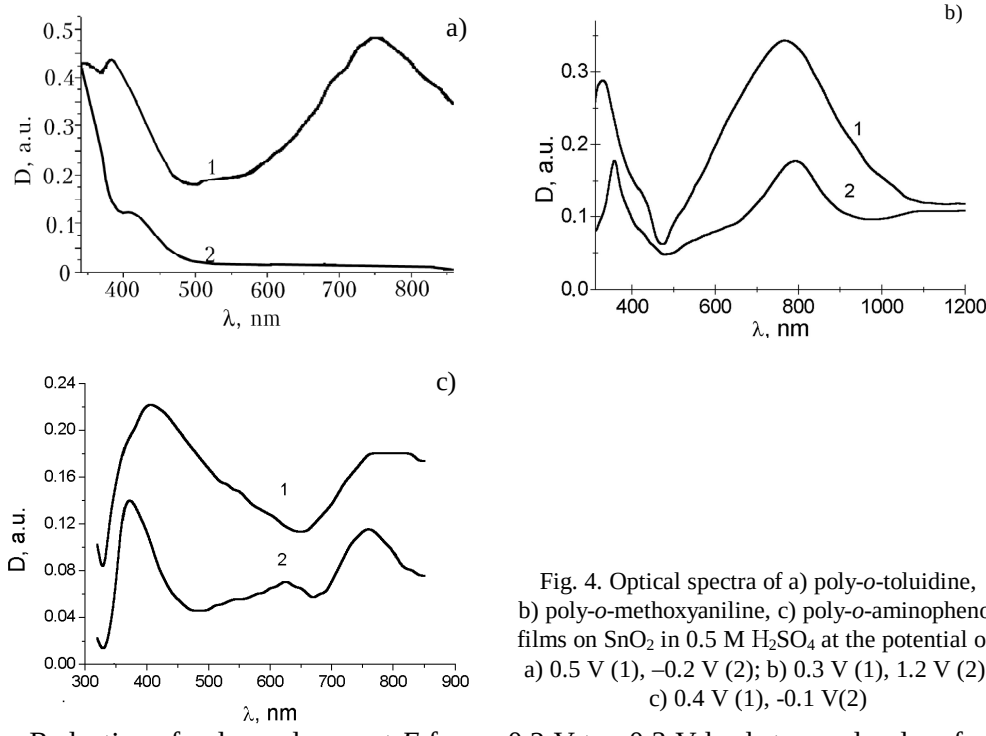

Fig. 4. Optical spectra of a) poly-*o*-toluidine, b) poly-*o*-methoxyaniline, c) poly-*o*-aminophenol films on SnO_2 in 0.5 M H_2SO_4 at the potential of: a) 0.5 V (1), –0.2 V (2); b) 0.3 V (1), 1.2 V (2); c) 0.4 V (1), -0.1 V(2)

Reduction of polymer layers at E from –0.2 V to –0.3 V leads to a colourless form of polyaminoarenes with the absorption band at 340–420 nm ($\pi \rightarrow \pi^*$ transition), which is illustrated by curve 2 in Fig. 4a. This band corresponds to leucoemeraldine benzene –amine polymer, which has an unconjugated backbone [3]. The anode polarization of SnO_2 electrode to 0.3–0.6 V causes the appearance of the green colour of PANI, POMA and POTI films, and of rose-red colours of POAP. As is shown in Fig. 4a, b, these transitions for POMA and POTI films similar to PANI [3] are accompanied by arising wide absorption maxima in the visible region of the spectra (700–850 nm). In the case of POAP under anode polarization from –0.1 V to 0.4 V, the intensity of absorption bands in the interval of 600–700 nm increases (Fig. 4c) as a result of polymer oxidation and doping by sulfate anions [9]. A small red shift in the positions of these bands is also observed.

For polymers with linear polymer chain structure, such as POTI, POMA and PANI, the existence of absorption at 340–400 nm and 700–800 nm may be assigned to polaron or bipolaron bands [15]. The existence of a delocalized polaron band is attributed to semi-oxidized states of polyaminoarenes – emeraldine form [3, 10]. The polaron transition is dominant at a lower polarizing potential, while the bipolaron transition is dominant at a higher potential. In the potential interval $E > 0.6$–0.8 V, the blue (PANI, POTI), violet (POMA) and brown (POAP) colours of the films appear, which may be connected with the increase of pernigraniline content in the polyaminoarene. At a still higher potential ($E \geq 1.2$ V), the colour changes become irreversible. The decrease of

the optical density for POMA film, taken as an example, (curve 2 in Fig. 4b) takes place as a result of the electrochemical destruction. For all polyaminoarenes studied, the loss of doping level and decrease of the electrical conductivity of the films are observed. According to X-ray microprobe analysis, it has been determined that in the colourless form of polyaniline the contents of doping ions (e.g., sulfate) are close to 0%; in green form – to 6.2 at. %; blue – 3.3 at.% of S.

The features of electrochromic transitions in polyaminoarene films are connected with molecular structure of polymer chains. The incorporation of electron-donating substituents into a conjugated chain leads to the decrease of the polymer oxidation potential by increasing the energy of valence band electrons [15]. On the other hand, the existence of electron-donating substituents in polymer chain ($–OCH_3$, $–CH_3$) leads to the widening of potential range of colour transitions in POMA and POTI films in comparison to PANI [3]. Introduction of the hydroxyl substituent into aminoarene molecule leads to a decrease of the electron transport rate for oxidation of aminophenols and to the formation of rigid heterocycle structure of POAP. The structure obtained, as well as electrochemical and spectroscopic data permit to conclude that electrochromic transitions in conjugated polyaminoarenes are caused by chemical and structural factors. The colour variations depend on the doping level of polyaminoarene connected with oxidation-reduction of aminobenzene or iminoquinoid functional groups. The rate of electrochemical and electrochromic transformations is defined by charge transport in the polymer film associated with diffusion of anions on the polymer–solution interface.

References

[1] YANO J., Electrochem. Soc., 144, (1997), 477.
[2] GONÇALVES D., MATVIENKO B., BULHOES L.O.S., Synth. Metals, 83 (1996), 147.
[3] FOOT P.J.S., SIMON R., J. Phys. D: Appl. Phys., 22 (1989), 1598.
[4] CHOI S.-J., PARK S.-M., J. Electrochem. Soc., 149, (2002), E26.
[5] ZOTTI G., CATTARINN S., COMISSO N., J. Electroanal. Chem., 235 (1987), 259.
[6] GONÇALVES D., BULHOES L.O.S., Thin Solid Films, 243 (1994), 544.
[7] PLUSNINA T.A., AKSIMENTYEVA E.I., KOVALCHUK E.P., Elektrokhimiya, 30 (1994), 825.
[8] AKSIMENTYEVA O.I., ARTYM V.T., MELNIK O.I., PLUSNINA T.A., Acta Phys. Pol. A, 85 (1994), 237.
[9] GONÇALVES D., FARIA R.C., YONASHIRO M., BULHOES L.O.S., J. Electroanal. Chem., 487 (2000), 90.
[10] PALYS B., KUDELSKI A., STANKIEW A., JACKOWSKA K., Synth. Metals, 108 (2000), 111.
[11] DOBOSH D., *Electrochemical Constants*, Mir, Moscow, 1980.
[12] NYASULU F.W.M., MOTTOLA H.A., J. Electroanal. Chem., 239 (1988), 175.
[13] MAKSIMOV YU.M., KHALDUN M., PODLOVCHENKO B.I., Elektrokhimiya, 27 (1991), 739.
[14] LAVTRON E., *Electroanalytical Chemistry*, A. J. Bard (Ed.), Marcel Dekker, New York, 12 (1979), 53.
[15] SANKARAN B., REYNOLDS J.R., Macromolecules, 30 (1997), 2582.

Received 7 June 2002
Revised 31 October 2002

Materials Science, Vol. 20, No. 4, 2002

4-(4-Dimethylaminostyryl)pyridinium derivative: a solvent viscosity- and polarity-sensitive fluorescent sensor*

ALINA MIELNICZAK[1], BARBARA WANDELT[1**], STANISŁAW WYSOCKI[2]

[1]Technical University of Łódź, Department of Molecular Physics, Żeromskiego 116, Łódź 90 924, Poland

[2]Technical University, Department of Food Science and Biotechnology, Stefanowskiego 4/10, Łódź 90 924, Poland

Trans-4-(*p*-N,N-dimethylaminostyryl)-N-vinylbenzylpyridinium chloride (1) is a newly synthesised multichromophore chemosensor. This molecule displays strong intramolecular charge transfer properties. It fluorescences in a very favourable region (480–650 nm in polar and viscous solutions) for its use as a sensing system. Steady-state and time-resolved fluorescence spectroscopy have been used to characterize photophysical properties in viscous and non-viscous polar solutions. We investigated the influence of solvent viscosity on the rate constants of radiative and non-radiative processes of deactivation of (1) in aqueous solutions.

Key words: *multichromofore chemosensor; polarity sensitive fluorescence; reorientation processes*

1. Introduction

Multichromophore compounds exhibiting intramolecular charge transfer (ICT) and twisted intramolecular charge transfer (TICT) properties show ICT fluorescence bands that depend on the physical and chemical properties of the medium. This environmentally sensitive fluorescence, by virtue of varying fluorescence responses to solvent media, provides a wealth of information on the molecular properties of microenvironments. In particular, the dependence of TICT fluorescence on viscosity of the environment has been widely reported, and is thought to occur by a time-dependent

---

*Paper presented at the 4th International Conference on *Electronic Processes in Organic Materials*, ICEPOM-4, 3–8 June 2002, Lviv, Ukraine.

**Corresponding author, e-mail: bwandelt@ck-sg.p.lodz.pl.

intramolecular reorientation process [1–5]. The applications of environmentally sensitive fluorophores are limited by their fluorescence wavelength ranges. Although a number of fluorophores are used, only few of them have absorption and fluorescence spectra in the visible range. Among them dimethylaminostyrylpyridinium derivatives are important as they are easily composed into a polymer matrix. The dynamics of reorientation relaxation of molecules in solution with high friction between the rotating molecule and solvent, as it occurs for 4-(4-dimethylaminostyryl)pyridine (DMASP) derivatives, can be described by the Debye–Stokes–Einstein (DSE) hydrodynamic model. The reorientation relaxation time of the solvent molecules τ_{or} depends on the viscosity and on fluorescence quantum yield Φ_F, as shown by the following equations [1–3]:

$$\tau_{or} = C(\eta/T) \tag{1}$$

$$\tau_{or} = \tau \frac{\Phi_F}{\Phi_0 - \Phi_F} \tag{2}$$

where η is the shear viscosity of the solvent, T is the absolute temperature, C is the geometry-dependent rotational friction coefficient (which itself is dependent on temperature and viscosity [6]), τ is the lifetime of fluorescence of the dye, and Φ_0 is the fluorescence quantum yield when internal rotation of the molecule has ceased (at infinite η). If $\Phi_F << \Phi_0$ ($\Phi_0 = 0.35$) for the dye in a polymer matrix [2, 5], the above equations simplify to:

$$\Phi_F = \Phi_0 (C/\tau)(\eta/T) \tag{3}$$

This relationship has been proven for many compounds exhibiting ICT properties, including *p*-(dimethylamino)benzonitrile [1], substituted stilbenes [4], *p*-dialkylaminobenzylidenemalononitriles [2] and 4-(*p*-dimethylaminostyryl)pyridine derivatives [5, 7]. Increase of the viscosity of the environment surrounding of these fluorophores, suppresses the non-radiative transitions induced by intramolecular reorientation and diffusional collisions with the solvent molecules, and thus enhances the radiative processes [4, 5, 7].

Sensory systems based on DMASP exhibit environmentally sensitive photoinduced electron transfer and conformational changes in the meaning of viscosity and polarity interactions [3, 5, 7–9]. Recently, DMASP derivatives were reported to be sensitive to viscosity and temperature in aqueous solutions [5, 9]. These molecules are charged fluorophores with ICT fluorescence in the visible regions, about 600 nm that can be observed with excitation at 360 and 469 nm. Although the intensity of ICT emissions obtained by excitation at both 469 and 360 nm was affected by the viscosity of the local microenvironment, the emission obtained by excitation at 469 nm exhibited the greatest enhancement with viscosity, while that obtained by excitation at 360 nm was much less

sensitive to the changes in viscosity. In this paper, we present new data on the viscosity dependence of the reorientational dynamics of (1) in viscous aqueous glycerol and non-viscous methanol solvents. The goal of this study is to characterize the radiative and non-radiative deactivation processes for better understanding the solute–solvent interactions that influence the fluorescence of the sensing system.

2. Experimental

2.1. Materials

4-(4-Dimethylaminostyryl)pyridine (95%) and 4-vinylbenzyl chloride (90% *p*-vinylbenzyl chloride), acetonitrile, methylene chloride and carbon tetrachloride were purchased from the Aldrich Chemicals Co., and used without further purification. Methanol (99,9% HPLC grade) and glycerol (99% GC) were purchased from Sigma Chemicals Co., and used without purification. Aqueous solutions were prepared using double distilled deionised water.

2.2. Synthesis of *trans*-4-(*p*-N,N-dimethylaminostyryl) -N-vinylbenzylpyridinium chloride

Acetonitrile (10 cm^3) was added to a round bottom flask containing (0.246 g, 1.1 mmol) DMASP equipped with a magnetic stirrer, reflux condenser topped with a nitrogen inlet and a heating mantle. When DMASP was completely dissolved (for minimum 24 hours), it was stirred under nitrogen at the temperature of 60 °C, 4-vinylbenzyl chloride (0.256 g, 1.68 mmol) was added dropwise for over 15 min to give an orange reaction mixture. After gentle refluxing for ~48 h under nitrogen any remaining undissolved material was filtered off, leaving a clear, deep red mother liquor which was rotoevaporated to dryness. The product was recrystallized from methylene chloride and carbon tetrachloride and dried under vacuum (20 mm Hg) at 35 °C overnight. Yield of the product – dark red crystals – was 0.378 g (78.5%).

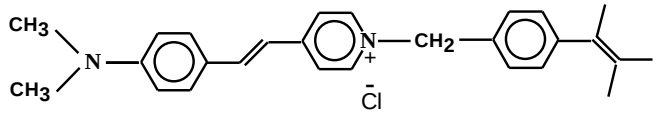

Fig. 1. Molecular structure of *trans*-4-(*p*-N,N-dimethylaminostyryl) -N-vinylbenzylpyridinium chloride (1)

The ^{1}H NMR spectra were recorded using Bruker Avance DPX 250:

^{1}H NMR ($CDCl_3$) δ 3.09 ppm (s. 6H, CH_3), 5.26 ppm (d. 1H, H_b), 5.72 ppm (d. 0.3H, *para* H_a), 5.79 ppm (d. 0.7H, *meta* H'_a), 6.04 ppm (s. 2H, CH_2), 6.66 ppm (m. 1H, H′), 6.69 ppm (d. 2H, H), 6.77 ppm (d. 1H, H), 7.26 ppm (t. 0.7H, *meta* H'_a), 7.35 ppm (d. 1.3H, *meta* H and *para* H), 7.53 ppm (d. 1H, H), 7.56 ppm (d. 0.6H, *para* H), 7.58 ppm (s. 0.7H, *meta* H), 7.75 ppm (d. 2H, H), 9.17 ppm (d. 2H, H). The structure of the molecule is schematically shown in Fig. 1.

2.3. Viscometry

The viscosities of the solvents were determined using capillary Ubbelohde dilution type viscometers which were submerged in a bath at the temperature of 25±0.1 °C. Solutions of various viscosities were prepared from water and glycerol mixtures and the average kinematic viscosity was taken as the mean of four measurements. Then the average kinematic viscosity was converted to intrinsic viscosity and corrected for density. The viscosities of highly concentrated aqueous glycerol solutions were obtained from published tables [10]. Low-viscosity binary solutions were prepared from water and methanol mixtures.

2.4. Spectroscopy

Absorption spectra were taken using a UV-VIS Varian Cary spectrometer and fluorescence spectra using a Perkin Elmer LS 50 spectrofluorimeter. Time-correlated single photon counting system (Edinburgh Analytical Instruments Co.) was used in fluorescence lifetime measurements. The fluorescence decays were analysed by a last squares reconvolution procedure using the software package provided by Edinburgh Instruments. 10 nm excitation and emission slits were used when both steady-state and time-dependent fluorescence spectra were recorded.

To avoid aggregation and self-quenching processes, the dye concentration of 10^{-5} M was used. The cuvette holder was heated with the accuracy of ± 0.1 deg. Fluorescence quantum yields (Φ_F) were determined at 25 °C relative to the quantum yield of rhodamine B in ethanol (Φ = 0.69; excitation at 366 nm) as a standard (Φ_{st}), using the following equation [11]:

$$\Phi_F = \Phi_{st} \frac{I_F}{I_{st}} \frac{A_{st}}{A_F} \tag{4}$$

where I_F and I_{st} are the fluorescence emission peak area of the dye solution and the standard solution, respectively; A_{st} and A_F are the absorbances of the standard solution and the dye solution, respectively.

3. Results and discussion

Figure 2a shows UV-Vis absorption spectra of (1) in water and in viscous solutions of mixture of glycerol with water. The absorption band appears as a typical ICT broad transition in the 350–550 nm region. The single broad absorption band of (1) exhibited a λ_{max} at 459 nm, very similar to that obtained for other DMASP derivatives [5, 8]. There is a bathochromic shift of the λ_{max} when (1) is in the aqueous glycerol solutions (Fig. 2a) up to 494 nm in 99% glycerol, and in aqueous methanol (Fig. 2b) up to 489 nm for 100% methanol. Excitation of (1) at 469 nm resulted in a broad structureless emission band with a maximum at 600 nm in water, as shown in Fig. 3a.

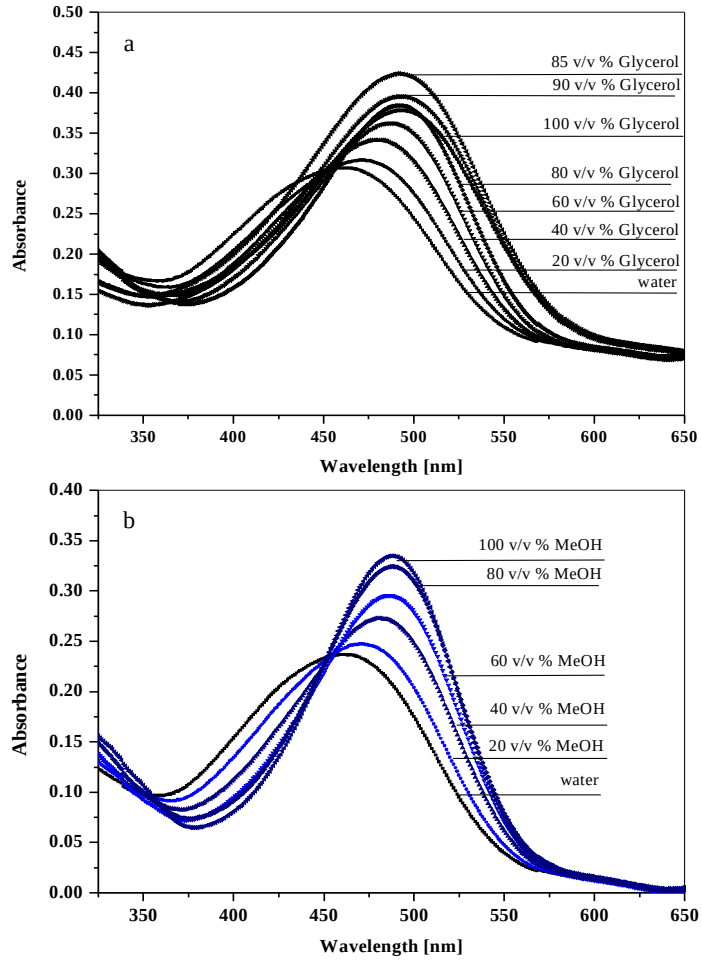

Fig. 2. Absorption spectra of (1) (10^{-5} M) in binary aqueous solvents: a) glycerol–water, b) methanol–water

The band slightly moves to shorter wavelengths with an increase of glycerol concentration in the mixed solvent but the intensity increases dramatically when the concentration of glycerol as well as its viscosity increase. Similarly, when (1) was in mixed methanol and water solvent shown in Fig. 3b, the shift of maximum wavelength was about 5 nm. Excitation of (1) at 360 nm resulted in a broad structured emission spectrum that could be decomposed by curve-fitting analysis ($r > 0.995$, standard error ±10%) into Gaussian emission peaks. The deconvoluted peak with a maximum at 600 nm appeared to be similar to the broad emission band obtained by excitation at 469 nm as was previously presented for other DMASP derivative, *trans* -4-(*p*-N,N-dimethylaminostyryl)-N-phenethylpyridinium bromide [5]. The quantum yields of the ICT of longer wavelengths [5] were calculated and shown in Table 1.

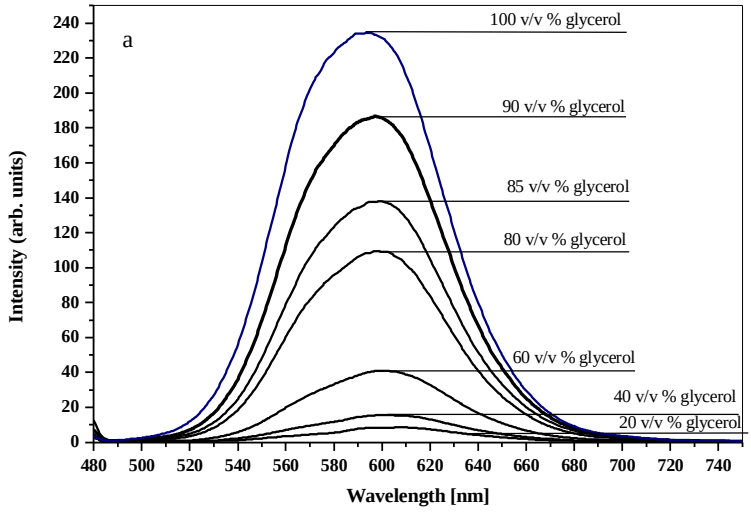

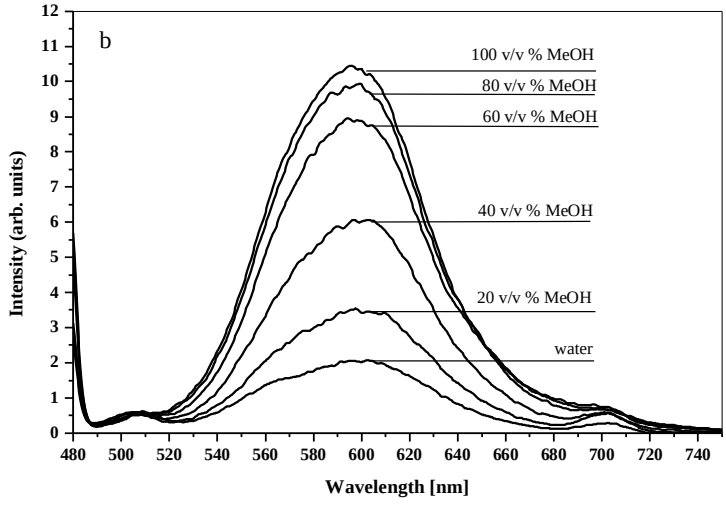

Fig. 3. Fluorescence spectra of (1) (10^{-5} M) in binary aqueous solvents when excited at 469 nm: a) glycerol–water, b) methanol–water

The intensity of this ICT fluorescence was comparable to that obtained by excitation at 469 nm and it corresponds to the data obtained for DMASP derivative [5]. The ICT fluorescence by excitation at 360 nm was observed for (1) in binary water –methanol solvents and is at about 500 nm, the emission at 600 nm is negligible. Presumably the structure of the molecule is slightly different. For the aqueous vbDMASP the Stockes shift is about 140 nm, and shifts to 100 nm for pure glycerol while for the methanol–water binary solvent of vbDMASP it shifts to 108 nm.

Table 1. Fluorescence quantum yield for (1) in viscous and non-viscous aqueous solvents

Component's concentration (v/v %)	Viscous solutions Glycerol–water			Non-viscous solutions Methanol–water		
	Viscosity (T = 298 K) cP	Quantum yield×10^2		Viscosity (T = 298 K) cP	Quantum yield×10^2	
		Exc. 469 nm	Exc. 360 nm		Exc. 469 nm	Exc. 360 nm
0 (pure H_2O)	0.89	0.111	0.137	0.89	0.109	0.137
20	1.54	0.205	0.290	1.53	0.221	0.182
40	3.18	0.379	0.371	1.67	0.282	0.245
60	8.82	1.001	0.582	1.48	0.349	0.310
80	45.90	2.936	1.110	1.07	0.399	0.362
85	96.00	3.764	1.593	–	–	–
90	267.00	5.135	1.835	–	–	–
100 (glycerol or methanol)	934.00	7.300	2.241	0.54	0.355	0.317

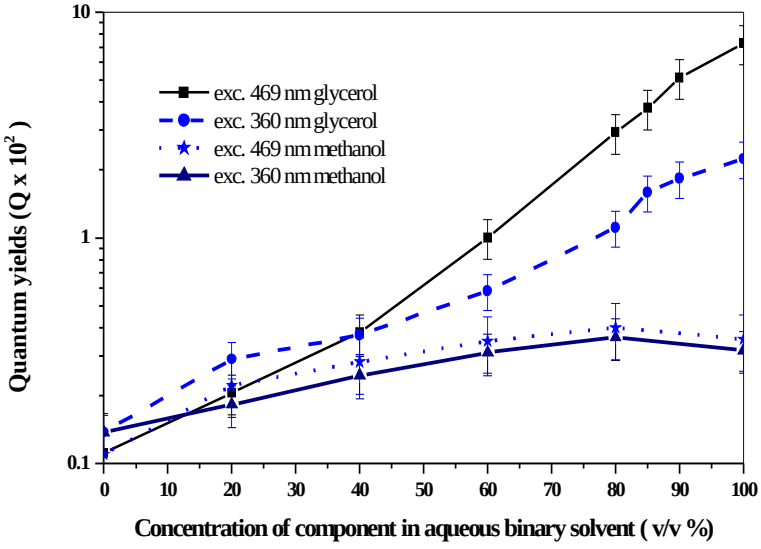

Fig. 4. Fluorescence quantum yield of (1) (10^{-5} M) in binary aqueous solvents when excited at 469 and 360 nm. The experimental values are means of four measurements

Figure 4 shows the quantum yield of fluorescence of (1) dependent on the concentration of binary solvent. The fluorescence quantum yield for (1) in aqueous glycerol increases with the concentration of glycerol but it slightly changes for that in the aqueous methanol binary solvent. The results suggest that the quantum yield of the molecule is strongly affected by the reorientation relaxation processes in agreement with Eq. (1).

Table 2. Fluorescence lifetime τ, ns for (1) in viscous and non-viscous aqueous solvents

Component's concentration (v/v %)	Viscous solutions Glycerol–water		Non-viscous solutions Methanol–water	
	Exc. 360 nm	Exc. 469 nm	Exc. 360 nm	Exc. 469 nm
0 (pure H_20)	0.188*	0.115*	0.188*	0.115*
20	0.223*	0.141*	0.220*	0.127*
40	0.276*	0.182*	0.265*	0.144*
60	0.355±0.07	0.261±0.06	0.332*	0.161*
80	0.546±0.03	0.424±0.05	0.452±0.14	0.193±0.04
85	0.628±0.16	0.539±0.04	–	–
90	0.641±0.15	0.5895±0.04	–	–
100 (glycerol or methanol)	0.98	0.744*	0.542±0.11	0.240±0.06

*The data were obtained by extrapolation of linear dependence of 1/τ vs. of binary solvent components' concentration (v/v %).

We measured the lifetimes of fluorescence of (1) when excited at 469 and 360 nm in viscous and non-viscous polar solutions. The data are gathered in Table 2.

The lifetime increases with the concentration of the viscous component in the binary solvent and much less for the non-viscous binary solvent, the lifetime for (1) in glycerol-based solvent is three times as high as for methanol-based solvent, if excitation was at 469 nm. When solution of (1) was excited at 360 nm, lesser increase of the fluorescence lifetime is observed (Table 2). This indicates that the lifetime of fluorescence is affected by viscosity as well as by electrostatic interactions but the effect of viscosity is much higher.

The basic photophysical equation which correlates the quantum yield and lifetime of fluorescence of the molecule with rate constants of radiative and non-radiative processes can be defined as follows [5]:

$$k_r = \frac{\Phi_F}{\tau_F}; \qquad k_{nr} = \frac{1-\Phi_F}{\tau_F} \tag{5}$$

where: Φ_F – quantum yield at a given concentration of the solvent and wavelength, τ_F – fluorescence lifetime at a given concentration of the solvent.

Figures 5a, b show the rate constants of radiative and non-radiative processes of (1) in the binary aqueous solvent systems, viscous and non-viscous, respectively. The increase of the rate constants of radiative processes due to (1) in viscous glycerol –water solutions with an increase of the glycerol concentration in the mixture is accompanied by a decrease of the rate constants of non-radiative processes.

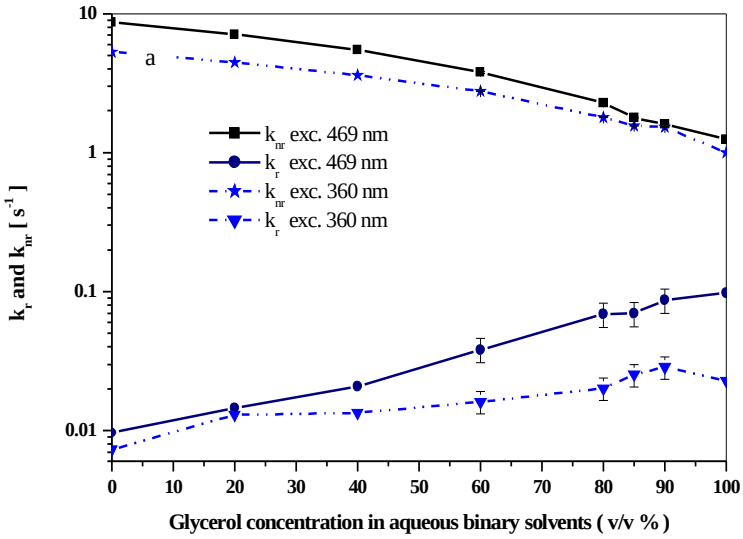

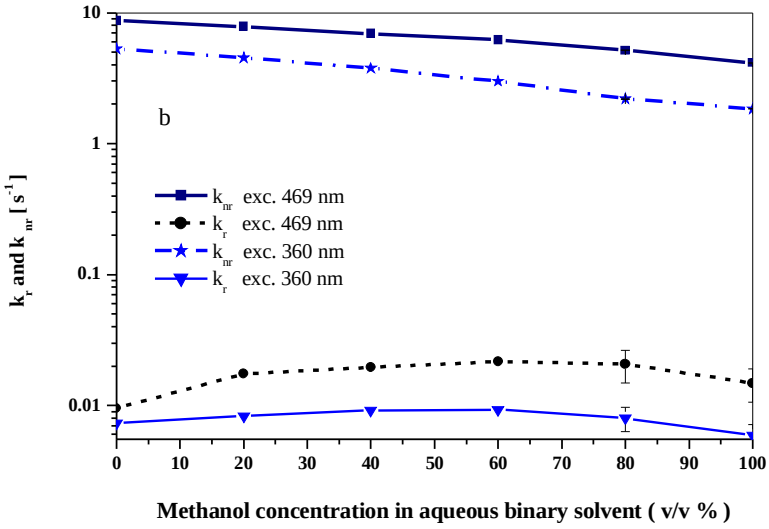

Fig. 5. Rate constants of radiative and non-radiative process for 1 in binary solvents vs. solvent concentration when excited at 469 and 360 nm. The experimental values are means of four measurements; a) glycerol–water, b) methanol–water

In opposite, for non-viscous methanol–water binary solvent the rate constants of radiative deactivation slightly increase with addition of methanol (10 v/v %) and almost do not change with the concentration of methanol in the binary solvent. In opposite (Fig. 5b), for non-viscous methanol–water binary solvent the rate constants almost do not change with the concentration of methanol in the binary solvent.

Conclusions

The vbDMASP probe molecules exhibit an intense absorption band in the visible region. The long-wavelength $S_0 \rightarrow S_1$ absorption band was observed to move to generally lower energies with the increasing concentration of glycerol in the mixture with water, which results in increasing viscosity. Fluorescence emission spectra ($S_1 \rightarrow S_0$) exhibited the same sensitivity to solvent viscosity demonstrating the role of non-radiative deactivation of the excited state of the dye. The decrease of the rate constant of non-radiative deactivation processes with the increase of glycerol concentration in the aqueous solution is accompanied by an increase of radiative deactivations. The long-wavelength fluorescence emission of vbDMASP observed in the glycerol–water binary solvent is undoubtedly due to an intramolecular $\pi^* \rightarrow \pi$ charge-transfer transition. A question can be raised, however, as to whether the conformation of the multichromophore compound and the fluorescence observed in viscous solvents will change when the compound is incorporated to polymer matrix. We have no answer to this question yet but no change of the absorption and fluorescence spectra, in the meaning of maximum wavelength and its CT character, has been observed when the molecule was

covalently incorporated in the polymer matrix. The vbDMASP has the possibility to be easily incorporated in the polymer matrix.

Acknowledgements

This work was financially supported by KBN grant No. 7 T09B 011 21.

References

[1] GRABOWSKI Z.R., Pure. Appl. Chem., 64 (1992), 1249.
[2] LOUTFY R.O., ARNOLD B.A., J. Phys. Chem., 86 (1982), 4205.
[3] ABDEL-MOTTALEB M.S.A., Laser Chem., 4 (1984), 305.
[4] LAPOUYADE R., CZESCHKA K., MAJENZ W., RETTIG W., GILABERT E., RULLIERE C., J. Phys. Chem., 96 (1992), 9643.
[5] WANDELT B., TURKEWITSCH P., STRANIX B.R., DARLING G.D., J. Chem. Soc. Faraday Trans., 91 (1995), 4199.
[6] BESSIRE D. R., QUITEVIS E.L., J. Phys. Chem., 98 (1994), 13083.
[7] ABDEL-MOTTALEB M.S.A., SHERIEF A.M.K., ISMAIEL L.F.M., DE SCHRYVER F.C., VANDERAUWERAER M.A., J. Chem. Soc., Faraday Trans. 2., 85 (1989), 1779.
[8] LOEW L.M., COHEN L.B., DIX J., FLUHLER E.N., MONTANA V., SALAMA G., JIAN-YOUNG WU, J. Membrane Biol., 130 (1992), 1.
[9] TURKEWITSCH P., WANDELT B., DARLING G.D., POWELL W.S., J. Photochem. Photobiol., A, 117 (1998), 199.
[10] *CRC Handbook of Chemistry and Physics*, R.C. Weast (Ed.), 68 Ed., CRC Press Inc. Boca Raton FL USA, New York, 1987, D-221, D-269.
[11] PARKER C.A., REES W.T., Analyst, 85 (1960), 587.

Received 17 June 2002
Revised 4 November 2002

Materials Science, Vol. 20, No. 4, 2002

On the mechanism of formation of the photoelectret state in 4-nitro-4′-aminodiphenyl thin films*

MYKOLA KRAVTSIV

Drohobych State Pedagogical University, I. Franko Str. 24, 82100 Drohobych, Ukraine**

The mechanism of photoelectret formation in organic polycyclic compounds is discussed on the example of 4-nitro-4′-aminodiphenyl. It is established that the magnitude of photoelectret field is associated with the magnitudes of the external electric field and the pyroelectric field. Photogenerated and injected holes are the main source of photoelectret charge in these materials. The magnitude and kinetics of photoelectret state depend on the polarity of illuminated electrodes.

Key words: *photoelectret state; organic semiconductors; trapping centres; pyroeffect*

1. Introduction

It is known that photoelectret state is formed in photosensitive high-resistant semiconductors in the presence of deep trapping levels for majority carriers and of electrode barriers [1]. The generation of non-equilibrium carriers in inorganic and organic semiconductors is difficult in some details but the mechanism of photoelectret state (PhES) formation is the same: inhomogeneous distribution of charge carriers in trapping centres along the electric field. PhES in inorganic semiconductors has been investigated in detail but it did not find a wide practical application. A search for new photoelectrets among organic semiconductors gave positive results. For example, photoconductivity, PhES and pyroeffect, independent of external electric field, successfully combine in 4-nitro-4′-aminodiphenyl (NADPh). This opens new perspectives for practical application of the above material in optical memory, optical transmission, etc. [2]. The material was also selected due to an overlap of photoconductivity and pyroeffect in some spectral regions that

*Paper presented at the 4th International Conference on *Electronic Processes in Organic Materials*, ICEPOM-4, 3–8 June 2002, Lviv, Ukraine.

**E-mail: sndlnd@drohobych.net.

permits the PhES investigations in the presence and absence of pyroelectric field in the function of wavelength.

2. Experimental

NADPh thin-film samples were manufactured in the form of sandwich-cells, which were obtained by consecutive application of the bottom aluminium electrode, organic material and the top aluminium electrode on the substrate (quartz, glass ceramic, polymer film) by the thermal deposition in vacuum. The working area of the samples corresponded to the overlapping area of lower and upper electrodes and was equal to 25×10^{-8}–16×10^{-6} m^2, while the thickness of the photosensitive pyroelectric (photopyroelectric) amounted to 0.5–1.0 μm. Purity of the organic materials was ensured by the recrystallization and controlled by a stability of the melting temperature.

Irradiation of photopyroelectric sensitive elements was carried out using a xenon-krypton lamp, blackbody and monochromator. Pyroeffect and PhES kinetics were investigated with an electrometric amplifier and oscillograph.

Thermally stimulated currents were measured using the photopolarization method described in details previously [1].

3. Results and discussion

The molecule of NADPh contains two heterogroups: a strong acceptor group $-NO_2$ and a donor one $-NH_2$:

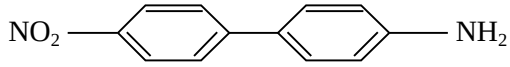

Polycrystalline NADPh consists of conglomerates of small single crystals [3]. The organic film is deposited in such a manner (the substrate is heated during the deposition) that the spontaneous orientation of these conglomerates occurs and they possess a dipole moment distinct from zero. NADPh molecule has dipole moment of 6.4 D in the ground state increasing to nearly 20 D in the first excited singlet state [4], due to the transfer of one of the nitrogen lone-pair (lp) electrons of amino group to the nitro group possessing strong acceptor properties.

NADPh thin films exhibit strong absorption in UV spectral region (Fig. 1). The long-wavelength shift of the absorption edge, in comparison with the spectrum of non-substituted diphenyl, is caused by the introduction of a heterogroup.

The photoconductivity spectrum to some extent follows the absorption spectrum with the exception of the long-wavelength region. The polarity of illuminated electrode has the essential influence on the spectral characteristic of photoconductivity. Under the

illumination of positive electrode, the photoconductivity maximum at 375 nm is much higher than under the illumination of negatively biased electrode. The reverse picture is observed for the maximum at 540 nm. The photoconductivity measurements confirm that the holes are the majority carriers in NADPh [5].

Experimental data point to PhES formation during the photocurrent flow. The PhES field is directed oppositely to the biasing field direction. The PhES magnitude depends on the sign of the potential of the illuminated electrode, the light intensity and the magnitude of external electric field. Investigations of spectral dependencies of the photoelectromotive force showed that symmetric barriers, assisting the PhES formation, are formed on both contacts.

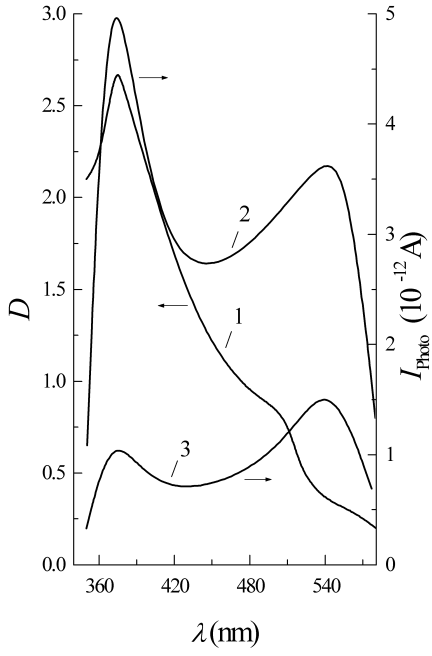

Fig. 1. Spectra of optical absorption (1) (sample thickness – 0,15 μm) and photoconductivity at the irradiation of positive (2) and negative (3) electrodes for thin film of 4-nitro-4′-aminodiphenyl (sample thickness – 0,15 μm and ~1 μm)

After achieving its maximal value, the photocurrent relaxes to a certain level. On repeated illumination, the photocurrent does not reach the maximal value but initially increases exponentially with following saturation to some stationary value. This feature indicates that the formation of PhES results in a decrease of the total electric field in the sample. The magnitude of the PhES field is approximately one order of magnitude lower than that of the biasing field.

Under the influence of external electric field, which is much higher than pyroelectric one, non-equilibrium carriers, both formed under the illumination and injected from the electrodes, move towards electrodes. The dynamics of PhES field formation is determined by the drift of holes, which are the majority charge carriers in NADPh, to the negatively biased electrode.

Barriers of approximately 1 eV high, hindering a free exchange of carriers between the organic material and electrode, exist at the interfaces between organic material and the aluminium electrodes [6]. Due to the presence of these barriers, the charge carriers are trapped with high probability in near-electrode region, creating an additional charge at the interfaces. It is possible that a part of trapped carriers will be released from traps under the influence of light, temperature, electric field, etc.

The depth of trapping centres responsible for the PhES can be determined, as a rule, by thermally stimulated current method in photoelectret regime. In the case of NADPh samples, the investigation of thermally stimulated currents [7] yield the trap depths

amounting to 0.3 and 0.6 eV. On the other hand, the depths 0.3 and 0.7 eV were obtained from the temperature dependencies of photocapacitance for investigated sandwich cells [8]. Thus, two types of trapping centres with the depths of 0.3 and 0.7±0.1 eV take part in the PhES formation processes.

Despite the fact that photoelectret charge decays with time (Fig. 2) due to detrapping process, the residual charge after the saturation at ~10^4 s is sufficient for effective application of PhES phenomenon in this material.

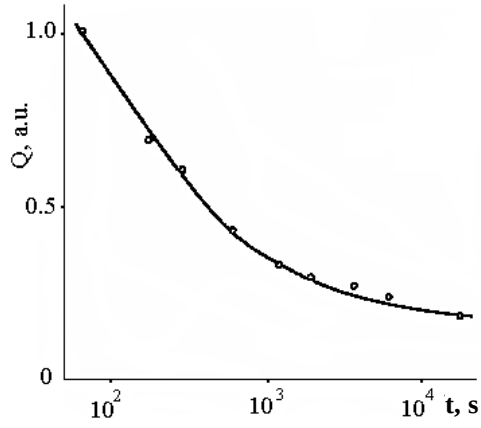

Fig. 2. Kinetics of PhES decaying
in NADPh thin films in darkness at 300 K

The regularities of PhES formation and disappearance for inorganic semiconductors can be used for the description of processes in NADPh. For example, the dependencies of PhES field on the biasing electric field (Fig. 3) and on the intensity of polarizing field (Fig. 4) have a similar character. It is clear that the saturation of PhES field in both cases is connected with filling traps. At the same time, some PhES peculiarities associated with the differences between inorganic and organic semiconductors occur.

An efficient process of PhES formation occurs, in analogy to inorganic semiconductors, at the wavelength corresponding to photoconductivity maxima. The presence of electrode barriers, strong optical absorption in UV region as well as different origin of photoconductivity maxima require a detailed consideration of PhES formation mechanism in 375 nm and 540 nm regions.

At 375 nm practically all light is absorbed in the contact region where the generation of electron–hole pairs takes place. Under the illumination of the positive electrode, the holes drift into the material bulk towards the non-illuminated electrode, where the trapping occurs. The electrons located near the illuminated electrode cannot form a sufficient heterocharge because due to optical excitation and hole injection from aluminium electrode. Thus, the space charge is formed, mainly, near the negatively charged electrode.

Hole injection from illuminated electrode is absent during the illumination of negatively charged electrode by 375 nm light. So, only carriers generated by the light in organic material make contribution into the photoconductivity. The holes drift to illuminated electrode, where part of them is trapped in the trapping centres. Because the area where the positive space charge is formed is permanently under illumination, the process of PhES formation is accompanied by a partial release of this charge. The region of the space charge is formed near the non-illuminated electrode.

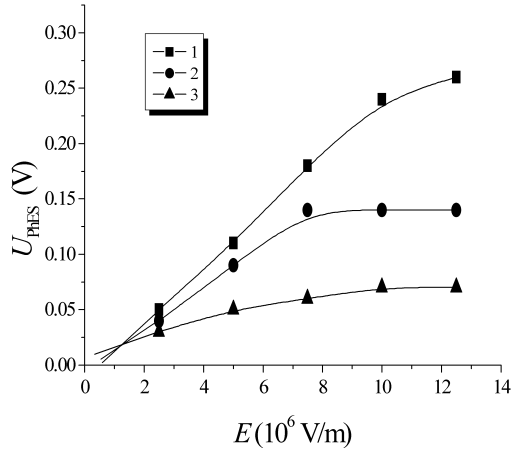

Fig. 3. Dependence of the PhES field on the external electric field in 4-nitro-4′-aminodiphenyl thin film: 1 – at the illumination of negatively charged electrode by 375 nm light; 2 – at the illumination of negatively charged electrode by 540 nm light; 3 – at the illumination of positively charged electrode by 375 nm light

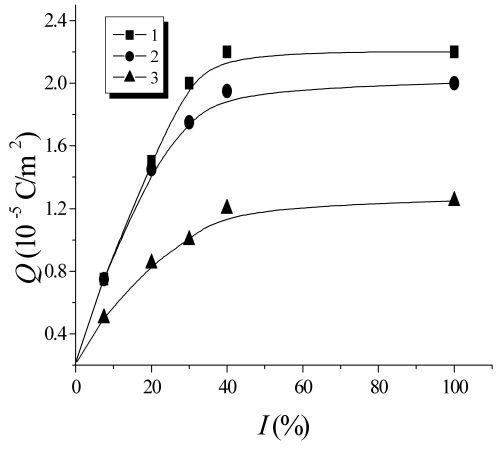

Fig. 4. Dependence of the PhES charge on the light intensity in

4-nitro-4′-aminodiphenyl thin film: 1 – at the illumination of negatively charged electrode by 375 nm light; 2 – at the illumination of negatively charged electrode by 540 nm light; 3 – at the illumination of positively charged electrode by 375 nm light

Though the hole conductance is dominant in NADPh, the electron type of conductance associated with the electron drift due to electron photoinjection from the electrode into the sample body cannot be excluded completely.

The carriers trapped in the NADPh bulk in trapping centres are released due to different processes. The emptying of trapping centres may be due to the thermal detrapping. The probability of such a process is determined by the simple Boltzmann dependence being more probable for the shallow centres than from deep ones. The optical detrapping of carriers is also possible. The absorbed light can release the carriers directly (the phonon is absorbed by the trapped charge carrier) or through the formation of triplet excitons interacting afterwards with the trapped charge carrier [9].

The dark polarization, caused by equilibrium charge carriers, plays a noticeable role in the whole polarization. The electrode injection is so intensive that at the investigation of dark polarization by depolarization method, illuminating the positively charged electrode by 375 nm light in the external circuit we observed the current flowing in the same direction as the dark current. This means that the photoinjection current is larger than the current caused by the dark polarization decay. On increasing the PhES charge, i.e., on increasing the exposition to light during the PhES formation, the photodepolarization current exceeds the photoinjection current.

It must be mentioned that in the above case the PhES field is not completely destroyed, because the positive heterocharge close to the unilluminated elecctrode remains uncharged. This charge can be destroyed by the illumination of whole bulk of the sample, for example, by the 550 nm light. The experimental results confirm that only the light of 550 nm wavelength causes the complete destruction of PhES.

In our conditions, the PhES is destroyed after 20–300 s of the illumination of samples with light from the region of long-wavelength photoconductivity maximum. A nonuniform rise of PhES charge in the initial moment of depolarisation at different polarity of illuminating electrode can be mainly explained by the existence of the pyroeffect. The pyroelectric field assists the PhES formation under the influence of external electric field on illuminating the positive electrode, and prevents this process on illuminating the negative electrode. The heat time constant for investigated films is 0.4 s and the Maxwell relaxation time is 30 s. From this it follows that the influence of pyroelectric charge on PhES becomes apparent only at the initial moment of PhES formation and destruction. The relative importance of this effect decreases with the increasing external electric field.

A slower rise of PhES charge is explained by the accumulation of negative PhES charge, which is partially compensated by the hole injection from the illuminated positively electrode, into the near-electrode layer. Under illumination of negatively biased

electrode during the PhES formation, the hole injection becomes slower and PhES charge creation is mainly due to non-equilibrium carriers.

Conclusions

The investigations of photopolarization and photodepolarization reported in this paper showed that in NADPh thin films the process of PhES formation and destruction is mainly realized due to non-equilibrium holes generated by light in the sample bulk and owing to holes injected from illuminated aluminium electrode. The magnitude of PhES field is determined by the biasing electric field and by pyroelectric field.

Acknowledgements

The technological support of colleagues from Scientific Research Institute of Organic Intermediates and Dyes (Moscow, Russia) is kindly acknowledged.

References

[1] KOVALSKIJ P.M., SHNEIDER A.D., *Photoelectret Effect in Semiconductors* (in Russian), Vyshcha Shkola, Lvov, 1977.
[2] KOVALSKIJ P.M., KRAVTSIV M.M., STANKO M.G., SHPOTYUK O.J., Ukr. Phys. J., 38 (1993), 1728.
[3] DOROZHKIN L.M., LAZAREV V.V., PLYUSHKOV G.M., CHAYANOV B.A., Quantum Electronics, 10 (1983), 1107.
[4] SVERDLOVA O.V., *Electron Spectra in Organic Chemistry* (in Russian), Khimiya, Leningrad, 1973.
[5] KOVALSKIJ P.M., KRAVTSIV M.M., MANZHARA V.S., STANKO M.G., YURKIVSKA L.I., Ukr. Phys. J., 35 (1990), 532.
[6] KOVALSKIJ P.M., PhD Dissertation, Drohobych State Pedagogical Institute, 1990, 358.
[7] ZOLOTARYOV V.F., SEMAK D.G., CHEPUR D.V., Phys. Stat. Sol. (a), 21 (1967), 437.
[8] KOVALSKIJ P.M., KRAVTSIV M.M., MACKUS P., LIPSKIS K., J. Non-Cryst. Solids, 90 (1987), 657.
[9] POPE M., SWENBERG CH.E., *Electronic Processes in Organic Solids* Clarendon Press, Oxford, 1982, (Russian transl., Moscow, 1985)

Received 3 June 2002
Revised 7 November 2002

Materials Science, Vol. 20, No. 4, 2002

Energy transfer in peptides based on phthalimide derivatives of aliphatic aminoacids*

N. YUKHIMENKO[1**], I. SAVCHENKO[1], A. KOLENDO[1],
V. SYROMYATNIKOV[1], J. BŁAŻEJOWSKI[2], W. WICZK[2]

[*]Kyiv Taras Shevchenko National University, 60 Volodymyrs'ka St., 01033, Kyiv, Ukraine

[**]University of Gdańsk, 18 Sobieskiego Str., 80-952 Gdańsk, Poland

Model peptides containing phthalimide derivatives of aliphatic aminoacids with various number of methylene groups in side chains have been synthesized and investigated spectroscopically. The study aimed at the creation of polymers with the intramolecular triplet–triplet excitation energy transfer. In all compounds investigated, efficient triplet–triplet energy transfer is observed, resulting in the phosphorescence only from phtalimide π-electronic system in frozen solutions at 77 K.

Key words*: peptides; electronic excitation; energy transfer; conformational analysis*

1. Introduction

The critical distance of a triplet exciton jump is known to be 1.8–2.0 nm [1–3]. This distance was calculated as an average value for copolymers of vinyl carbazole with octyl methacrylate with various contents of the first co-monomer units. Using a certain content of quenching admixtures, identical in all samples, the decrease of intensity of phosphorescence in comparison with the appropriate low molecular weight analogue was measured, as well as changes of delayed fluorescence intensity. In order to check the reliability of this value, from our point of view, it is convenient to use low molecular weight models. These models must have two π-electronic systems at a defined distance from one to another. Their lowest excited energy levels must ensure a triplet–triplet excitation energy transfer. The spectral investigations of such model compounds in low-concentration solutions guarantee the absence of intermolecular excitation energy transfer, whereas their conformational analysis enables one to estimate distances for energy transfer.

---

[*]Paper presented at the 4th International Conference on *Electronic Processes in Organic Materials*, ICEPOM-4, 3–8 June 2002, Lviv, Ukraine.

[**]Corresponding author, e-mail: svg@.chem.univ.kiev.ua.

As appropriate model compounds we chose compounds with non-conjugated benzyl and phthalimide groups. In our previous work [4], it was shown that their unselective photoexcitation caused an efficient intramolecular excitation energy transfer from benzyl to phthalimide π-system that results (frozen solutions at 77 K) in phosphorescence of the latter group only.

We have synthesized model compounds (Fig. 1b) containing the above-mentioned π-electronic systems at various distances from one another. The aim of this work is the evaluation of a critical distance between the π-systems, above which the excitation energy transfer will be not complete, that will be evident in an occurrence of a phosphorescence of the benzyl π-electronic system. The arrangement of the first excited singlet and triplet electronic energy levels of phthalimide and benzyl π-electronic systems are shown in Fig. 1.

a) b)

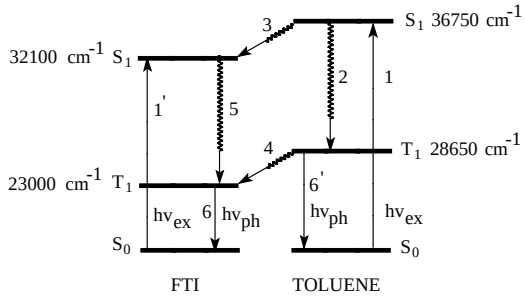

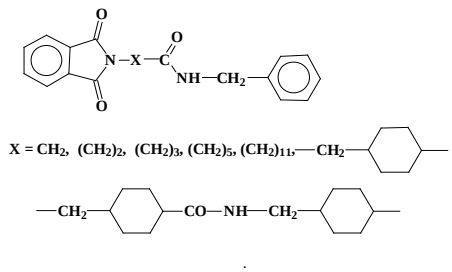

c)

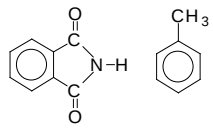

Fig. 1. Energy transfer in compounds containing phthalimide and benzyl fragments: a) π-electronic moieties, b) scheme of excited energy levels, c) model compounds

According to the scheme shown in Fig. 1, a partial S–T conversion (way 2) takes place under an unselective excitation of the model compounds (path 1 and 1′) except S–S crossing (path 3). After the complete triplet–triplet conversion of excitation energy (way 4), in the spectrum of their phosphorescence in diluted solutions only the phosphorescence of phthalimidic π-electronic system is observed (way 6). At an incomplete T–T conversion, the phosphorescence of benzyl fragment should be observed at shorter wavelengths (path 6′).

2. Experimental

Chemicals. The starting phthalimides of amino acids 1a–f were obtained by the condensation of equimolar amounts of phthalic anhydride and corresponding amino acids. The peptides 2a–f and 1g were synthesized using a standard technique [5] (Scheme. 1):

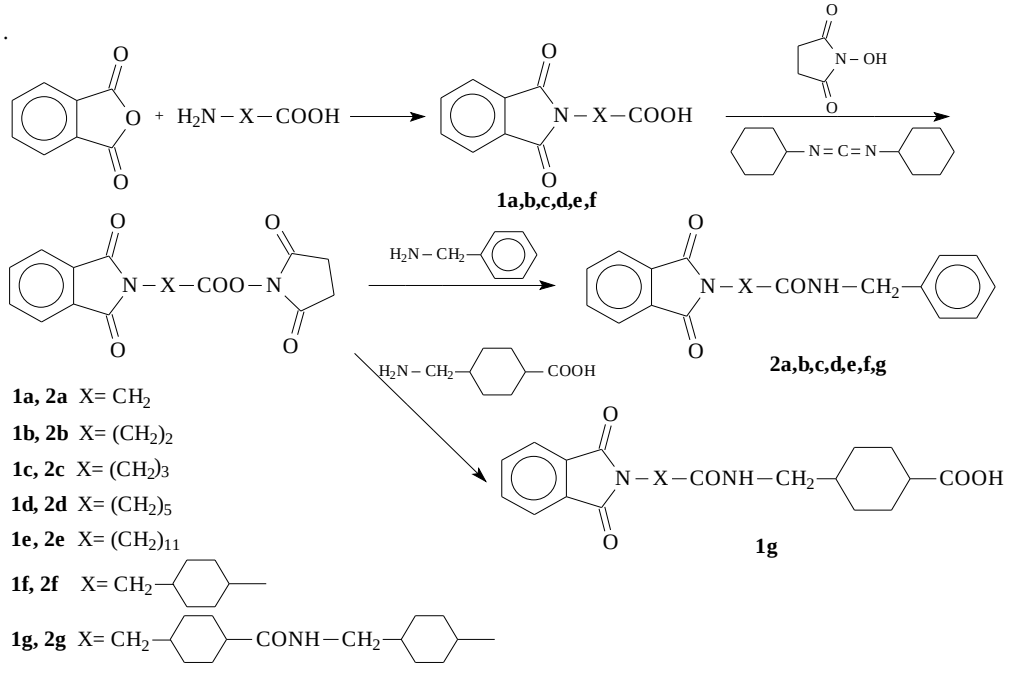

Scheme 1. Synthesis of starting phthalimides of amino acids: N1-benzyl-2-(1,3-dioxo-2,3-dihydro -1H-2-isoindolyl)acetamide – **2a** (m.p. = 225 °C, yield 70%), N1-benzyl-3-(1,3-dioxo-2,3-dihydro -1H-2-isoindolyl)propanamide **2b** (m.p. = 207–209 °C, yield 75%), N1-benzyl-4-(1,3-dioxo-2,3-dihydro-1H-2-isoindolyl)butanamide **2c** (m.p. = 157 °C, yield 80%), N1-benzyl-6-(1,3-dioxo-2,3-dihydro -1H-2-isoindolyl)hexanamide **2d** (m.p. = 133 °C, yield 87%), N1-benzyl-12-(1,3-dioxo-2,3-dihydro -1H-2-isoindolyl)dodecanamide **2e** (m.p. = 125 °C, yield 72%), N1-benzyl-4-(1,3-dioxo-2,3-dihydro -1H-2-isoindolylmethyl)-1-cyclohexanecarboxamide **2f** (m.p. = 190 °C, yield 70%), N1-benzyl -4-[4-(1,3-dioxo-2,3-dihydro-1H-2-isoindolylmethyl)cyclohexyl-carboxamidomethyl] -1-cyclohexanecarboxamide **2g** (m.p. = 269-271°C, yield 61%) were synthesized

The purity of the compounds synthesized was checked by thin-layer chromatography (TLC). Ethanol and methanol (Fluka AG), both of spectral grade, were used as solvents.

Spectral measurements. The structures of new compounds were characterized by NMR-spectroscopy. All measurements were carried out with a Bruker-100 NMR spectrometer. Acetone-d_6 was used as a solvent, and tetramethylsilane – as an internal standard. IR spectra were recorded with an UR-10 spectrometer in KBr pellets. The UV

absorption spectra were measured with a SPECORD UV VIS spectrophotometer in ethanol solutions ($C = 10^{-5}$ mol/dm^3).

Fluorescence was measured with a Perkin-Elmer LS-50 spectrofluorimeter. The excitation and emission spectra were both recorded at the 2.5 nm bandwidth in ethanol solution. The emission spectra were measured by adjusting excitation wavelengths to the maxima in the absorption and fluorescence excitation spectra. Fluorescence excitation spectra were recorded at the wavelengths corresponding to the maxima in the emission spectra or sometimes at selected wavelengths at the edges of the emission bands. Phosphorescence measurements were carried out using equipment based on ISP-28 quartz spectrograph in alcohol solutions at 77 K.

Calculations. The conformational analysis for compounds **2a–g** and the distribution of distances between π-electronic systems of benzyl and phthalimide was carried out by computer simulation (MM^+) with the subsequent geometry optimization (in each local minimum) in the semi-empirical AM1 approximation. The simulation was carried out for the ambient temperature. Only conformers with the heat of formation not exceeding 4 kcal/mol from optimal till energy of conformer were selected. As the duplicates similar structures with a difference of energy of 0.3 kcal/mol were considered.

3. Results and discussion

The structures of all compounds obtained were examined by spectral methods. We calculated the average distances between π-electronic systems for model compounds **2a–g**. The results of calculations are given in Fig. 2. It can be seen that while for compound **2a**, the average distance between systems is 0.35 nm, the elongation of the chain by one methylene group (**2b**) leads to 20% of molecules with the minimal distance between systems of about 0.7 nm. A further increase of the number of methylene groups between the π-systems (from 3 up to 11, **2c–2e**) results in the decrease of a portion of extended conformers (1–2%, **2d**), due to the increase of chain flexibility.

The use of "hard" cyclohexane rings as spacers allows one to achieve a considerable amount of extended conformers (Fig. 1) **2f–2g**. For compound **2f**, the distance between phthalimide and benzyl systems is 0.6–0.95 nm, and shorter conformers are absent. The addition of a second cyclohexane ring in the basic chain (**2g)** allows us to obtain more than a half of molecules with the distance between rings amounting to 1.0–1.3 nm and about 10% of molecules with the minimal distance equal to 1.5–1.6 nm.

So in Figure 3, the model of conformer **2g** with maximal length and minimal distance between phthalimide and benzyl π-electronic systems of 1.63 nm is represented.

In Figure 4, the phosphorescence spectra of compounds **2a–g** are shown. For comparison, the phosphorescence spectra of toluene and phthalimide are given. It is evident that only the emission from the phthalimide π-electronic system (with the maximum at

about 460 nm) is observed in the samples pointing to a complete intramolecular triplet–triplet energy transfer from toluene to phthalimide π-electronic system.

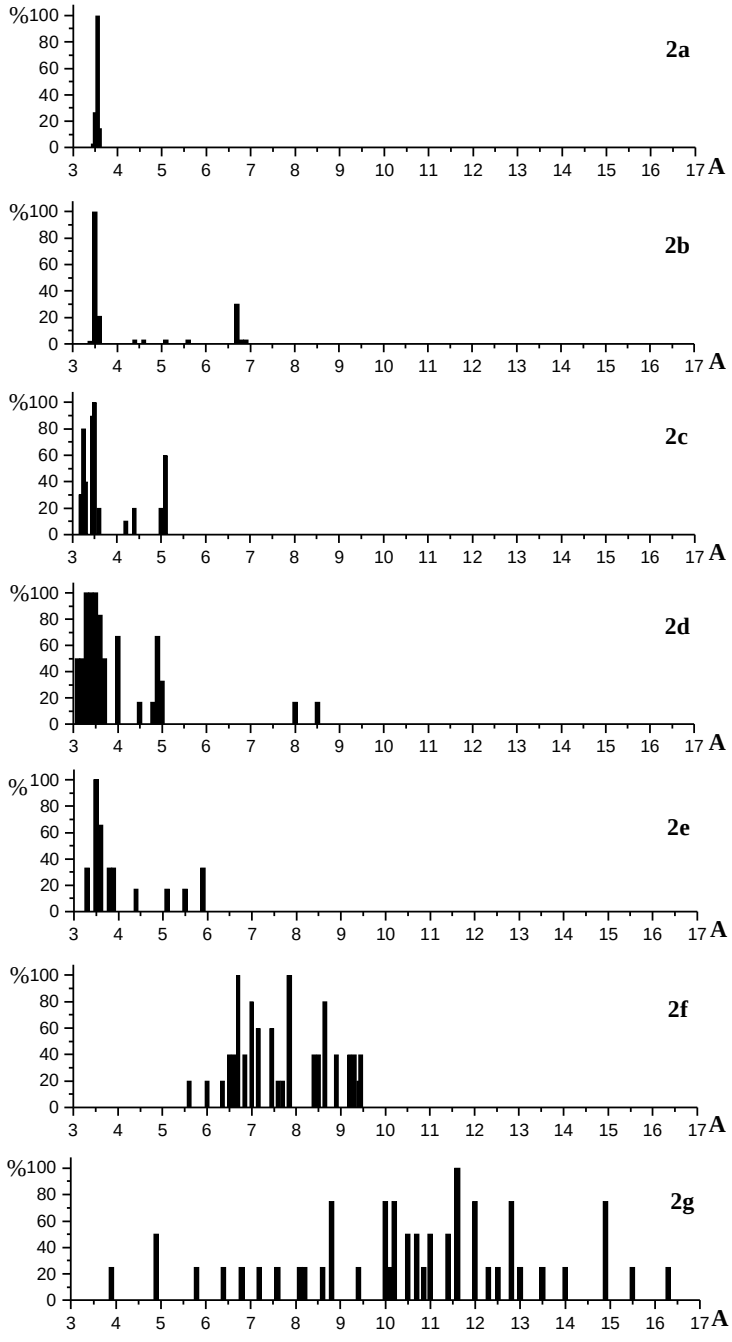

Fig. 2. Estimation of distances between phthalimide and benzyl π-electronic systems for the conformers **2a–g**. The relative contributions of various conformers were normalized to the most probable structure. The distances are expressed in Ångström units

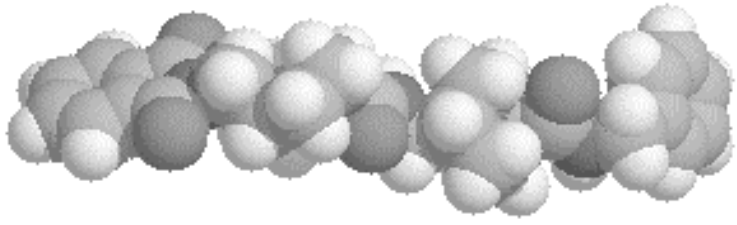

Fig. 3. Model of a compound **2g** molecule with a minimal distance between phthalimide and benzyl π-electronic systems of 1.63 nm

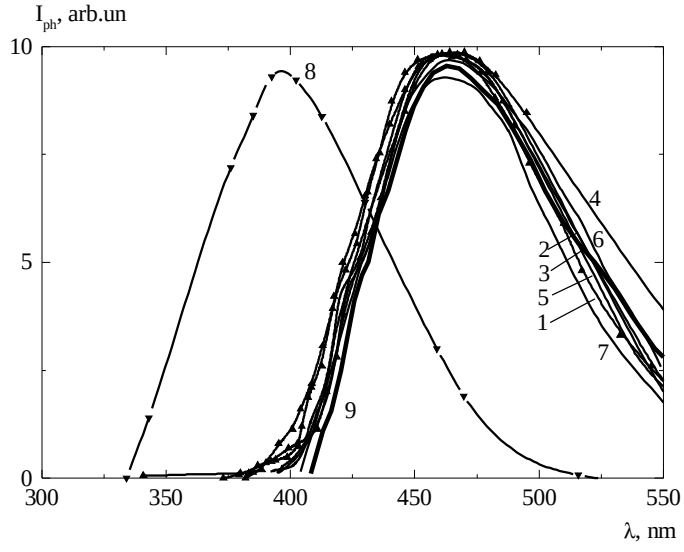

Fig. 4. Phosphorescence spectra of: 1 – 2a; 2 – 2b; 3 – 2c; 4 – 2d; 5 – 2e; 6 – 2f; 7 – 2g; 9 – phthalimide in ethanol at 77 K ($C = 10^{-5}$ mol/l, $\lambda_{ex} = 254$ nm), 8 – toluene ($C = 10^{-2}$ mol/l, $\lambda_{ex} = 254$ nm)

Conclusions

It was shown that the increase of a spacer length consisting of methylene groups does not result in the increase of the distance between π-electronic systems. Thus it is possible to obtain only 1–2% of conformers with the distances between π-electronic systems equal to about 0.8–0.85 nm. By using cyclohexane rings as spacers, the flexi-

bility of chains is decreased, and for **2g** about 60% of molecules with a minimal distance between rings 1.0–1.3 nm and about 10% of molecules with 1.5–1.6 nm can be obtained. Availability of a complete intramolecular excitation energy transfer in the frozen solutions of all compounds investigated is proved by spectral methods. The longest distance between the donor and acceptor π-electron systems achieved in the systems under study do not allow for the inhibition of the triplet energy transfer. Our results thus indicate that the critical distance of a "simple" triplet exciton jump, at which the excess of the excitation energy transfer will be incomplete, exceeds 1.6 nm.

References

[1] OGULCHANSKY T., YASHCHUK V., MASLYUK A., BEREZNITSKII G., KACHKOVSKI O., Mol. Cryst. Liq. Cryst., 361 (2001), 25.

[2] YASHCHUK V., SYROMYATNIKOV V., OGULCHANSKY T., KOLENDO A., PROT T., BLAZEJOWSKI J., KUDRYA V., Mol. Cryst. Liq. Cryst., 353 (2000), 287.

[3] ERMOLAEV V.L., BODUNOV E.N., SVISHNIKOVA E.B., SHAKHBERDOV T.A., *Radiationless transfer of electron excitation* (in Russian), Nauka, Leningrad, 1977.

[4] SAVCHENKO I., SYROMYATNIKOV V., KOLENDO A., Polish-Ukrainian Conference "*Polymers of special applications*", Radom, Poland, 2000, p. 104.

[5] GERSHKOVYCH A.A., KIBIREV A.A., *Chemical analysis of peptides* (in Russian), Naukova Dumka, Kiev, 1992.

Received 3 June 2002
Revised 8 November 2002

Materials Science, Vol. 20, No. 4, 2002

Nanofiller-modified varnishes for electrical insulation

B. GÓRNICKA*, J. ZAWADZKA, B. MAZUREK,
L. GÓRECKI, B. CZOŁOWSKA

Electrotechnical Institute Division in Wrocław,
M. Sklodowskiej-Curie 55/61, 50-369 Wrocław, Poland

Investigation into improvements in impregnating varnishes used for electrical insulation. The comparative results of the thermoanalytical testing and temperature dependence of the bonding strength of varnishes with various cross-linking reactive agents in the standard version and in the modified by introducing nanofillers version are presented. On the basis of the testing it was found that the thermal and mechanical properties of the varnishes modified by nanofillers have been greatly improved. New varnishes modified by nanofillers may be useful for a very high speed or inverter-fed electrical motors applications.

Key words: *impregnating varnish; nanofiller; bond strength; thermoanalytical methods; thermal endurance*

1. Introduction

Properties of available impregnating varnishes do not satisfy requirements of some applications, e.g. in very high-speed electrical motors (bond strength is not sufficient) or in inverter-fed motors (vulnerable to partial discharges). The varnishes need to be modified to improve their properties.

Insulating varnishes can be divided into two groups: solvent varnishes and solventless varnishes (with reactive diluents). Solventless varnishes can be improved by incorporating various reactive diluents that can increase bond strength and thermal endurance. Reactive monomers, other than styrene, are usually more expensive. In this project, we chose still another way of improving bonding properties of varnishes by incorporating a new class of fillers, i.e. nanofillers.

Nanofillers influence material properties at molecular level, and have potential to be far more homogeneously distributed than regular fillers and thus are effective at low concentrations (1–10 wt. %), keeping the cost down. Although interaction between

*Corresponding author.

nano-scale structures and polymer matrices is still unknown, nano-composites offer significant improvement of performance over base polymers. They can be designed for desired application requiring enhanced tensile strength, conductivity, thermal resistance, flammability, etc. [1–4].

The goal of this project was to fabricate nanofilled varnishes and investigate their properties for modern electrical motor applications.

3. Experimental

3.1 Samples

Six types of solventless varnishes with various reactive monomers (styrene, biallyl phtalate, vinyltoluene) and one type of solvent varnish with and without nanofiller were used (Table 1). The nanofiller was based on surface-modified layered silicates consisting of a sheet-like structure where the dimensions in two directions far exceeded the particles thickness. The thickness of the layers (platelets) was of the order of 1 nm and the aspect ratio was above 100. The type of nanofiller and its concentration were selected based on the results of processability and thermoanalytical tests.

3 wt. % of nanofiller was applied to solventless varnishes and 2 wt. % to solvent varnish. The nanofillers were dispersed in dissolved varnishes at ambient temperature.

Table 1. Tested varnishes based on unsaturated polyestreimide resin

No.	Reactive diluent	Number of components, impregnating method	Code
Solventless varnishes			
1	diallyl phtalate (P)	one-component (1) dipping varnish (D)	P1D
2	styrene (S)	two-components (2) trickle varnish (T)	S2T
3	styrene (S)	one-component (1) trickle varnish (T)	S1T
4	vinyltoluene (V)	one-component (1) dipping varnish (D)	V1D
5	styrene (S)	two-component (2) trickle varnish (T)	S2T′*
6	styrene (S)	two-component (2) dipping varnish (D)	S2D
Solvent varnish			
7	blend of solvents	dipping varnish (D)	D

*S2T′ – the same type of varnish as S2T but from different manufacturer.

3.2 Processing parameters

Varnishes are applied in motors by conventional impregnating methods, such as dipping or trickling and their processing parameters must suit the method used. The results of measurements of impregnation parameters (viscosity, gelation time and gel

temperature) for standard and modified by nanofiller varnishes are compared in Table 2.

Table 2. Viscosity, gelation time and gel temperature for standard varnishes and modified by nanofiller

No.	Varnish	Catalogue data		Testing data			
		Standard varnish		Standard varnish		Modified varnish	
		Viscosity /s	Gelation time /min /gel temperature /°C	Viscosity /s	Gelation time /min /gel temperature /°C	Viscosity /s	Gelation time /min /gel temperature /°C
1	P1D	340–370	20–60/110	340	40/110	352	45/110
2	S2T	45–105	3/120	38	3/120	46	3.5/120
3	S1T	45–105	1.5–2/120	58	1.5/120	62	2/120
4	V1D	150–170	2–3/130	155	3/130	162	3/130
5	S2T	22–26	2–3/120	27	3/120	28	3/120
6	S2D	100–120	6/120	114	6/120	131	7/120
7	D	60–80	4–6 h/120	85	5h/120	92	5.5h/120

It can be noticed that the varnish with diallyl phtalate as a reactive monomer (PID) shows the highest viscosity and gelation time. The data presented in Table 2 indicate that the varnish viscosity and range of the gelling parameters are not significantly changed by the presence of a nanofiller. The fact that the processing parameters do not deteriorate due to application of nanofiller is substantial for the impregnation processes of motor windings.

3.3. Thermoanalytical testing

Standard and the modified varnishes in a liquid and cured conditions have been tested using thermoanalytical methods. The test parameters applied were the following: temperature range: 25–800 °C, rate of furnace temperature rise: 10 °C/min, sample mass: 100 mg, test environment: air, reference substance: Al_2O_3. One measurement was performed for each varnish.

On the basis of the simultaneous recording of TG, DTG, DTA and T curves, the range of gel temperature, loss of mass during gelling and solid content for liquid varnishes and the initial temperature of decomposition (5% loss of mass) for cured varnishes have been determined. For cured samples the relative temperature index RTI_{TG} by the Di Cerbo method [5] has also been assessed.

The varnishes show maximum temperature of exothermic peak between 130–180 °C. The loss of mass during gelling is 10–17% for all solventless varnishes with and with-

out nanofillers, except for the varnish with diallyl phtalate PID (6%). The lowest initial temperature of decomposition (270 °C) and relative temperature index (139) were also obtained for the PID, while for all of the other solventless varnishes the initial temperature of decomposition was in the range of 300–320 °C and relative temperature indexes in the range of 146–171.

Table 3. The result of thermoanalytical testing of the standard and modified varnishes

No.	Varnish	Liquid varnish					Cured varnish	
		Range of gel temperature /°C			Loss of mass during gelling** /%	Solid content** /%	Initial temperature of decomposition /°C	Relative temperature index RTI_{TG} /°C)
		T_i	T_{max}	T_t				
1	P1D	150	180	230	6	96	270	139
1*	P1D*	150	180	230	6	96	275	–
2	S2T	80	140	160	17	83	300	146
2*	S2T*	80	130	160	15	85	310	–
3	S1T	120	150	190	16	84	300	160
3*	S1T*	110	145	200	16	84	320	–
4	V1T	120	150	190	10	90	320	171
4*	V1T*	120	145	200	10	90	320	157
6	S2T	95	135	180	11	89	320	159
6*	S2T *	100	140	190	13	87	330	–
6	S2D	80	130	170	14	76	310	146
6*	S2D*	80	140	200	14	76	320	162
7	D	120	160	220	55	45	270	171
7*	D*	80	155	230	55	45	320	–

*Varnishes with a nanofiller.
** The accuracy of reading from TG curves was ±2%.

Thermoanalytical testing has confirmed that important processing parameters of varnishes have not significantly changed after adding nanofillers. Table 3 shows that the initial temperature of decomposition of modified styrene varnishes has actually increased by about 10–20 °C in comparison with the standard ones. However, for varnishes with diallyl phtalate (P1D) and with vinyltoluene (VID) the initial temperature of decomposition did not change after modification.

3.4. The bond strength testing

The testing of the bond strength has been made at a temperature range from 23 °C to 180 °C according to IEC standard [6]. At each point six measurements were performed and the scatter of the results was ±6%.

Table 4 shows the ratios of the varnish bonding strength with filler and the bonding strength without filler for various temperatures. This ratio, denoted here as a *k*-factor, is higher than one and thus indicates that the bond strength of a varnish increases after adding a nanofiller. At the test temperatures close to the curing temperature of a varnish (130 °C for styrene varnishes), the *k*-factor attains the maximum value.

Table 4. The *k*-factor for various varnishes at different test temperatures

Varnish	Reactive monomer	The factor *k* at various test temperatures/°C				
		23	105	130	155	180
P1D	diallyl phtalate	0.79	–	0.79	0.76	0.94
V1D	vinyltoluene	0.98	–	1.19	1.32	1.00
S1T	styrene	1.01	–	1.20	1.18	1.30
S2T	styrene	1.22	–	1.53	1.25	1.16
S2D	styrene	1.32	1.76	1.63	1.50	–
PK 180	styrene	1.34	–	1.57	1.25	1.30
D	blend of solvents	1.44	–	1.67	1.40	1.38
S2T	styrene	1.50	1.45	1.52	1.38	1.57

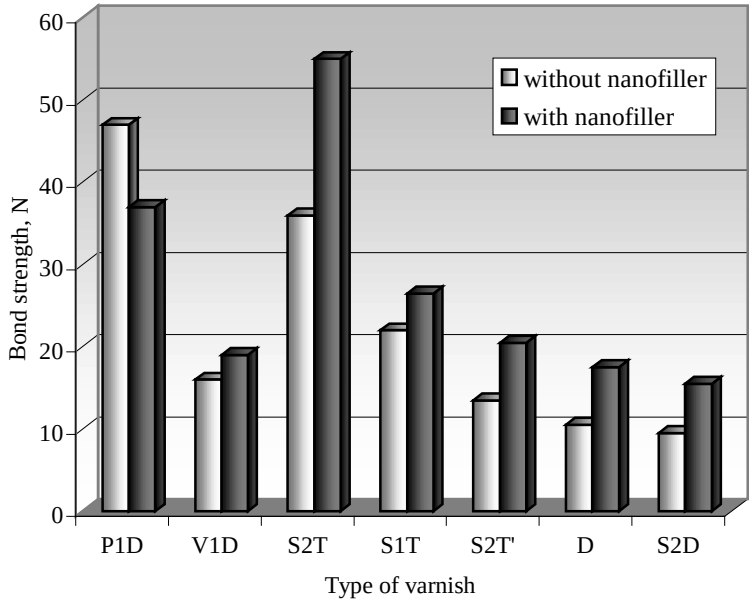

Fig. 1. The bond strength for varnishes with and without nanofiller at 130 °C

In Figure 1, the bond strength of different varnishes with and without nanofillers measured at 130 °C is presented. Figure 2 shows the temperature dependence of the bond strength for the S2T varnish with and without nanofiller.

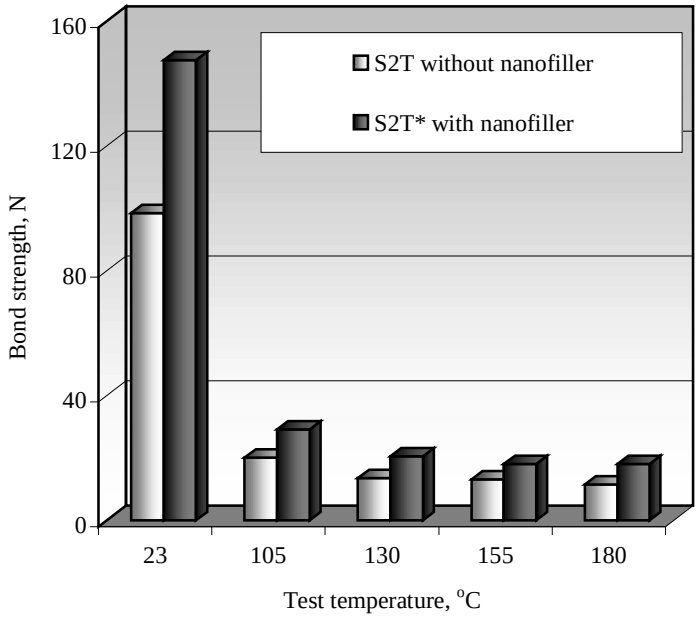

Fig. 2. The temperature dependence of bond strength for varnish S2T with and without nanofiller

The data presented in Table 4 and in Figs. 1, 2 indicate that after incorporation of nanofillers the bond strength of most varnishes significantly increases, up to 67%, except for PID and VID. While for VID varnish (containing vinylotoluene) no improvement was observed, the PID's (varnish with diallyl phtalate) bond strength decreased after modification. Due to high viscosity of these two non-styrene varnishes (Table 2), the nanofiller did not have any positive effect on their thermal and mechanical properties (Tables 3 and 4). For highly viscous varnishes the interlayer spacing of the applied processing method was too most likely small for polymer chains to penetrate.

Conclusions

The comparative test for varnishes used in motor insulation and modified by loading low amounts of nanofiller have been presented. It was found that adding 2–3% of nanofiller to varnishes with various cross-linking agents:

- did not change processing parameters,

- increased the bond strength of styrene varnishes by about 30%,
- increased the thermal endurance of styrene varnishes.

For highly viscous (non-styrene) varnishes development of a better method of dispersing nanofiller particles is required. New nanofiller-modified styrene varnishes exhibit improved mechanical and thermal properties and might be useful for applications in high-speed motors. The nanofiller-modified varnishes will be tested for inverter fed electrical motor applications, including the effect of partial discharges.

Acknowledgements

The authors are grateful to the State Committee for Scientific Research for a financial support through the grant No. 8 T10A 074 21.

References

[1] SCHADLER L., APPLE T.M., BENICEWICZ B.C., SIEGEL R.W., STERNSTEIN S.S., ASH B.J., NUGENT J., ROGERS D., ZHU A., *Mechanical and Molecular Behavior of Nanoparticle/Polymer Composites*, http://www-unix.oit.umass.edu/~nano/NewFiles/FN14_RPI.pdf.

[2] MAUL P.L., *Plastic Nanocomposites: The Concept Goes Commercial*, http://www.nanocor.com/tech_papers/plastic_nanocomposites.asp.

[3] HAY J.N., SHAW S.J., *A Review of Nanocomposites 2000*, http://www1c.btwebworld.com/nano/nanocomposites_review.pdf.

[4] *Advanced Materials and Nanotechnology Research*, The Resselaer Nanotechnology Center, http://www.rpi.edu/dept/research/nanotech_abstract2.html

[5] DI CERBO P.M., *Using Thermogravimetric Analysis to Determine Varnish/Magnet Wire Coating Compatibility*, Insulation/Circuits, 1 (1975) , 21.

[6] IEC 1033:1991. *Test methods for determination of bond strength of impregnating agents to an enamelled wire substrate*.

Received 22 July 2002
Revised 30 October 2002

Materials Science, Vol. 20, No. 4, 2002

Molecules with bonds such as Xe–O between moieties and their application

P. O. KONDRATENKO[1*], YU. M. LOPATKIN[2], N. P. KONDRATENKO[3]

[1]Supreme Certifying Commission, Vul. Khreshchatyk 34, 01001 Kyiv, Ukraine

[2]Sumy State University

[3]Taras Shevchenko Kyiv National University

The molecules with the bond such as Xe–O (the bond is formed owing to the interaction of completely occupied atom orbital (AO) of xenon and partially occupied AO of triplet oxygen between moieties are investigated. These investigations have shown that all such molecules (diazoquinones, salt of diazonium, azides etc.) are characterized by considerable activity in lower excited states or upon the transfer of an additional electron into them. They allowed us to establish that the photodissociation of the diazonium cation or the molecule of azide is carried out owing to the predissociation into the dissociative $\pi\sigma^*$ state, and the σ^* MO is located on the dissociative bond. The photodissociation of diazoquinones is carried out from the lower singlet $\pi\pi^*$ state. The transfer of the electron into salt of benzenediazonium and phenylazides provides the necessary conditions for the dissociation of the molecule, nevertheless, it provides the opportunity of the sensitization of the dissociation process to the visible region of the spectra with dyes only of diazonium salts. The sensitization of the photolysis of azide is possible only with high-energy radiation that also allows us to use this substance, for example, for the registration of ionizing radiation.

Key words: *diazo; sensitization; photodissociation; registration*

1. Introduction

The salts of diazonium and azides are widely known as the photosensitive components of the photographic materials, which do not contain halogenides of silver [1]. And though these compounds have been known since the end of the XIX century, their photochemical properties have not been sufficiently examined.

We have analyzed the properties of the excited states of these compounds, within the frameworks of a new class of compounds that can promote more understanding of the

[*]Corresponding author, e-mail: pkondrat@unicyb.kiev.ua.

photochemical properties of the large number of compounds and the expansion of opportunities of their use as the photosensitive components for the photographic and phototechnological processes. This new class of compounds are the compounds with the bonds such as Xe–O between molecule moieties.

The classification of the chemical bonds in molecules (valence, ionic, donor–acceptor, hydrogen) is sufficiently developed. A distinct type of the bond in this classification is the chemical bond between the atom with the completely occupied atom orbitals (AO), for example, of the inert gas atom (xenon, krypton) or the anion of halogen (Cl^-, Br^-, I^-) and the oxygen atom. In order to create the chemical (donor –acceptor) bond, preliminary excitation of the oxygen atom from the state with the electronic configuration $(2p_z)^2(2p_x)^1(2p_y)^1$ into the state with the electronic configuration $(2p_z)^2(2p_x)^2(2p_y)^0$ is necessary. The result of such a process is the formation of molecules such as ClO_n^- or IO_n^- (n = 1–4) and the molecule XeO_n. It is known [2] that the molecules such as ClO_n^- or IO_n^- in water solutions act as the electron acceptors, despite the presence of interelectronic repulsion. It is clear that the neutral molecule XeO_n will be a considerably stronger oxidant that leads to the explosion of this substance at contact even with weak donors [2].

The opportunities of formation of molecules are extended at the expense of the above-mentioned type of bonds. Thus instead of the atoms Xe and O we investigated molecules, which would have the same properties as the specified atoms, namely, one of molecules should have the completely occupied molecular orbital (MO) (including n–MO), and another one – to be in the triplet state.

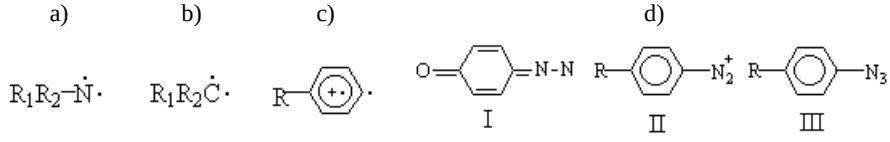

Fig. 1. Molecular structures of: a) carbenes, b) nitrenes, c) aryl cations, d) diazoquinone (I), salts of diazonium (II), azides (III)

To the first type of molecules there belong: molecular nitrogen (N_2), molecules (including cyclic) with heteroatoms, on which n–MO is located (R_1–O–R_2, R_1–S–R_2, R_1–N=R_2, R_1–NH–R_2, R_1–CO–R_2 etc., where R_1, R_2 are any molecule moieties) and others. The second type is represented by the molecular structures such as carbenes (Fig. 1a), nitrenes (Fig. 1b), aryl cations (Fig. 1c) and others. Besides the anion of halogen or the atom of oxygen can play a role of one of the moieties mentioned.

2. Experimental and calculations

The experimental and theoretical investigations of the compounds of the types mentioned above, such as diazoquinone (I), salts of diazonium (II) and azides (III) (Fig. 1d) were carried out.

Experimental investigations concerned spectroscopic and photochemical properties of those compounds, and the theoretical one – the quantum-chemical calculations (methods MNDO and AM1 [3]*) of the excited states of molecules. For comparison the calculations of the molecules ClO_n^- and IO_n^- were carried out, which could help to understand the properties of the molecule XeO_n.

Luminescence of the solutions was excited using a mercury lamp DRSh-1000 equipped with colour filters. Spectra were recorded with the Specord M-40 spectrophotometer.

3. Results and discussion

3.1. Molecules ClO_n^- and XeO_n

The results of calculations have shown that in the molecules under consideration all π MO are populated with electrons. The transfer of one electron from the π^* MO into the σ^* MO corresponds to the lower singlet state S_1, at that the σ^* MO is formed owing to the interaction of the p_z–AO of the interactive atoms. The quantum transition $S_0 \rightarrow S_1$ or $S_0 \rightarrow T_1$ does not result in the dissociation of the molecule. The dissociation is possible only at the $\sigma \rightarrow \sigma^*$ excitation (the energy surfaces of the $S(\sigma\sigma^*)$ and $T(\sigma\sigma^*)$ states are clearly dissociative).

As the molecules $HalO_n^-$ (Hal is the atom of halogen) act in solutions as acceptors of electrons, we have also calculated the energy surface $HalO_n^{2-}$. It turned out that it is exclusively dissociative that is, the transfer of an electron into $HalO_n^-$ results in the separation of the anion of oxygen ($ClO_n^- + e^- \rightarrow Cl^- + O^-$). In vacuum, the process of the transfer of the electron is impossible, as the reaction proceeds with increasing energy of the system owing to the inter-electronic repulsion. Nevertheless, in water solutions there will be the gain of energy at the expense of the interaction of $HalO_n^{2-}$ with the molecules of the solvent (of the polarization of the solvent).

---

*We have established that the calculation by means of less exact methods, such as CNDO/2 or MINDO allows receiving similar data, with respect to the shapes of the potential surfaces of the excited states of molecules, and drawing the same conclusions concerning the mechanisms of the photodissociation of molecules.

The elimination of the effect of considerable inter-electronic repulsion at the transition to XeO_n results in essential increasing of its oxidizing properties. As the result, XeO_n in any aggregative state explodes in the presence of even weak donors of electrons.

In connection with such a difference of properties of $HalO_n^-$ and XeO_n later on we shall compare the properties of two similar structures, which would differ in charge in the basic state, and of the same structure in the basic and restored (plus one electron) states.

3.2. Diazoquinone and cation of diazonium

Now we shall consider the structures I and II. The results of the calculation have shown that the dissociation of diazoquinone is possible only from the $S(\pi\pi^*)$ state, which is the S_1 state of the molecule (Fig. 2). The value of the energy barrier for the process of the dissociation from this state makes only 0.17 eV that will ensure high efficiency of the dissociation of the molecule. All other states appeared inactive concerning the process of the dissociation, owing to that the product of the photolysis will be in the excited singlet state. Molecule I has large affinity to the electron (about 3 eV). This value does not depend on the length of the C–N bond, as the σ^* MO is not involved at that, and, consequently, the energy of the C–N bond almost will not change. It is the basic reason that the molecule will not be able to dissociate after the capture of the electron.

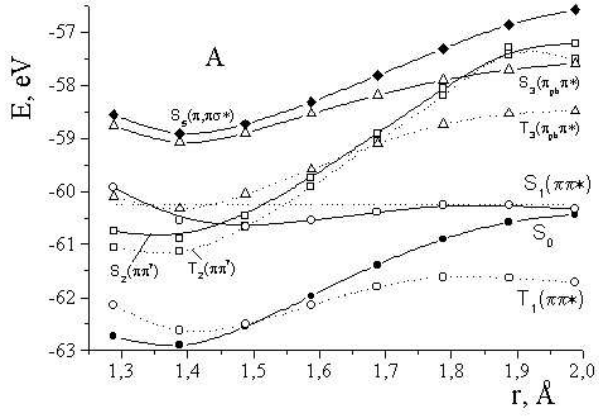

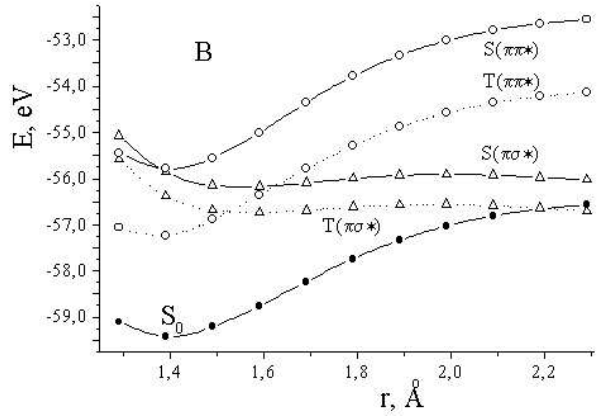

Fig. 2. The energy diagram of diazoquinone (A) (ΔE ($S_1(\pi\pi^*)$) = 0.166 eV) and *p*-hydroxyphenyldiazonium (B) (ΔE ($T(\pi\sigma^*)$) = 0.166 eV)

The protonation of molecule I with the formation of cation II entirely changes the properties of the molecule. Now the $S(\pi\sigma^*)$ and $T(\pi\sigma^*)$ states become dissociative, in which the cation will pass owing to the predissociation from the $S(\pi\pi^*)$ state. Most likely the hydroxyphenylic cation in the excited singlet state will be the basic product of the dissociation, then its relaxation occurs into the basic triplet state. The energy barrier for the dissociation from the $S(\pi\sigma^*)$ state does not exceed 0.2 eV, and from the $T(\pi\sigma^*)$ state – 0.17 eV.

As the result, the capture of the electron by cation II was expected. Its affinity to the electron in the equilibrium geometrical configuration is 5.9 eV and grows up to 8.25 eV at lengthening of the C–N bond up to 0.2 nm. The energy surface of the restored cation II has no barrier at the lengthening of the C–N bond. Hence, the phototransfer of the electron into cation II will cause its dissociation into the aryl radical and the molecule of nitrogen.

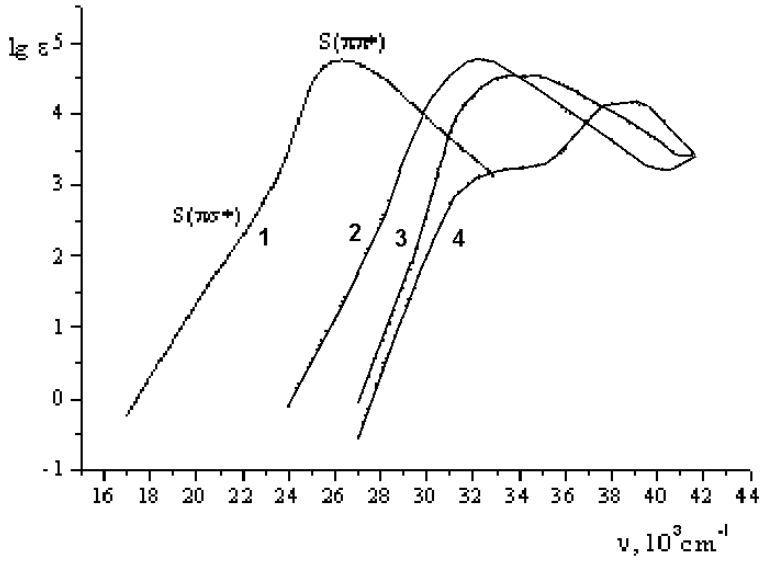

Fig. 3. The spectra of absorption of water solutions of *para*-substituted salts of benzenediazonium. The substituents: 1 – $N(C_2H_5)_2$, 2 – OCH_3, 3 – Br, 4 – H

The replacement of the substituent in cation II does not change the mechanisms of the dissociation – from the dissociative singlet and triplet $\pi\sigma^*$ states, in which the cation will pass owing to the predissociation from the $S(\pi\pi^*)$ state.

Experimental investigation and theoretical calculations show that energy of the excitation into the $S(\pi\pi^*)$ state naturally grows with increasing of electron–acceptor properties of the substituent (from NH_2 to NO_2). Both the $\pi \rightarrow \pi^*$ and $\pi \rightarrow \sigma^*$ quantum transitions can be experimentally observed (Fig. 3), as the weak $\pi \rightarrow \sigma^*$ quantum transitions (they are seen only as the long-wave break on the band of absorption at the room temperature and as the band in the frozen solutions [4, 5]) are in the region of smaller energy than the long-wave $\pi \rightarrow \pi^*$ transition. It is seen from Fig. 3 that the extinction coefficient for the $\pi \rightarrow \sigma^*$ quantum transition is some orders smaller than for the $\pi \rightarrow \pi^*$ transition. As the $\pi\sigma^*$ state is dissociative, the direct excitation into the weak band will cause the dissociation of the diazonium cation with the same quantum efficiency as at the excitation into the $S(\pi\pi^*)$ state [5]. Hence, on account of the electronic configuration of the diazonium cation, the relaxation of the excitation energy proceeds entirely through the $\pi\sigma^*$ state.

In all the cases there is the a small energy barrier for the dissociation of the cation from the $S(\pi\sigma^*)$ state. In rigid solvents, particularly in frozen matrices, the process of the dissociation can be hindered owing to the steric factors. It will result in the $S(\pi\sigma^*) \rightarrow T(\pi\sigma^*)$ conversion and dissociation of the cations only from the $T(\pi\sigma^*)$ state. The process of the photodissociation has high efficiency even in a frozen solution up to 4.2 K.

3.3. Azides

Azides (III) belong to the group of compounds with the bonds between molecular moieties (such as Xe–O). These molecules consist of the linear group N_3 and the moiety R. The atom of hydrogen or alkaline element, any multi-atom moiety (radical) can play the role of the last one. The substituted phenylazids (PA) have the most widespread application.

Azides, as well as the salts of diazonium, similarly as XeO_n tend to explode. The transfer of the electron into XeO_n and CD causes the dissociation of the molecule, which may initiate the process of the explosion. Let us now consider similar processes in azides.

The results of the calculations of energy levels of phenylazide have shown that in this case the efficiency of the photodissociation will be high both from the $S(\pi,\sigma^*)$ and the $T(\pi,\sigma^*)$ states. The energy barrier at the $T(\pi,\sigma^*)$ state makes only 0.06 eV that enables proceeding the photodissociation practically at any temperature. We have shown experimentally that the photodissociation of phenylazide in frozen alcohol solutions (4.2 K) or in polymeric layers really took place. It also appeared that the molecular nitrogen crystallizes in certain sites of the solvent (of the polymeric layer). When heating the sample, the nitrogen passes through the gas phase and creates vesicles in the polymeric matrix owing to high pressure of gas. Thus the theoretical calculations of the energy structure and mechanisms of the photodissociation of azides are entirely confirmed experimentally.

The transfer of the electron into the phenylazide molecule results in increasing the energy of the electronic system by 1 eV at the equilibrium geometry of the molecule. The energy surface of phenylazide with the superfluous electron corresponds to the dissociative surface. Hence, during the transfer of the electron into phenylazide its dissociation will take place. Nevertheless, as it results from the calculation and from our experiments, the sensitization of this process by dye molecules is not possible. Most likely, the transfer of the electron may proceed from the matrix or dye molecule only at high-energy excitation.

Conclusions

The theoretical and experimental investigation of the molecules with the bond such as Xe–O between molecular moieties are carried out. The mechanisms of the photodissociation of the specified compounds and their acceptor properties capable to provide the opportunity of the sensitization of photolysis of the specified compounds by dyes were established. Comparison of properties of the compounds under investigation with their prototypes (ClO_n^-, IO_n^- and XeO_n) enabled understanding the essential differences in the properties of diazoquinones and of diazonium salts, which differ only by presence of the positive charge on the cation of diazonium. The analysis of the research results has allowed to show that:

- there exist whole classes of molecules (diazonium salt, azides and etc.) capable to the photodissociation at the excitation to the long-wave band of absorption due to the predissociation into the $\pi\sigma^*$ state, at that the σ^* MO is located on the dissociative bond; these molecules do not fluoresce or phosphoresce owing to the effective relaxation of the excitation through the $\pi\sigma^*$ state;
- the results of calculations concerning the excitation of the diazocations and molecules of azides into the $\pi\pi^*$ and $\pi\sigma^*$ states, are matched with the experimental data concerning the spectra of absorption, according to which there is the weak band of $\pi \rightarrow \sigma^*$ absorption at the long-wave side from the band of $\pi \rightarrow \pi^*$ absorption;
- the transfer of the electron to the salt of benzenediazonium and phenylazides provides necessary conditions for the dissociation of the molecule, nevertheless, it provides the opportunity of the sensitization to the visible region of the spectra by dyes only of diazonium salts that is **the basis for creation of the sensitized diazo materials**; the sensitization of the photolysis of azide is possible only to high-energy radiation;
- the experimental investigation of photolysis of diazonium salts and azides at low temperature (4.2 K) confirm the results of the calculation concerning the dissociative character of the $\pi\sigma^*$ state.

References

[1] DINABURG M.S., *Photosensitive Diazo Compounds And Their Uses*, London, Focal Press, 1964.
[2] PIMENTAL G.C., SPRATLEY R.D., *Understanding Chemistry*, Holden and Day, 1971.
[3] DEWAR M.J.S., ZOEBISCH E.G., HEALY E.F., STEWART J.J.P., J. Am. Chem. Soc., 107 (1985), 3902.
[4] ZHARKOV I.P., KONDRATENKO P.O., Optika i Spektroskopiya, 47 (1979), 877.
[5] ZHARKOV I.P., KONDRATENKO P.O., KURIK M.V., Ukr. fiz. zh., 25 (1980), 1263.

Received 19 July 2002
Revised 31 October 2002

Materials Science, Vol. 20, No. 4, 2002

Thermostimulated processes of production of metal nanoparticles in oxide films formed by the sol-gel method

YU. V. BOKSHITS, L. T. POTAPENKO, S. V. SEREZHKINA, G. P. SHEVCHENKO*

Physico-Chemical Research Institute, Belarussian State University, 220050 Minsk, Belarus

Our study demonstrates that using the sol-gel method to form thin Me–SiO_2 films with composite sols containing nanoparticles of hydrous silica and silver/gold metal or germanium dioxide makes it possible to vary metal particle size (on reductive heat treatment in hydrogen for GeO_2) and size distribution, thus affecting optical characteristics of the films. Ge particles formed in GeO_2–SiO_2 system are smaller than those formed by reducing pure GeO_2 films. Silica sols produced with sodium metasilicate were found to stabilize the silver and gold nanoparticles formed by chemical reduction.

Key words: *sol-gel method; Me–SiO_2; system; thin film; nanoparticles*

1. Introduction

Nowadays, research in the field of physics and chemistry of nanodisperse and nanostructured systems is proceeding vigorously, the systems posessing a number of specific properties. Much attention is given to investigations of nanodisperse, chemically stable metals (silver, gold) and nanocrystals of various semiconductor compounds. They are of interest due to their unique optical, photophysical and other properties [1–6]. Their size-dependent optical properties make them usable as elements of optical devices with controllable parameters. Furthermore, they are of interest because they can provide a basis for production of superstructures such as colloidal crystals and two- and three-dimensional film systems with ordered nanoparticle arrangement (two- and three-dimensional superlattice).

Revealing non-linear optical characteristics of glasses doped with ultrafine noble metals (Ag, Au) has considerably increased interest in thin-film "metal-oxide" systems formed by the sol-gel method. This paper presents the results of the study of thermo-

*Corresponding author, e-mail: shevchenko@.bsu.by.

stimulated process yielding "metal-oxide" film systems based on composite sols. Using such sols considerably extends the possibility of controlling properties of the film systems, as compared to metal-ion-containing oxide sols used to form film systems.

2. Experimental

Thin-film "Me-oxide" (Me is for Ag, Au) systems were formed on the basis of respective composite sols produced by chemical reduction of metal ions incorporated in an oxide matrix. Stable silica sols (pH = 3–4 and pH = 8–9) were used. The sols were produced by acidic or alkaline hydrolysis of tetraethyl orthosilicate (TEOS) or from sodium metasilicate using an ionite. Sodium borohydride and hydrazine hydrate were used as reductants to produce silver nanoparticles in the oxide matrix, while sodium borohydride were used to produce gold nanoparticles, the mole ratios being Ag^+/BH_4^- ($N_2H_4 \cdot H_2O$) = 1/2; $AuCl_4^-/BH_4^-$ = 1/1, respectively. SiO_2 sols produced from sodium metasilicate are good stabilizers for metallic nanoparticles. Stable composite silica sols produced by TEOS hydrolysis are formed only in the presence of a stabilizer (hexadecanethiol, thioglycerol, $C = 10^{-6}$ mol·l^{-1}). Metal atoms concentrations in all the composite sols were 10^{-3} mol·dm^{-3} with Me/Si atomic ratio of 0.0014. The table gives the particle size for silica phase in the oxide sols used to form Ag^0 and Au^0 nanoparticles.

Table. Properties of $Ag–SiO_2$ and $Au–SiO_2$ films depending on the heat treatment conditions

Reducing agent	Precursor of SiO_2 sol	Initial layer d_{av}/nm	Heated for 40 min at 500 °C	
			d_{av}/nm*	d_{av}/nm**
$Ag–SiO_2$ films				
$NaBH_4$	TEOS	30	50	23
$N_2H_4 \cdot H_2O$	TEOS	36	34	30
$NaBH_4$	Na_2SiO_3	7,5	16	10
$N_2H_4 \cdot H_2O$	Na_2SiO_3	24	50	10
$Au–SiO_2$ films				
$NaBH_4$	TEOS	30	35	50
$NaBH_4$	Na_2SiO_3	13	28	14

* In H_2.
** In air (for $Ag–SiO_2$ and $Au–SiO_2$) and then in H_2 (for $Ag–SiO_2$).

Composite $GeO_2–SiO_2$ sols were used as precursors to form $Ge–SiO_2$ films. The sols were formed either by simultaneous hydrolysis of TEOS and $GeCl_4$ in alcohol solutions with mole ratios TEOS/$GeCl_4$ = 5/1, TEOS/H_2O = 1/10 or by mixing one-

component SiO_2 and GeO_2 sols, SiO_2/GeO_2 mole ratio being 5/1. The pure sols of SiO_2 (pH = 9) and GeO_2 (pH = 9) were produced by alkaline hydrolysis of TEOS and by the method based on solubility differences of hexagonal GeO_2 in aqueous ammonia of different concentrations [7], respectively.

Ag–SiO_2 and GeO_2–SiO_2 films were formed via layer-by-layer spin coating of the respective composite sols on quarz glass substrates. Each layer deposition was followed by air-drying for 10 min at 150 °C. Au–SiO_2 films formed by the same method were of low optical density, therefore casting a composite sol on quarz glass substrates followed by air-drying for 10–12 h at room temperature was used instead. The dried Me–SiO_2 films were heated at 500 °C for 40 min either in the air or in hydrogen, as well as successively under both gases (40 min each). Temperature was raised by 5 °C per minute. The calculated thickness of the films was about 40 nm for double-layered Ag–SiO_2 and about 1 μ for Au–SiO_2 films. To produce Ge–SiO_2 films, the initial GeO_2–SiO_2 layers were reduced in hydrogen flow at 500 °C and 650 °C for 2 h. Four-layered Ge–SiO_2 films were 40 nm or 0.5 μ thick, depending on the method of the initial sol production (by TEOS and $GeCl_4$ co-hydrolysis or by mixing pure SiO_2 and GeO_2 sols).

Me–SiO_2 (Me is for Ag, Au, Ge) films formed were characterized by optical spectroscopy and electron microscopy (EM). Optical absorption spectra were recorded with a SPECORD M40 UV-VIS double-beam spectrophotometer in the wavelength range of 200–800 nm, particle size and shape in sols and films were determined using EM-125K electron microscope. IR spectra of GeO_2–SiO_2 powders separated from the sols were obtained with a Spectrum 1000 FT-IR spectrometer in the range of 400–4000 cm^{-1}. DRON-3 (CoKα radiation) was used for X-ray diffraction analysis.

3. Results and discussion

Ag(Au)–SiO_2 films

According to the EM data, acidic (pH = 3.5) silica sols produced by ion-exchange method from sodium metasilicate are composed of regularly shaped spherical particles with their sizes ranging from 5 to 40 nm, while those produced by alkaline hydrolysis of TEOS are composed of spheroidal particles 20–100 nm in size (Fig. 1a, 2a). Figures 1b, c and 2b, c give the data on sizes and size distributions of silver particles formed in the oxide sols, sodium borohydride and hydrazine hydrate being used as reductants. The silver particles produced are mostly smaller than those constituting the oxide matrix. The sizes of the former (ranging from 3,5 to 70 nm) depend on the types both of the precursors from which the oxide sols were produced and the reductants used. Optical spectra of the composite sols in the visible region differ both in the silver plasmon resonance maximum position (which varies from 390 to 415 nm) and in the absorption

bandwidth. Powders separated from the sols are of various yellow-gray, gray and brown colours.

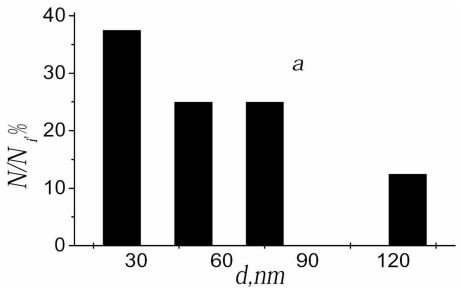

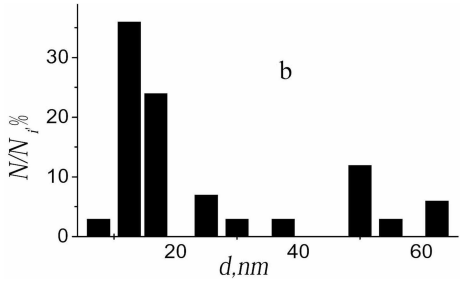

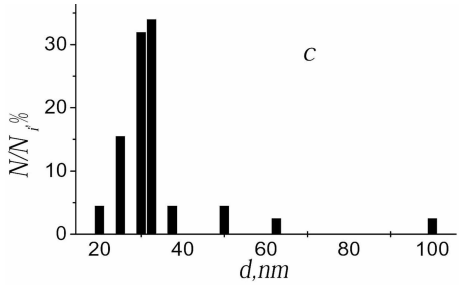

Fig. 1. Particle size distribution for: SiO_2 in the sol produced by alkaline TEOS hydrolysis (a) and silver in the composite sols (b, c). Reductants: b) sodium borohydride, c) hydrazine hydrate

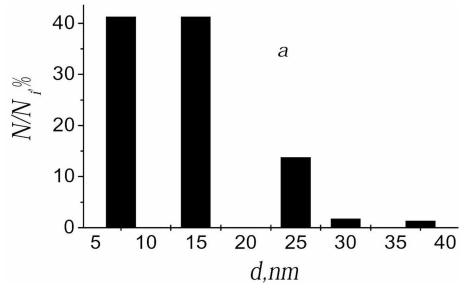

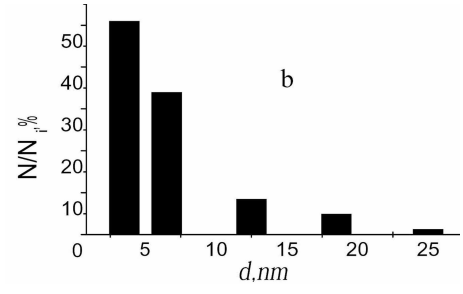

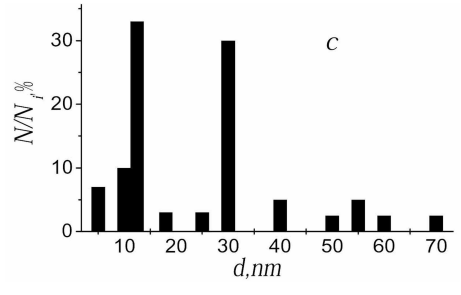

Fig. 2. Particle size distribution for: SiO_2 in the acidic sol produced by ion-exchange from sodium metasilicate (a), and silver in the composite sols (b, c). Reductants: b) sodium borohydride, c) hydrazine hydrate

Heating Ag–SiO_2 films in the air at 500 °C results in their discoloration, the temperature at which it occurs being little affected by the method of the sol production. Heating a discoloured sample in hydrogen (500 °C, 40 min) results in formation of

silver particles accompanied by the nanocomposite colour reappearing. The sizes of the particles re-formed are either the same or 1,5–2 times smaller than those of the initial ones. When the particles become hermetically encapsulated, the composite looses its ability to discolour on further oxidative heating. Annealing the initial films in hydrogen results in the larger and polydisperse silver particles. The proportion of the small particles (5–20 nm) decreases and a fraction of the larger aggregates (up to 50–90 nm) appears (see Table). Optical properties of $Ag–SiO_2$ films formed from the composite sols differ significantly depending on the way of their production (with different sol precursors and reductants used) and heat treatment conditions (Fig. 3).

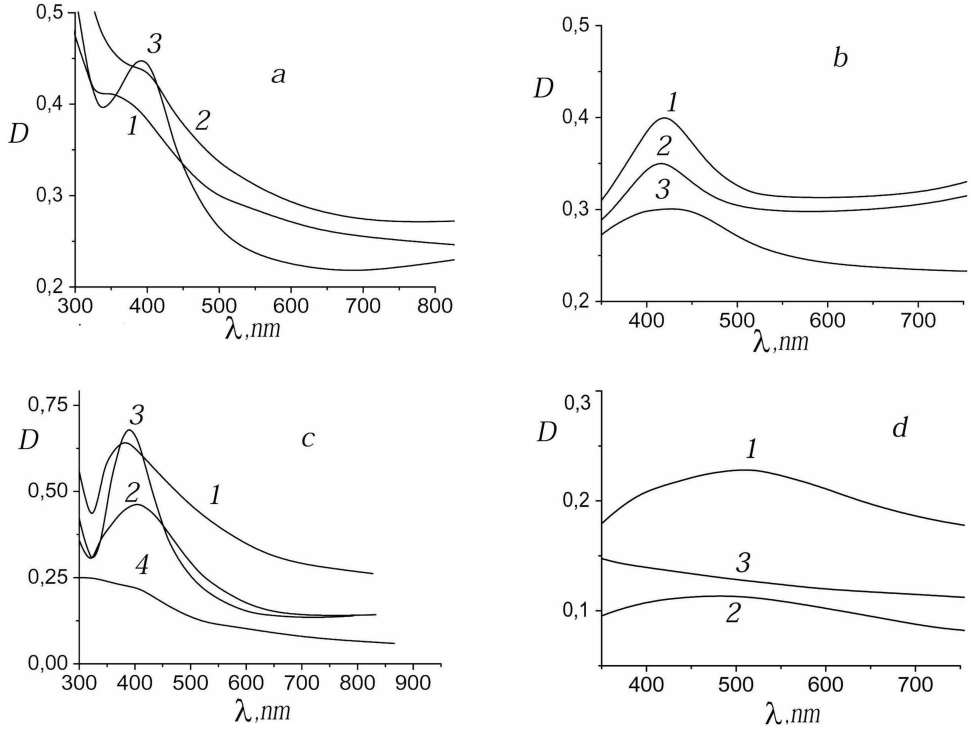

Fig. 3. UV-visible absorption spectra of silver-containing films formed from composite sols. Reductants: sodium borohydride (a, b), hydrazine hydrate(c, d). Matrices: alkaline SiO_2 sol produced from TEOS (a, c), acidic SiO_2 sol produced from sodium metasilicate (b, d). Layers: 1) initial 2) heated in hydrogen 3) heated successively in the air and in hydrogen 4) air-heated

For the films formed from the composite sols produced with TEOS, heating in the "air-hydrogen" mode results in a sharper plasmon maximum with the optical density increasing. As for the films formed from the composite sols produced with sodium metasilicate as the silica sol precursor, the same heating mode results in the broader plasmon band and the optical density decreasing. For the films formed by heating in hydrogen (for both precursors of the oxide sol) there occurs a red shift of the silver

plasmon absorption band due to an increase both in size and in polydispersity of the silver particles.

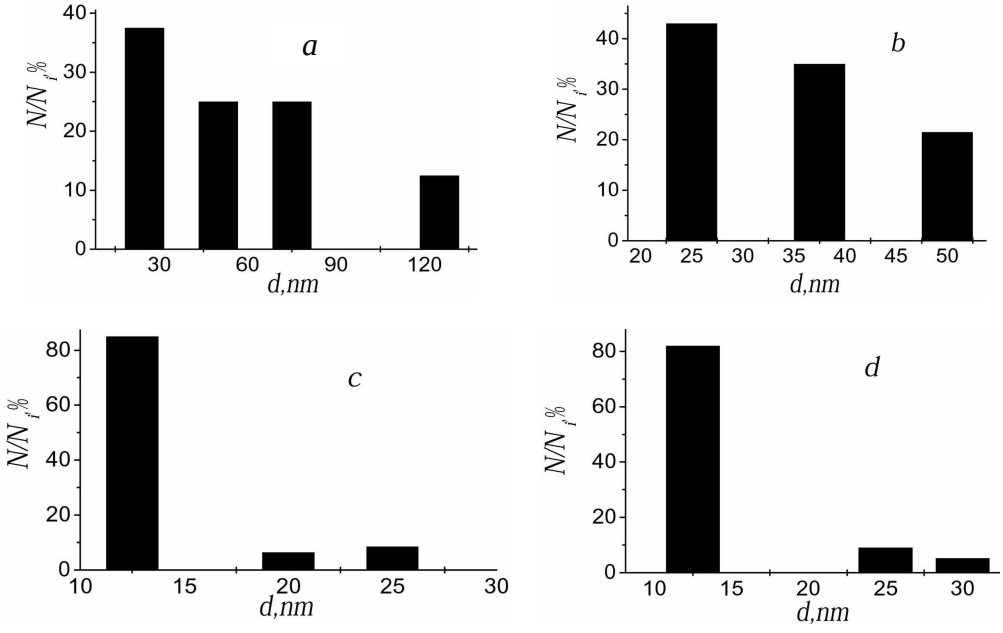

Fig. 4. Particle size distribution for SiO_2 in alkaline sols produced from TEOS (a) and sodium metasilicate (c), and for gold (b, d) in respective composite sols with sodium borohydride used as the reductant

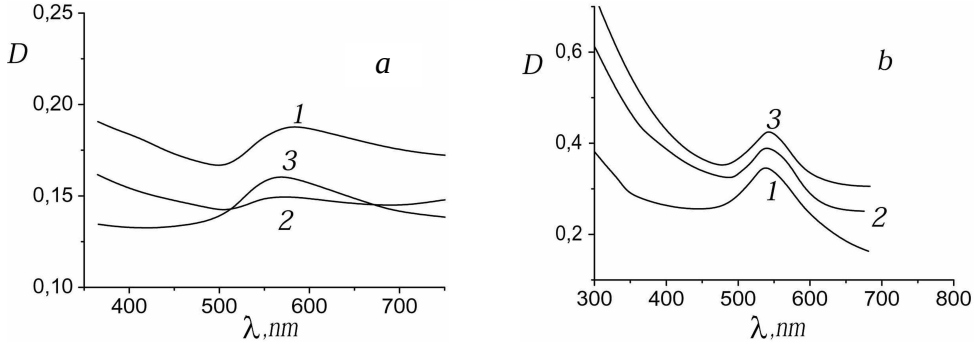

Fig. 5. UV-visible absorption spectra of gold-containing films formed from composite sols, sodium borohydride used as the reductant. Matrices: alkaline SiO_2 sols produced from sodium metasilicate (a), TEOS (b). Layers: 1) initial 2) air-heated 3) hydrogen-heated

The particles of gold in Au–SiO_2 films formed from respective composite sols used with particle sizes of 10–50 nm (Fig. 4b, d). In contrast to those of silver in the similar oxide matrices they do not oxidize when heated in the air. The particle size increases 1,5–2 times for different types of silica sols used (see Table). On heating Au–SiO_2 lay-

ers in hydrogen, larger gold particles are also formed by aggregation of the small ones. In spite of the particle size growth on heating, the shape of the optical absorption spectrum of the films remains essentially the same, the optical density only being slightly changed throughout the visible spectrum (Fig. 5). The changes in the optical density of both Au–SiO_2 and Ag–SiO_2 films on heating depend on the chemical nature of the oxide sol precursors. For the composite films based on sodium metasilicate, the decrease of the optical density observed on heating is due to their structurization resulting in the films becoming thinner. An increase in optical density is observed for the TEOS-based films, which can be related to the burnt remains of TEOS (particularly, carbon) contributing to the film absorption.

Ge–SiO_2 films

GeO_2 reduction with hydrogen in films formed from pure GeO_2 sols has previously been found to begin at 470–480 °C and to proceed with appreciable rate at 500 °C, the films turning red-brown because of ultrafine Ge particles formation [7].

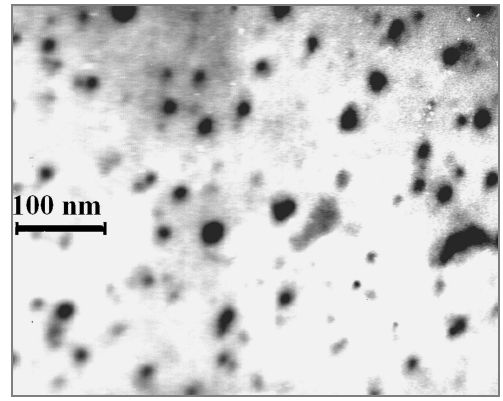

Fig. 6. TEM image of Ge-particles in Ge–SiO_2 film formed from GeO_2–SiO_2 sol produced by co-hydrolysis of TEOS and $GeCl_4$

The conditions of GeO_2 reduction to Ge in GeO_2–SiO_2 films under investigation differ significantly from those of pure GeO_2 films reduction. Heat treatment in hydrogen has been shown to be necessary to completely reduce GeO_2 in GeO_2–SiO_2 films formed from sols produced by co-hydrolysis. Virtually no reduction has been observed below 600 °C. The increased temperature of GeO_2 reduction to Ge in such films compared to that observed in films of pure GeO_2 may be explained by formation of mixed Si–O–Ge bonds in the sol produced by co-hydrolysis hindering GeO_2 reduction. IR-spectroscopy data confirm the presence of Si–O–Ge bonds. Absorption bands appear in GeO_2–SiO_2 powder spectrum (not shown) in the range of 600–700 cm^{-1} which are characteristic of the Si–O–Ge bond vibrations. The formation of such bonds is likely to explain the hindered GeO_2 crystallization in the GeO_2–SiO_2 system as opposite to that of pure GeO_2

(GeO_2 in SiO_2 matrix remains amorphous at the temperature of 500 °C, when the pure GeO_2 is already crystalline).

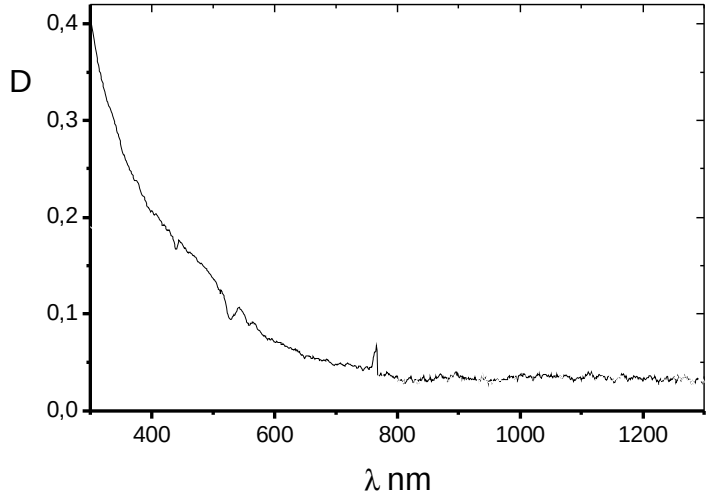

Fig. 7. Optical absorption spectrum of Ge–SiO_2 film prepared by reducing of GeO_2–SiO_2 layer in hydrogen

TEM-investigations have shown that spheroidal particles (5–15 nm in size) are formed in sols produced by co-hydrolysis of TEOS and $GeCl_4$. Particles of diamond -like germanium (10–15 nm in size) are formed in films produced from such sols and reduced at 650 °C for 2 h (Fig. 6). Optical absorption spectra of the reduced films are presented in Fig. 7 (GeO_2–SiO_2 precursor films do not absorb in that wavelength range). The films are characterized by an absorption edge (about 600–700 nm) blue -shifted from that of a bulk sample. Considering the above data concerning the Ge particle size in the films under study, it is unlikely that such a position of the absorption edge is related to the quantum size effect. It seems more likely that the shift observed is due to the light scattering on the assembly of particles, the size of it being smaller than the wavelength (according to the Mie theory) [8].

GeO_2 hydrogen reduction to Ge in GeO_2–SiO_2 films formed from the sols produced by mixing pure GeO_2 and SiO_2 sols proceeds at 500 °C. It is only the diamond -like germanium phase that is found in powders separated from the GeO_2–SiO_2 sols and heated at 500 °C for 2 h, indicating that heating in hydrogen for 2 h is enough to reduce GeO_2 to Ge in the films, too. According to the EM data, GeO_2–SiO_2 sols, prepared by mixing pure sols, contain spheroidal particles of sizes 10–25 nm for GeO_2 and 50–70 nm for SiO_2. In Ge–SiO_2 films produced from Ge particles of diamond-like structure are formed, of the sizes in the same range as those of GeO_2. Thus, there is no noticeable enlargement of the particles on reducing GeO_2 with hydrogen in SiO_2 matrix, in contrast

to the reduction of pure GeO_2, for which a general trend of the particle size increase has been observed [9].

Thus, using the sol-gel method to form thin Me–SiO_2 films from composite sols containing nanoparticles of hydrous silica and silver/gold metal or germanium dioxide makes possible varying the metal particle sizes and size distribution, thus affecting optical characteristics of the films. Silica nanoparticles prevent aggregation of Ge particles formed in the Ge–SiO_2 system. Silica sols produced from sodium metasilicate were found to stabilize silver and gold nanoparticles formed by chemical reduction.

Acknowledgements

Authors are grateful to the Basic Research Foundation of Belarus and Belarusian State University for the financial support of this work.

References

[1] *Nanoparticles and Nanostructured Films: Preparation, Characterisation and Applications*, J.H. Fendler (Ed.), Wiley, Weinheim, 1998.
[2] HENGLEIN A., J. Phys. Chem., 97 (1993), 5457.
[3] LINK S., EL-SAYED M.A., J. Phys. Chem., 103 (1999), 8410.
[4] OKAMOTO S., KANEMITSU Y., Phys. Rev., B., 54 (1996), 16421.
[5] PAINE D.C., CARAGIANIS C., KIM T.Y. et al., Appl. Phys. Lett., 62 (1993), 2842.
[6] YUE L., HE Y., J. Appl. Phys., 81 (1997), 2910.
[7] SHEVCHENKO G.P., SEREZHKINA S.V., POTAPENKO L.T., SVIRIDOV V.V., Vestsi NAN Belarusi, Ser. Khim. Navuk, 1 (2001), 28 (in Russian).
[8] HEATH J.R., J. Chem. Phys., 101 (1994), 1607.
[9] SVIRIDOV V.V., SHEVCHENKO G.P., POTAPENKO L.T., Inorg. Mat., 9 (1997), 1057 (in Russian).

Received 19 July 2002
Revised 31 October 2002